GLUTAMATE TRANSPORTER FUNCTION AT EXCITATORY SYNAPSES

by

Yanhua Huang

A dissertation submitted to the Johns Hopkins University in conformity with the requirements for the degree of Doctor of Philosophy

Baltimore, Maryland

January, 2006

Abstract

Glutamate uptake by high-affinity plasma membrane transporters is essential for maintaining a low ambient level of glutamate and avoiding neurotoxicity. At excitatory synapses, glutamate transporters help to terminate glutamate transients following release, restrict diffusion of glutamate between synapses, recycle glutamate for subsequent release, as well as provide glutamate for metabolic purposes. Five different glutamate transporters have been identified in the mammalian central nervous system (CNS); GLAST (EAAT1) and GLT-1 (EAAT2) are found predominantly in glial cells, and EAAC1 (EAAT3) and EAAT4 are expressed by neurons. Despite our knowledge about the localization and density of these transporters, their relative contribution to uptake of synaptic glutamate and their differential impact on transmission are poorly understood. This is mainly because antagonists selective for each type of glutamate transporter have not yet been developed. In this study, we performed electrophysiological recordings in wild-type and genetically modified mice defective in selective glutamate transporters to address the following questions: (1) What are the relative contributions of neuronal and glial glutamate transporters to glutamate uptake at excitatory synapses and (2) how do different types of glutamate transporters influence transmission at excitatory synapses? We examined synaptic clearance of glutamate at two representative excitatory synapses in the rodent brain: climbing fiber-Purkinje neuron synapses in the cerebellum, where neuronal glutamate uptake can be directly measured; and oriens-lacunosum moleculare interneuron synapses in the hippocampus, where

glutamate clearance at perisynaptic locations can be monitored. We found that at climbing fiber-Purkinje neuron synapses, neuronal transporter EAAT4 but not EAAC1 contributes to the clearance of glutamate, and astroglial transporters remove the majority of synaptic glutamate; at the hippocampal interneuron synapse, astroglial but not neuronal transporters regulate the occupancy of perisynaptic metabotropic glutamate receptors during transmission. We also observed that GLT-1, the predominant astroglial glutamate transporter, is expressed by a selective population of neurons, the hippocampal CA3 pyramidal neurons. The potential function of GLT-1 in these neurons is discussed.

Thesis Advisor: Dwight E. Bergles, Ph.D.

Reader: David J. Linden, Ph.D.

Acknowledgements

I would first like to thank my advisor, Dr. Dwight E. Bergles, for giving me guidance, trust and unwavering support throughout my graduate years. He has not only taught me the bolts and nuts of doing electrophysiology, but pointed out the path to me to becoming an excellent researcher and communicator of science. His critical advices and keen scientific insights have greatly facilitated the progression of this work. In addition, his dedication and his perfectionist approach to doing science have always been my immediate source of inspiration, which in retrospect, only intensified the exhilaration of scientific discovery.

I would also like to thank the other members of my thesis committee, Drs. Jeffrey Rothstein, David Linden, Paul Worley and King-Wai Yau, for their contributions to this work. In particular, I would like to thank Dr. King-Wai Yau, who first introduced the Hopkins Neuroscience graduate program to me, and soon later introduced Dwight to me. He has since given me tremendous encouragement and support throughout my graduate years, for which I am grateful and will always cherish.

I thank all the wonderful members of the Bergles lab for their friendship and their effort in developing a collegial environment over the years. It has been both an exciting and educational experience to have us shared each other's talents on a daily basis. I would like to especially thank Jennifer Ziskin for her invaluable friendship and trust, and her willingness to share. I also thank Dr. Shih-Chun Lin and Dr. Martin Paukert for their encouragement, advice and help over the years. Thanks to Naoko

Nishiyama, who is always caring and giving. I would also like to thank our collaborators at Hopkins, Dr. Jeffrey Rothstein and his lab members, Margaret Dykes-Hoberg and Dr. Melissa Regan in particular, for their efforts in producing fruitful collaborations indispensable for this work.

I am greatly indebted to my family, whose love and patience have sustained me over the long years. My parents, Zhen Huang and Xianlan Jin, have always been my faithful audience to listen to my progress and frustrations, and they have always been encouraging me to communicate science in common language. My sister Jinghua Huang shares many of my interests and has been a great companion, at the other end of the phone line, to explore together with me life and careers of profession.

Last but not least, I would like to thank my friends at and around Hopkins, who constantly remind me that there is a world beyond 725 N. Wolfe St.; and that science is, after all, a human endeavor. My special thanks go to our Life Fellowship members, without whom I would not have worked as hard as I had hoped and meanwhile enjoyed life as much as I had ever dared to imagine. Among them are Dr. Anding Shen, Lily (Ching-Ling) Lo, Dr. Zhiying He and Ling Wang. Special thanks to my classmates Chih-Ying Su and Gek Ming Sia, who offered me immeasurable help during my first graduate year to finish all my courses smoothly. Special thanks to Marlin Dehoff for his continual encouragement and his kindly effort in explaining the American culture to me in all aspects over the years.

Table of Contents

List of Figures

Chapter I

Introduction

Importance of clearance of extracellular glutamate

The amino acid L-glutamate is the major excitatory neurotransmitter in the mammalian central nervous system (CNS). Proper handling of this neural currency is required for most aspects of brain function including cognition, learning and memory, as well as development of the CNS (for review, see Danbolt, 2001). Glutamate is also a potent neurotoxin, whose accumulation in the extracellular space causes extensive activation of glutamate receptors located on neuronal and glial cell membranes, which can lead to excitotoxic damage to cells. Glutamate is synthesized and stored in high concentrations in glutamatergic neurons (~ 10 mM, see Ottersen et al., 1996), and is released upon specific stimuli (e.g. action potential firing) into extracellular space. It is critical to constrain the movement and lifetime of extracellular glutamate not only to prevent excitotoxicity, but to create a low-noise background for effective and sustained glutamate transmission.

Glutamate transporters represent the main mechanism to remove extracellular glutamate

The identification of mechanisms for clearance of extracellular glutamate was a critical step in the final establishment of glutamate as a neurotransmitter. More than 20 years after the initial discovery of potent glutamate uptake capacity in brain tissues

(Balcar and Johnston, 1972; Johnston, 1981; Logan and Snyder, 1972), five different plasma membrane glutamate transporters were cloned (Saier, 1999; Slotboom et al., 1999). Human isoforms (and their rodent homologs) are named EAAT1 (GLAST), EAAT2 (GLT-1), EAAT3 (EAAC1), EAAT4 (rEAAT4), and EAAT5 (rEAAT5). Splice variants for GLT-1 in rodents (named GLT-1a, -1b, -1c, and -1v) have been further identified (for review, see Grewer and Rauen, 2005). GLT-1 and GLAST are present at very high densities in brain tissue, and all five transporters exhibit high capacities for glutamate transport (see below, or review by Danbolt, 2001). The transport capacity is determined by the following stoichiometry (based on measurements of EAAC1 and GLT-1): each glutamate molecule is taken up together with $3Na^+$ and $1H^+$ in exchange for $1K^+$ (Levy et al., 1998; Zerangue and Kavanaugh, 1996). This coupling predicts a transport capacity that can reach a concentration gradient greater than $1x10^6$, lowering ambient glutamate concentration to a few nanomolar at equilibrium (Zerangue and Kavanaugh, 1996). Disrupting the expression or activity of these transporters results in excessive activation of glutamate receptors, abnormal neuronal activity, and eventual excitotoxic degeneration (Rothstein et al., 1996; Tanaka et al., 1997). Considerable effort is being expended to understand the mechanisms responsible for transporter dysfunction in diseases (Cleveland and Rothstein, 2001), including the contribution of reverse transport – the inappropriate transport of glutamate out of the cell – to glutamate release during acute ischemic episodes (Rossi et al., 2000). In brief, glutamate transporters play a crucial role in preventing the accumulation of extracellular glutamate, which, apart from

passive diffusion, represents the primary mechanism for glutamate clearance in the CNS.

Glutamate transporters are a key component for excitatory synapses

When the glutamate uptake mechanism was initially discovered, it was speculated that the uptake machinery was present at the glutamate-releasing nerve terminals to conveniently recycle glutamate for continuous release. However, subsequent studies using immunohistochemistry and electron microscopy revealed that glutamate transporters are distributed on post- but not pre-synaptic neuronal membranes, and on glial cell membranes surrounding synapses (free review, see Danbolt, 2001). Electrophysiological recordings have also shown that glutamate transporter activity can be detected in postsynaptic neurons and adjacent glial cells 0.1-1 ms following presynaptic release (Bergles et al., 1997; Bergles and Jahr, 1997; Otis et al., 1997), suggesting that functional glutamate transporters are indeed present close to the release sites. These transporters prevent accumulation of glutamate in the synaptic cleft so as to reduce background noise for transmission. Transporters also set up diffusion barriers to prevent glutamate "spillover" to neighboring synapses to ensure transmission fidelity (Arnth-Jensen et al., 2002; Asztely et al., 1997; Diamond, 2001; Tsvetkov et al., 2004). Importantly, because presynaptic nerve terminals are largely devoid of transporters, glutamate is recycled via a detour through glial cells to replenish the releasable pool: glutamate is taken up into glial cells by transporters, converted to glutamine through glutamine synthetase, and recycled back to neurons in

the form of glutamine (the "glutamate-glutamine cycle"), before eventually converted to glutamate through glutaminase (for review, see Danbolt, 2001). Glutamate taken up by neurons can also enter metabolic pathways to synthesize other molecules including the inhibitory neurotransmitter GABA (for review, see Danbolt, 2001); and glutamate uptake by astroglial cells can even stimulate glycolysis and lactate production in astrocytes, providing readily consumable energy sources for adjacent neurons (Voutsinos-Porche et al., 2003). In summary, glutamate transporters extend their homeostatic maintenance operations to excitatory synapses: they remove glutamate to maintain low background noise for transmission; they restrict diffusion of glutamate between synapses to ensure the fidelity of transmission; and they recycle glutamate for sustained release and energy production.

Glutamate transporters can influence receptor occupancy at excitatory synapses

The function of glutamate transporters at excitatory synapses goes beyond the extension of their homeostatic maintenance operations. Accumulating evidence now suggests that glutamate transporters are able to impact transmission by competing with receptors for glutamate binding and thus regulate receptor activation (for review, see Huang and Bergles, 2004). This has been studied using electrophysiological recordings of glutamate receptor-mediated EPSCs, and analyzing the change in EPSC size and duration upon application of transporter inhibitors. These studies have shown that glutamate transporters are able to restrict the size and duration of EPSCs at a number of CNS synapses (Arnth-Jensen et al., 2002; Barbour et al., 1994; Brasnjo and

Otis, 2001; Diamond, 2001; Otis et al., 1996; Tong and Jahr, 1994). The reasons for their ability to regulate receptor occupancy during transmission are as follows. (1) The density of glutamate transporters in brain tissue is very high; it has been estimated in the stratum radiatum of hippocampal CA1 region that the concentration of glial transporters alone (about 8,500 molecules per μm^2 astroglial cell membrane, (Lehre and Danbolt, 1998)) is significant compared to the synaptic release capacity (Danbolt, 2001). Within 1 ms of release, the 4,000 glutamate molecules in a vesicle will encounter ~8,000-12,000 transporters, many more than the 15-50 AMPA receptors that they activate (for review, see Attwell and Gibb, 2005). In addition, studies on the subcellular distribution of glial glutamate transporters have shown that the densities of transporters are higher on the astroglial membranes facing neuropil, nerve terminals, axons and dendritic spines, than those facing other astrocytes, cell bodies, pia mater or the basement membrane of capillary endothelium (Chaudhry et al., 1995), suggesting that glutamate transporters are more heavily involved in synaptic function. (2) The affinity of glutamate transporters is comparable to that of glutamate receptors; the EC_{50} for glutamate transporters is 3 – 97 μM (Arriza et al., 1997; Arriza et al., 1994; Fairman et al., 1995); the EC_{50} values for AMPA and NMDA receptors are 46 μM and 0.6 μM respectively (Attwell and Gibb, 2005), and for mGluRs are 4 – 60 μM (Pin and Duvoisin, 1995). (3) Glutamate transporters bind glutamate rapidly. The rise times of glutamate-evoked transporter currents in outside-out patches of astroglial cell membranes (Bergles and Jahr, 1997; Wadiche et al., 1995) and in whole-cell recordings in response to photolysis (Grewer et al., 2000)

indicate that they bind glutamate as rapidly as ionotropic glutamate receptors (Jonas and Sakmann, 1992). Therefore, although the entire transport cycle takes a longer time to complete (see below), the initial fast binding of transporters may be sufficient to rapidly buffer glutamate and win the race against receptors. (4) All five types of glutamate transporters exhibit a high capacity for transport, as determined by the shared stoichiometry (see above). However, the transport efficiency for many transporters is close to 50% (Bergles et al., 2002; Otis and Kavanaugh, 2000), meaning that glutamate, once bound, is as likely to unbind as it is to be translocated. Therefore, although the initial fast binding of transporters can effectively reduce glutamate concentration from its maximum value, subsequent dissociation of glutamate from transporters can slow down the decay of glutamate transient at low concentrations and prolong activation of receptors (for review, see Grewer and Rauen, 2005). In summary, the high affinity, high density, rapid binding, high capacity and low efficiency of glutamate transporters enable them to regulate the spatial and temporal concentration profile of glutamate in the extracellular space, and therefore regulate receptor occupancy at individual synapses, as well as to regulate the cross-activation of receptors at neighboring synapses (see Figure I-1).

Other factors contribute to the regulation of receptor occupancy by glutamate transporters

In addition to the intrinsic properties of glutamate transporters, the potential impact of transporters on excitatory transmission is further determined by additional parameters

at each individual synapses, including (1) the probability and frequency of release, (2) the structure of synaptic compartment, (3) the kinetic properties of glutamate receptors, (4) and the localization of transporters in relation to synaptic receptor molecules. (1) Glutamate transporters exhibit slow turn-over rates (10 ~75 ms, depending on the particular transporter (Bergles and Jahr, 1997; Bergles and Jahr, 1998; Otis and Jahr, 1998; Wadiche and Kavanaugh, 1998)), which predicts that their availability for glutamate binding decreases as the release frequency increases. Once the release interval is shorter than the turn-over time, glutamate transporters will not have had sufficient time to complete the transport cycle before the next round of release occurs. Therefore glutamate transporters can, if the density is relatively low in vicinity of receptors, serve as a high-pass filter for receptor activation, particularly for extrasynaptic receptors whose activation requires diffusion of glutamate out of the synaptic cleft. This may in part explain why activation of mGluRs and extrasynaptic NMDA receptors typically requires high frequency stimulation (Clark and Cull-Candy, 2002; Tempia et al., 1998). Similarly, in cerebellar Purkinje neurons where high-frequency stimulation of parallel fibers leads to activation of extrasynaptic mGluRs, inhibition of glutamate transporters reduces the number of stimuli necessary for mGluR activation at a given frequency (Reichelt and Knopfel, 2002). (2) CNS synapses are ensheathed by glial cell processes to different extents, which is predicted to lead to differences in local concentration and accessibility of transporters to glutamate. One dramatic example is demonstrated in the hypothalamus. During lactation dramatic structural rearrangements occur when astrocytes retract their

processes from excitatory synapses (Theodosis and Poulain, 1993). Following these morphological changes, activation of presynaptic mGluRs is enhanced because of a lack of proximal glutamate transporters (Oliet et al., 2001). A similar phenomenon has been observed in the cerebellum. Viral mediated expression of GluR2 selectively in Bergmann glia, an astrocyte-like cell, renders their AMPA receptors impermeable to calcium and causes these cells to retract their processes (Iino et al., 2001). An analysis of parallel fiber and climbing fiber mediated excitatory postsynaptic currents (EPSCs) in Purkinje neurons under these conditions of reduced ensheathment revealed that glutamate clearance from synapses was dramatically impaired (Iino et al., 2001). (3-4) For receptors located directly opposite release sites, such as the ionotropic glutamate receptors, their initial occupancy by glutamate is rarely altered by perisynaptically localized transporters (but see Diamond and Jahr, 1997; Tong and Jahr, 1994). However, blocking transporters may prolong the glutamate transient in the synaptic cleft, which either prolongs activation (Barbour et al., 1994; Kinney et al., 1997; Otis et al., 1996; Takahashi et al., 1995; Takahashi et al., 1996), or facilitates desensitization (Otis et al., 1996; Renden et al., 2005) of the postsynaptic receptors, depending on the local concentration of glutamate achieved and the kinetic properties of receptors. In contrast, mGluRs are typically located on peri- or extra-synaptic membranes; activation of these receptors therefore requires diffusion of glutamate away from the synaptic cleft. At cerebellar parallel fiber-Purkinje neuron synapses, inhibition of glutamate transporters facilitates diffusion and potentiates mGluR activation (Reichelt and Knopfel, 2002). Recent studies by Wadiche and Jahr

(Wadiche and Jahr, 2005) also revealed an inverse correlation at this synapse between the density of EAAT4 transporters and synaptic activation of mGluRs. In contrast, AMPA receptor-mediated transmission at the same synapse was not affected by changes in EAAT4 transporter density. These studies suggest that the impact of glutamate transport on synaptic transmission may be generalized only with caution, considering the diversity of synaptic structures and the expression profiles of transporters and receptors.

Understanding the differential contributions of transporters to synaptic clearance

To fully understand the function of glutamate transporters in excitatory transmission, it is necessary to recognize the individual contributions of different types of glutamate transporters. Compared to other neurotransmitters, the clearance pathway for glutamate is much more elaborate, as there are more than five types of transporters for glutamate, but only two types for GABA (GAT-1,2), and one for each of the monoamines, norepinephrine (NET), dopamine (DAT), and serotonin (SERT). Finer control over extracellular glutamate dynamics may be achieved by spreading the task of glutamate uptake among different transporters, as they are expressed by distinct populations of cells (for review, see Danbolt, 2001). GLAST and GLT-1 are primarily expressed in astroglial cells throughout the CNS, and their expression varies between different brain regions and during development. GLT-1 is the quantitatively dominating glutamate transporter in the mature forebrain, particularly in the

hippocampus, cerebral cortex, and striatum, whereas GLAST has the highest level of expression in the cerebellum, inner ear, and retina. GLT-1 has also been suggested to exist in certain neurons at the presynaptic terminals (Chen et al., 2004), but these immuno-electronmicroscopy (immuno-EM) results are not yet confirmed by functional studies. In contrast to GLAST and GLT-1, EAAC1 and EAAT4 are expressed by neurons. EAAT4 is highly expressed in cerebellar Purkinje cells, and is almost undetectable in other regions, where EAAC1 becomes the predominant neuronal glutamate transporter. EAAT5 expression is restricted to the retina. When considering neuronal and glial transporter function at excitatory synapses, there are advantages and disadvantages for both groups of transporters. The average density of astroglial transporters is greater than that of neuronal transporters (for review, see Danbolt, 2001). Inaddition, astrocytes possess many features that create an environment optimized for efficient uptake, including a high resting potential that facilitates voltage-dependent glutamate transport, a high resting conductance that prevents fluctuation of the membrane potential, and a low intracellular concentration of glutamate. By contrast, transporters operating in neuronal membranes must fight against a higher electrochemical gradient, and a more depolarized and constantly fluctuating membrane potential. Nonetheless, neuronal transporters may be positioned closer to the synaptic cleft than glial transporters; distribution of the latter is determined by the extent of ensheathment of synaptic structure by glial cell processes.

Development of tools to investigate the differential function of glutamate

transporters

Investigation of the individual contributions from different types of glutamate receptors has proven to be challenging, partly because pharmacology is lagging far behind the molecular identification of transporters and selective antagonists for each type of them have yet to be developed. Only one specific transporter antagonist, dihydrokainate (DHK), has been well characterized so far, which has a ~100x higher affinity for GLT-1 over other transporters. Several other selective transporter antagonists, WAY213613 and WAY-855 have recently been developed during the course of this study, and they exhibit > 40x higher affinity for GLT-1 over other transporters (personal communication; and Dunlop et al., 2003).

Although selective transporter antagonists are largely unavailable, efforts have been made to take advantage of the fact that glutamate transporters are segregated into neuronal and glial cell compartments. To determine their specific functions, selective manipulation of single cells or single cell populations has been an alternative way to alter the operation or synaptic localizations of neuronal and glial transporters, and to study their differential impact on transmission. In two of the above-mentioned examples, when glial cell processes are dissociated from excitatory synapses either in the hypothalamus during lactation or in the cerebellum following viral infection of Bergmann glia with GluR2, there are changes in receptor activation during transmission. These observations point to the essential role of glial cell processes in delivering transporters to sites of release, and highlight the importance of glial transporters at excitatory synapses. To investigate the function of neuronal

transporters, several studies took advantage of the dependence of transport on voltage and intracellular K^+ to selectively inhibit uptake in the postsynaptic neurons. Complete replacement of K^+ with $Tris^+$, a cation that does not support glutamate transporter cycling, increases the parallel fiber-evoked mGluR EPSCs in Purkinje neurons (Brasnjo and Otis, 2001). In the hippocampus, activation of extrasynaptic NMDA receptors is potentiated when postsynaptic glutamate transporters are inhibited either by high positive membrane potential or by depletion of intracellular K^+. These studies suggest that postsynaptic transporters (e.g. EAAC1 and EAAT4) also may shield receptors during transmission. Furthermore, recent studies by Wadiche and Jahr (2005) also reveal an inverse correlation among different cerebellar lobules between the density of EAAT4 transporters and the size of mGluR-mediated synaptic currents in Purkinje neurons, although it is not yet conclusive if EAAT4 expression alone is sufficient to explain the observed differences in synaptic mGluR activation, considering that the comparison is made between two cerebellar cortical lobules, and that the EAAT4 expression level is only one of many potential variables.

Other than pharmacology and single cell manipulations there have been alternative approaches to address the individual contribution of glutamate transporters to the clearance of glutamate. These approaches include chronic administration of antisense oligonucleotide to inhibit the synthesis of the targeted glutamate transporter (Rothstein et al., 1996), and generation of selective transporter knockout animals. To further differentiate the contributions from different types of glutamate transporters, gene-specific knockout mice have been generated (Peghini et al., 1997; Tanaka et al.,

1997; Watase et al., 1998). EAAC1 knockout mice show no CNS phenotype (Peghini et al., 1997); GLT-1 knockout mice have increased susceptibility to acute forebrain injury, and they cannot survive till adulthood due to lethal spontaneous epileptic seizures (Tanaka et al., 1997); GLAST knockout mice are mildly discoordinated, more susceptible to cerebellar injury (Watase et al., 1998), and develop exacerbated noise-induced hearing loss (Hakuba et al., 2000). In addition, detailed examination of synaptic physiology in glial transporter knockout mice revealed that in GLT-1 deficient mice, there is increased basal activity of NMDA receptors in the hippocampal CA1 region, which impairs NMDA receptor-dependent long-term potentiation at Schaffer collateral synapses (Katagiri et al., 2001); and in the cerebellum of GLAST deficient mice, Purkinje neurons remain to be innervated by multiple climbing fibers even in adulthood (Watase et al., 1998). These results indicate that glutamate transporters play distinct roles in clearing glutamate from the extracellular space, and that different phenotypes of glial transporter knockout mice may reflect the regional differences of GLT-1 and GLAST expression. Nonetheless, it remains to be determined the individual contribution of transporters to clearance at a given synapse.

Methods to monitor glutamate transporter activity

Glutamate transport is associated with movements of a variety of substances across the membrane, which provides the means to monitor transporter activity. Glutamate uptake leads to accumulation of substrates (e.g. glutamate and H^+) on one side of the

membrane, which can be monitored by measuring radiolabeled substrates accumulation or optical measurements of cytosolic pH changes. Glutamate uptake also leads to net charge movement because two positive charges are carried into the cell during each cycle of transport (Levy et al., 1998; Zerangue and Kavanaugh, 1996), and binding of glutamate to the transporter increases its conductance to certain anions (Wadiche et al., 1995). The resulting change in voltage across the plasma membrane can be monitored by voltage-sensitive dyes, or by electrical recordings of transporter-associated currents (for review, see Danbolt, 2001). Transporter-associated currents are proportional to the movement of glutamate (Otis and Jahr, 1998; Zerangue and Kavanaugh, 1996), providing a quantitative measure for glutamate transporter activity in individual cells that can be resolved with high temporal fidelity.

Main objectives of this thesis

As summarized above, glutamate transporters prevent the accumulation of extracellular glutamate that would otherwise lead to tonic activation of receptors, disrupted signaling, and excitotoxic damage. At excitatory synapses, glutamate transporters regulate the spatial and temporal concentration profile of glutamate transients and therefore can potentially impact transmission by regulating receptor occupancy. This work combines electrophysiological recordings with usage of genetically modified mice defective in selective glutamate transporters to address the following questions: (1) What are the relative contributions of neuronal and glial glutamate transporters to glutamate uptake at excitatory synapses and (2) how do

different types of glutamate transporters influence transmission at excitatory synapses? In **Chapter II**, we investigated the relative contributions of neuronal transporters EAAC1 and EAAT4, as well as glial transporters (GLAST and GLT-1), to the clearance of synaptic glutamate at the cerebellar climbing fiber-Purkinje neuron synapse; this synapse is the only location in CNS where quantitative analysis for neuronal glutamate transporter activity during transmission is possible. We found that EAAT4 but not EAAC1 contributes to the synaptic uptake of glutamate by Purkinje neurons. Postsynaptic EAAT4 transporters remove ~10% of total released glutamate at this synapse, and the rest is presumably taken up by glial transporters. We also identified a novel conductance mediated by GluR5-containing kainate receptors at this synapse, whose presence led to an overestimation of the Purkinje neuron contribution to synaptic uptake in previous studies. For other CNS synapses where direct measurements of total neuronal or glial uptake are not possible, we used an extrasynaptically localized glutamate receptor to estimate the relative contributions of neuronal and glial transporters to clearance (**Chapter III**). We found that at an excitatory synapse in the hippocampus, the glial transporters GLT-1 and GLAST, but not the neuronal transporter EAAC1, have a significant impact on the occupancy of extrasynaptic mGluRs during transmission. Thus, at these two groups of excitatory synapses glial transporters dominate the clearance of glutamate following release, raising the question of whether transporters on neuronal membranes are important to regulate transmission. In **Chapter IV**, we describe the synthesis and characterization of a caged transporter substrate, 4-methoxy-7-nitroindolinyl-D-aspartate, for rapid and

selective activation of glutamate transporters in their native membranes. Using photolysis approach, we describe the observation (**Chapter V**) that GLT-1, the predominant astroglial glutamate transporter, is also expressed by a selective population of neurons, the hippocampal CA3 pyramidal neurons. The potential function of GLT-1 in these neurons is discussed.

Figure I-1. The location of glutamate transporters and receptors at a typical excitatory synapse. Unlike receptors, glutamate transporters are excluded from the synaptic cleft. EAAT1 (GLAST) and EAAT2 (GLT-1) are present at high densities in the membranes of astrocytes that often ensheath synapses. EAAT3 (EAAC1) is found in the soma and dendrites of neurons, but is also found in GABAergic terminals (not shown). Glutamate transporters shield extrasynaptic NMDA receptors and mGluRs from glutamate as it diffuses from the cleft, and prevent glutamate from reaching receptors at nearby synapses. Inhibition of these transporters potentiates excitatory responses mediated by these receptors, and allows glutamate spillover, which suggests that transporter regulation might be used to regulate synaptic efficacy. Note that presynaptic mGluRs have been omitted from this diagram.

Figure I- 1

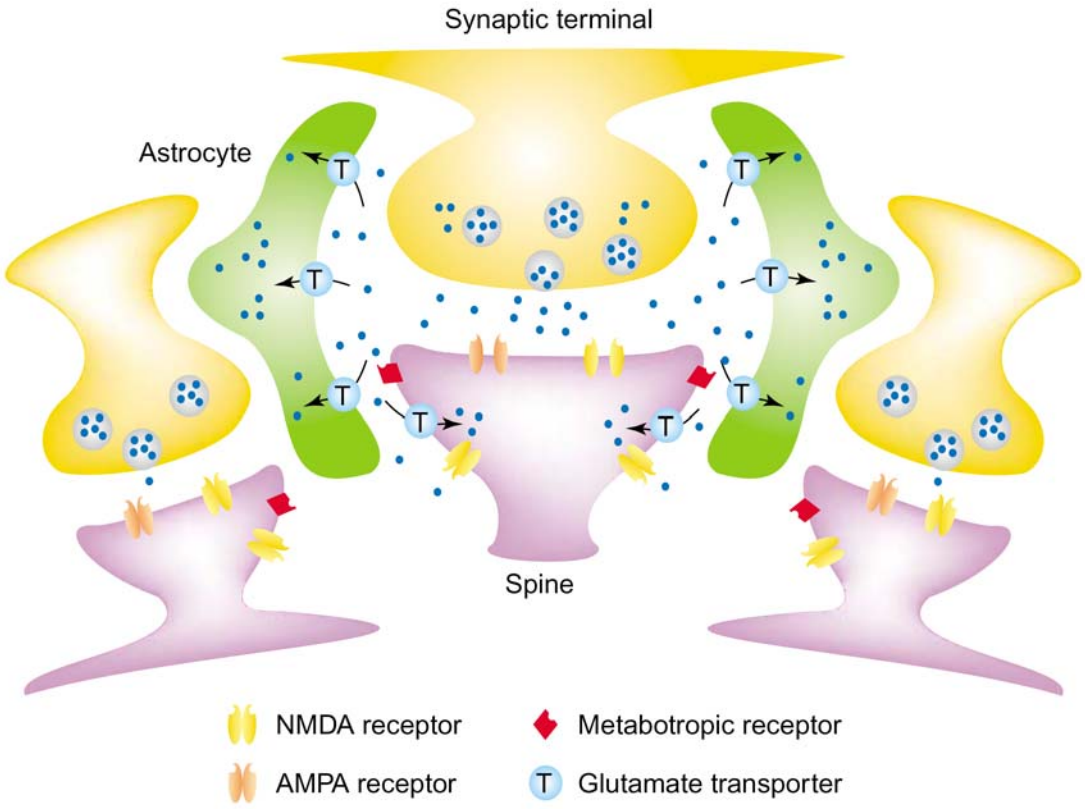
Synaptic terminal
Astrocyte
T
Spine
NMDA receptor
AMPA receptor
Metabotropic receptor
Glutamate transporter

Chapter II

Climbing Fiber Activation of EAAT4 Transporters and Kainate Receptors in Cerebellar Purkinje Cells

Introduction

Our knowledge about neuronal glutamate uptake is based largely on studies of climbing fiber-Purkinje cell (CF-PC) synapses in the cerebellum, the only CNS synapses where both anion and stoichiometric (coupled) currents associated with glutamate transport have been resolved in the postsynaptic neuron. In addition to EAAC1, PCs express EAAT4, a transporter that exhibits a 10-fold higher affinity for glutamate than other glutamate transporters (Fairman et al., 1995). Measurements of the charge transferred during CF synaptic transporter currents have been used to estimate the amount of glutamate taken up by PCs (Auger and Attwell, 2000; Otis et al., 1997). An initial study concluded that at least 22% of the glutamate released at CF synapses was removed by PCs, more if EAAC1 also contributes to uptake currents (Otis et al., 1997). Although this estimate was based on measurements of transporter-associated anion currents, a recent study described a CF-induced synaptic current that was attributed to the movement of charge directly coupled to glutamate transport (Auger and Attwell, 2000); this study concluded that PCs remove the majority of glutamate (56 − 230 %) released at CF synapses. However, this putative transporter current was only partially inhibited by TBOA (Auger and Attwell, 2000), an antagonist that blocks all glutamate transporters (Shigeri et al., 2001; Shimamoto

et al., 1998), raising questions about the accuracy of these estimates.

To determine both the contribution of EAAC1 and EAAT4 to uptake of synaptic glutamate, and the reason for the partial sensitivity of the putative synaptic transporter current to TBOA, we recorded CF responses in cerebellar slices prepared from mice deficient in neuronal transporters. We find that EAAT4 is responsible for the glutamate transporter currents recorded at CF-PC synapses. In addition, our results indicate that previous studies have overestimated the amount of glutamate captured by PCs, because non-AMPA glutamate receptors account for more than 40% of the putative coupled transporter current recorded from PCs. These non-AMPA receptors at CF synapses exhibited pharmacological and kinetic features characteristic of GluR5-containing kainate receptors and were responsible for about 5% of the CF EPSC.

Materials and Methods

Generation of mice deficient in neuronal transporters. *EAAC1*$^{-/-}$ and *GluR5*$^{-/-}$ mice were generated as described (Contractor et al., 2000; Peghini et al., 1997). For targeted disruption of the EAAT4 gene, the exon 7 including the sixth transmembrane segment was replaced by a neomycin-resistance gene. The linearized targeting vector was electroporated into E14 ES cells and one ES cell line with a single targeted allele was used for the generation of *EAAT4*$^{-/-}$ mice (H. Maeno, K. Watase, K. Wada, and K. Tanaka, unpublished observations). To generate *EAAC1*$^{-/-}$ x *EAAT4*$^{-/-}$ mice as well as other genotypes with comparable backgrounds, hybrids of the two lines (genotype:

EAAC1$^{+/-}$ x *EAAT4*$^{+/-}$) were used to generate two sets of mice. The first set had one mutant allele (*EAAC1*$^{-/-}$ or *EAAT4*$^{-/-}$) and one heterozygous allele (*EAAC1*$^{+/-}$ or *EAAT4*$^{+/-}$), which were then used to generate double mutants (*EAAC1*$^{-/-}$ x *EAAT4*$^{-/-}$) or single mutants (*EAAC1*$^{-/-}$ or *EAAT* $^{-/-}$). The second set had one wild-type allele (*EAAC1*$^{+/+}$ or *EAAT4*$^{+/+}$) and one heterozygous allele (*EAAC1*$^{+/-}$ or *EAAT4*$^{+/-}$), which were then used to generate wild-type mice (*EAAC1*$^{+/+}$ x *EAAT4*$^{+/+}$) as well as single mutant mice. All comparisons between different genotypes (Figures I-1, 2, & 3) were performed using mice generated in this manner. Additional double mutants were obtained from the subsequent mating of double mutants (Figures I-4 & 5). The genotype of all experimental animals was confirmed by PCR.

Immunoblotting and immunostaining. Mice were euthanized using approved animal welfare protocols and perfused by cardiac puncture with 4% paraformaldehyde/Phosphate buffered saline (PBS). Brains were removed and tissue blocks were cryopreserved for sectioning. For immunoblotting, tissue was rapidly frozen on dry ice, and stored at −70° C until assayed. Samples from P18-21 cerebellum were homogenized with a Brinkmann Polytron or by sonication in 20 mM Tris-HCl (pH 7.4) containing 10% sucrose, and protease inhibitor cocktail (Roche Diagnostics). These cerebellar extracts were subjected to 7.5% sodium dodecyl sulfate polyacrylamide gel electrophoresis (SDS-PAGE) and transferred to nitrocellulose membrane (Hybond ECL) by electroblotting (30 V, 60 min). Western analysis was performed as described (Rothstein et al., 1994). Bots were probed with affinity purified polyclonal antibody specific for EAAC1 (carboxy terminus-directed antibody

at 0.6 μg/ml), EAAT4 (carboxyterminus-directed antibody at 0.4 μg/ml) or actin (1:500; Sigma Chemical) using horseradish peroxidase-conjugated donkey anti-rabbit Ig (Amersham) (diluted 1:5000 in blocking solution) as secondary antibody. Immunoreactive proteins were visualized by enhanced chemilumine- scence (ECL). Immunoblots were run at least two times.

For immunohistochemistry, sections (50 μm) of cryopreserved mouse brain (P19-20) were cut on a sliding microtome then transferred to cold TBS (0.05 M Tris, 0.15M NaCl, pH 7.4). Sections were pre-treated with 3% hydrogen peroxide/ 0.1% Triton X-100 in TBS, rinsed and blocked (1 hour, 4° C) in TBS containing 5% normal goat serum, and 0.1% Triton X-100. Sections were incubated (48 − 72 hours, 4° C) in one of the affinity-purified anti-peptide antibodies (EAAC1 - 0.06, EAAT4 - 0.4 ug/ml) or anti-calbindin (1:2000, Sigma) antibody in TBS containing 2% normal goat serum, 0.1% Triton X-100. The monospecificity of the affinity purified antibodies had been previously confirmed using pre-adsorption overnight with excess (5 μM) corresponding synthetic oligopeptide, or 2) primary antisera omitted. Following the primary antibody incubation, sections were incubated (1 hr, 4° C) with biotinylated secondary antibody (Vector Labs) to rabbit IgG diluted 1:400 (for all glutamate transporter antibodies) in TBS containing 2% normal goat serum, then rinsed and incubated (1 hour, 4° C) in ABC reagent 1:200 in TBS (Elite kit, Vector Labs), followed by 0.05% diaminobenzidine/0.01% hydrogen peroxide in TBS. Tissue staining was performed on 2 animals from each group (wild-type, *EAAC1*$^{-/-}$, *EAAT4*$^{-/-}$, and *EAAC1*$^{-/-}$ x *EAAT4*$^{-/-}$).

Slice preparation. Parasagittal cerebellar slices were prepared from 15 to 19 day-old mice and 13 to 15 day-old rats @ 250 μm on a vibratome (Leica, VT1000S) in ice-cold artificial cerebrospinal fluid (ACSF) containing (in mM): NaCl (119), KCl (2.5), $CaCl_2$ (2.5), $MgCl_2$ (1.3), NaH_2PO_4 (1), $NaHCO_3$ (26.2), and glucose (11) saturated with 95% O_2/5% CO_2. Slices were incubated in ACSF at 37° C for 30 min, and then allowed to recover for at least 30 min at room temperature before experimentation.

Electrophysiological recordings. PCs were visualized through a 40x water immersion objective using infrared light, DIC optics, and a CCD camera (Sony XC-73). Whole-cell recordings were made under visual control with an internal solution consisting of (in mM): CsA (105), where A represents NO_3^- or $CH_3O_3S^-$ (MeS), TEA-Cl (20), EGTA (10), HEPES (20), Mg-ATP (2), Na-GTP (0.2), QX-314 (1), pH 7.3. CFs were stimulated with a theta glass pipette filled with ACSF. A constant-current isolated stimulator (Digitimer DS3) was used to supply a 100 μs pulse of 2-30 μA. Pipette position was adjusted to minimize the stimulus intensity required to generate an all-or-none CF-evoked response. Subthreshold stimulation did not induce EPSCs, indicating that there was no contamination by parallel fiber synapses. Synaptic currents were recorded with a MultiClamp 700A amplifier (Axon instruments), filtered at 2 − 3 kHz, amplified 20x (Brownlee 440), and then digitized at 10 kHz with a Digidata 1322A analog-to-digital converter (Axon instruments). Data were analyzed off-line using pClamp (Axon Instruments) and Origin (Microcal) software. All recordings were made at room temperature.

Data analysis. By optimizing the position of the stimulation pipette, it was possible to obtain CF EPSCs and rEPSCs that were well separated from the stimulus artifact. Although subtraction of the artifact was not performed, in most traces the artifact has been blanked for clarity. The rise time of synaptic currents was measured from 10 – 90% of peak amplitude. The decay kinetics of CF rEPSCs and EPSCs recorded in GYKI 53655 were calculated by fitting a single exponential ($y = y_0+A_1e^{-(x-x_0)/t_1}$) to the decay from ~ 10% below the peak. The decay of CF EPSCs under control conditions could not be fitted with a single exponential, therefore the half-decay time was measured to provide an indication of the decay time course. Reversal potentials for CF EPSCs and rEPSCs were measured by performing a linear regression fit of the I-V data from each individual experiment. The estimated reversal potentials have not been corrected for the junction potential. All results are presented as mean ± S.E.M.

Results

CF synaptic transporter currents from wild-type mice

To determine the relative contribution of EAAC1 and EAAT4 to the PC glutamate transporter current, we compared CF synaptic currents recorded from wild-type mice to those recorded from mice lacking EAAC1 (Peghini et al., 1997), EAAT4, or both EAAC1 and EAAT4 transporters. We confirmed that transporter expression was disrupted in *EAAC1*$^{-/-}$, *EAAT4*$^{-/-}$, and *EAAC1*$^{-/-}$ x *EAAT4*$^{-/-}$ mice by PCR (data not shown), western blot (Figure II-1*A*), and immunocytochemistry (Figure II-1*B*).

Despite the absence of neuronal glutamate transporters, these animals survived into adulthood (Peghini et al., 1997), did not exhibit obvious motor discoordination, and had grossly normal cerebellar architecture (Figure II-1*B*). In slices prepared from wild-type mice, CF stimulation elicited large amplitude all-or-none synaptic currents in PCs similar to those observed in rats (Perkel et al., 1990) (Figure II-2*A*). This CF EPSC was reduced to < 1% of its original amplitude upon application of antagonists of AMPA receptors (NBQX, 25 μM; GYKI 52466, 25 μM), NMDA receptors (RS-CPP, 10 μM) and $GABA_A$ receptors (SR-95531, 5 μM; bicuculline, 20 μM). The residual synaptic current (rEPSC) recorded in the presence of these antagonists was –23.0 ± 1.5 pA (n = 9) (Vm = –65 mV) when recordings were made with an internal solution that contained MeS as the primary internal anion, which does not permeate the glutamate transporter anion channel (Bergles et al., 2002), and exhibited the same threshold and all-or-none behavior as the CF EPSC (Figure II-2*B*). This current had rapid rise and decay kinetics (rise time: 2.3 ± 0.2 ms; decay tau: 9.1 ± 1.2 ms, n = 9) (Figure II-2*B*), similar to currents recorded from rat (Auger and Attwell, 2000), and was inhibited by 38.2 ± 2.9 % (n = 4) by DL-*threo*-*β*-benzyloxyaspartic acid (TBOA, 200 μM), a non-selective antagonist of glutamate transporters (Shigeri et al., 2001; Shimamoto et al., 1998). These results indicate that a stoichiometric or coupled transport current, reflecting the movement of charge directly associated with glutamate uptake, mediates a portion of the CF rEPSC. When recordings were made with NO_3^- as the primary internal anion, which is highly permeant through glutamate transporters (Wadiche et al., 1995), this residual current was larger (amplitude: –76.4

± 15.9 pA; $p < 0.05$) and decayed more slowly (rise time: 2.8 ± 0.4 ms, $p = 0.27$; decay tau: 37.2 ± 2.3 ms, n = 4; $p < 0.001$) (Figure II-2*C*), and was inhibited to a greater extent by TBOA (inhibition: 73.2 ± 2.8 %, n = 4; $p < 0.001$) (Figure II-2*C*), effects similar to that observed for transporter currents in outside-out patches (Auger and Attwell, 2000; Bergles et al., 2002). These data indicate that both stoichiometric (coupled) and anion (uncoupled) currents associated with glutamate transport can be recorded in PCs from wild-type mice in response to CF stimulation. We used these two features of glutamate transporters, the potentiation by permeant anions and the inhibition by TBOA, to address whether glutamate transporter currents were disrupted in mice lacking EAAC1 and/or EAAT4.

EAAT4 is responsible for the CF glutamate transporter current.

As shown in Figure II-3*A*, both the amplitude and decay time of CF rEPSCs from *EAAC1*$^{-/-}$ mice were increased when NO_3^- rather than MeS was used as the primary internal anion, similar to responses from wild-type mice (see Figure II-2). In contrast, there was no significant difference in the amplitude or decay time of CF rEPSCs from *EAAT4*$^{-/-}$ or *EAAC1*$^{-/-}$ x *EAAT4*$^{-/-}$ mice when NO_3^- rather than MeS was used as the primary internal anion (Figure II-3*A*, *B*). Furthermore, the amount of inhibition of CF rEPSCs by TBOA was reduced in *EAAT4*$^{-/-}$ mice, and there was no significant difference in TBOA inhibition between *EAAT4*$^{-/-}$ and *EAAC1*$^{-/-}$ x *EAAT4*$^{-/-}$ mice (Figure II-3*A*,*C*). These data indicate that EAAT4 is responsible for the anion-potentiated CF glutamate transporter current. However, because EAAT4

exhibits a much higher anion permeability than EAAC1 (Fairman et al., 1995; Wadiche et al., 1995), it is possible that EAAT4 could be the predominant transporter when NO_3^- is the main internal anion, but a minor component when permeant anions are not present. If EAAC1 contributes to the coupled transporter current (recorded with MeS), there should be a difference in the amount of inhibition by TBOA between *EAAT4*$^{-/-}$ and *EAAC1*$^{-/-}$ x *EAAT4*$^{-/-}$ mice. However, there was no significant difference in TBOA inhibition of CF rEPSCs between these animals (Figure II-3*C*). Furthermore, under these conditions, CF rEPSCs from *EAAT4*$^{-/-}$ mice were inhibited significantly less than CF rEPSCs from wild-type mice ($P < 0.05$). These data indicate that both stoichiometric and anion transporter currents recorded at CF synapses are mediated by EAAT4, rather than EAAC1.

The presence of a small TBOA-sensitive current in mice lacking both EAAC1 and EAAT4 suggested that TBOA may have secondary effects, or that PCs may express an additional glutamate transporter. Previous studies have shown that blocking glutamate transporters with TBOA causes glutamate to accumulate in the extracellular space (Arnth-Jensen et al., 2002; Jabaudon et al., 1999), which could inhibit release by activating presynaptic metabotropic glutamate receptors on CF terminals (Harrison and Jahr, 2003; Tamaru et al., 2001). Consistent with this possibility, TBOA increased the paired-pulse ratio (PPR) of CF rEPSCs by 37.9 ± 8.3 % ($n = 5$, $p < 0.01$) in *EAAC1*$^{-/-}$ x *EAAT4*$^{-/-}$ mice (Figure II-4*A*), suggesting that TBOA decreased the release probability of CF terminals. Furthermore, both the decrease in amplitude and the increase in PPR ratio were blocked when TBOA was applied in the

presence of the group I/II metabotropic glutamate receptor antagonist (*RS*)-*a*-methyl-4-carboxyphenylglycine (MCPG, 1 mM) (amplitude decreased by 0.6 ± 4.0 %, n = 7, $p = 0.62$; PPR increased by 1.5 ± 3.7 %, n = 5, $p = 0.44$) (Figure II-4*B*). These results indicate that the TBOA-induced decrease in amplitude of the CF response in *EAAC1*$^{-/-}$ x *EAAT4*$^{-/-}$ mice was due to a reduction in glutamate release from CF terminals, rather than an inhibition of latent glutamate transporters in PCs; in the absence of neuronal transporters, TBOA application presumably increases extracellular glutamate by inhibiting glutamate uptake into surrounding Bergmann glial cells (Bergles et al., 1997; Rothstein et al., 1994). We estimated the proportion of the CF rEPSC mediated by glutamate transporters by measuring the amplitude of the TBOA-sensitive current in the presence of MCPG. In recordings with MeS as the primary internal anion, EAAT4 transporters were responsible for 57.2 ± 3.9 % (n = 4) of the CF rEPSC in rats, and 36.4 ± 5.5 % (n = 4) of the CF rEPSC in wild-type mice (Figure II-4*C*).

Non-AMPA glutamate receptors at CF synapses

As shown above (see Figure II-2), and previously (Auger and Attwell, 2000), the CF rEPSC recorded from wild-type animals in the presence of 25 μM NBQX was only partially inhibited by TBOA (200 μM). Because TBOA blocks all high affinity, Na^+ dependent glutamate transporters with a K_m of 3 – 50 μM (K_i at EAAT4 = 4.4 μM) (Shigeri et al., 2001; Shimamoto et al., 2000), these data suggest that a significant portion of the CF rEPSC is not mediated by glutamate transporters. Consistent with

this hypothesis, a CF synaptic current remained in *EAAC1*$^{-/-}$ x *EAAT4*$^{-/-}$ mice in the presence of 25 μM NBQX and 25 μM GYKI 52466 (see Figure II-3*A*). To determine the properties of the receptors responsible for this current, we examined CF rEPSCs in *EAAC1*$^{-/-}$ x *EAAT4*$^{-/-}$ mice, avoiding contamination of this current by glutamate transporters. The reversal potential of the rEPSC was 8.6 ± 2.4 mV (n = 6) (Figure II-5*A*, *B*), similar to that of the CF EPSC (reversal potential = 8.2 ± 1.0 mV, n = 5; p = 0.46), suggesting that this current also is mediated by a non-selective cation channel. Although it is unlikely that the CF rEPSC is mediated by unblocked AMPA receptors given the slow dissociation rate of NBQX (Diamond and Jahr, 1997), and the non-competitive nature of antagonism by GYKI 52466, we tested this possibility by examining whether the rEPSC was sensitive to cyclothiazide, a compound that blocks AMPA receptor desensitization. As shown in Figure II-5*C*, cyclothiazide (CTZ, 200 μM) had no effect on the amplitude or decay time of the CF rEPSC, although it caused a dramatic slowing of the CF EPSC (Figure II-5*D*). The CF rEPSC was insensitive to NMDA receptor antagonists (RS-CPP, 10 μM; MK-801, 50 μM; and 7-Cl-kynurenate, 20 μM; recordings made in 0 Mg^{2+} ACSF) (5.9 ± 1.1 % inhibition, n = 3), consistent with the conclusion that PCs do not express functional NMDA receptors at this age (Hausser and Roth, 1997). The insensitivity to NMDA receptor antagonists also indicates that the CF rEPSC is not mediated by an aspartate receptor (Yuzaki et al., 1996). However, the CF rEPSC was largely blocked by 100 μM NBQX (83.0 ± 2.7 % inhibition, n = 4) (Figure II-5*E*, *F*), suggesting that this current is mediated by a glutamate receptor, rather than a receptor for another neurotransmitter.

This conclusion is supported by the observation that TBOA slowed the decay of the CF rEPSCs in *EAAC1*$^{-/-}$ x *EAAT4*$^{-/-}$ mice (decay tau: control, 8.1 ± 0.8 ms; TBOA, 11.1 ± 1.6 ms, n = 7, $p < 0.05$) (see Figure II-4*B*), which suggests that the ligand for these receptors is a substrate for glutamate transporters.

The sensitivity of the CF rEPSC to a higher concentration of NBQX suggested that the receptors underlying this current might have been partially blocked in 25 μM NBQX. To determine the actual size of this glutamate receptor current we measured the amplitude of the CF EPSC in GYKI 53655 (100 μM), a selective, non-competitive AMPA receptor antagonist (Paternain et al., 1995). As shown in Figure II-6*A*, GYKI 53655 inhibited the CF EPSC by 94.5 ± 0.1 % (n = 2) in cerebellar slices from wild-type mice, and by 94.8 ± 0.8 % (n = 4) in cerebellar slices from rats. The CF EPSC recorded in the presence of 100 μM GYKI was not contaminated by unblocked AMPA receptors, as CTZ did not affect the amplitude or time course of these residual responses (Figure II-6*B*). Although this non-AMPA EPSC was only a small fraction of the total CF EPSC, at –65 mV this current was –281.2 ± 18.5 pA (n = 3) in wild-type mice and ‾409.4 ± 63.6 pA (n = 7) in rats.

Low occupancy of non-AMPA receptors at CF synapses

CF EPSCs exhibit paired-pulse depression when two stimuli are applied at short intervals, due to the high release probability of CF terminals (Silver et al., 1998; Wadiche and Jahr, 2001). A striking difference in PPR was observed between CF EPSCs recorded under control conditions, and responses recorded in 25 μM NBQX or

100 μM GYKI 53655. As shown in Figure II-7*A*, the PPR of the CF EPSC was 0.73 ± 0.01 (n = 6), while it was 0.33 ± 0.03 (n = 6, $p < 0.001$) for the non-AMPA CF EPSC recorded in 100 μM GYKI 53655. As expected, the PPR of the non-AMPA EPSC was not significantly different from the PPR of the CF rEPSC recorded from *EAAC1*$^{-/-}$ x *EAAT4*$^{-/-}$ mice (0.34 ± 0.02, n = 6, $p = 0.325$) (Figure II-7*A*). These differences in PPR cannot be explained by voltage clamp errors arising from the differences in the size of the AMPA and non-AMPA currents, because the PPR of the CF EPSC was unchanged when the amplitude of the CF EPSC was reduced by 48.1 ± 1.0 % by holding cells slightly more positive (PPR @ –10 mV = 0.77 ± 0.01; PPR @ –2 mV = 0.77 ± 0.01, n = 3, $p = 0.777$). Recent results indicate that individual CF synapses may release multiple vesicles in response to a single stimulus, causing saturation of AMPA receptors (Wadiche and Jahr, 2001). This saturation of PC AMPA receptors leads to an underestimate of CF depression in paired-pulse protocols, because AMPA receptors are not able to provide an accurate measure of the first glutamate transient (Harrison and Jahr, 2003). Therefore, the greater depression of the non-AMPA EPSC suggested that these receptors might have a lower occupancy than AMPA receptors following release at CF synapses. To test this possibility, we examined the sensitivity of CF AMPA and CF non-AMPA responses (recorded in 100 μM GYKI 53655) to a reduction in release probability. As shown in Figure II-7B, partial block of presynaptic voltage-dependent Ca^{2+} channels with 5 μM Cd^{2+} ($CdCl_2$), caused a 28.3 ± 2.7 % (n = 5) reduction in peak amplitude of the non-AMPA EPSC, but only a 3.5 ± 0.9 % (n = 4, $p < 0.001$) decrease in the CF EPSC. This differential effect of Cd^{2+} on the two

components of the CF EPSC is not likely to have resulted from a preferential inhibition of the non-AMPA receptors themselves, because the non-AMPA current exhibited a linear I-V (see Figure II-5*A*) characteristic of receptors that are Ca^{2+} impermeable. These results indicate that the non-AMPA receptors experience lower occupancy following release at CF synapses.

Slow time course of non-AMPA EPSCs at CF synapses

The rise time of the non-AMPA response (recorded in 100 μM GYKI 53655) was significantly slower than the CF EPSC (rise time: AMPA, 0.8 ± 0.04 ms; non-AMPA, 1.7 ± 0.1, n = 8, $p < 0.001$); however, the non-AMPA response decayed more rapidly than the AMPA current (half decay time: AMPA, 8.7 ± 0.6 ms; non-AMPA, 5.9 ± 0.3, n = 8, $p < 0.001$) (Figure II-8*A*). The decay of the CF AMPA current may be prolonged due to saturation of AMPA receptors and slow clearance of glutamate (Barbour et al., 1994), which allows repeated binding to receptors and perhaps spillover onto nearby receptor clusters (Wadiche and Jahr, 2001). To address whether the slower decay of the CF AMPA response is a consequence of AMPA receptor saturation, we examined the decay of these two components when release probability at CF terminals is closer to that exhibited by most CNS glutamatergic terminals. Because the AMPA response in 5 μM Cd^{2+} was still close to saturation (see Figure II-7*B*), we raised the Cd^{2+} concentration to 12 μM. This reduced the peak amplitude of the AMPA response by 20.4 ± 1.8 % (n = 3) and the decay time to 4.7 ± 0.4 ms (half decay) (decay tau: 5.4 ± 0.4 ms, n = 3, $p < 0.01$) (Figure II-8*B*), similar to results

shown by Wadiche and Jahr (2001). In contrast, application of 5 μM Cd^{2+} did not alter the decay of the non-AMPA response (decay tau: control, 10.1 ± 0.4 ms; + Cd^{2+}, 9.6 ± 0.5 ms, n = 8, p = 0.101) (Figure II-8*C*). In Figure II-8*D*, the non-AMPA recorded in 100 μM GYKI 53655 is scaled to the peak amplitude of the AMPA response recorded under lowered release conditions (12μM Cd^{2+}), illustrating the significantly slower rise and decay of the non-AMPA response ($p < 0.001$).

Kainate receptors are responsible for the non-AMPA EPSC

Fast excitatory transmission is mediated by three classes of ionotropic glutamate receptors, AMPA, NMDA and kainate receptors. At synapses where both AMPA and kainate receptors are expressed, kainate receptor-mediated currents exhibit a smaller amplitude and slower kinetics (Lerma, 2003), similar to the non-AMPA receptor currents recorded at CF synapses. To determine whether kainate receptors are responsible for the non-AMPA CF EPSC, we measured the inhibition of this response by LY 382884, an antagonist that exhibits a ~ 100-fold greater selectivity for kainate receptors over AMPA receptors (Bortolotto et al., 1999; Lerma et al., 2001). As shown in Figure II-9*A*, CF non-AMPA responses (recorded in 100 μM GYKI 53655) were inhibited by 78.0 ± 0.2 % (n = 4) by 10 μM LY 382884, a concentration that does not inhibit AMPA receptors (Bortolotto et al., 1999), and by 88.5 ± 1.4 % (n = 4) by 50 μM LY 382884. The PPR was unchanged in the presence of LY 382884 ($PPR_{control}$: 0.31 ± 0.01; $PPR_{LY:}$ 0.32 ± 0.01, n = 5, p = 0.150), indicating that this inhibition did not result from presynaptic actions of this compound. These results suggest that the

non-AMPA CF response is mediated by kainate receptors.

PCs express both GluR5 and KA1 kainate receptors (Wisden and Seeburg, 1993), and LY 382884 has a higher affinity for GluR5-containing receptors (Bortolotto et al., 1999). To address the possible contribution of GluR5 to the CF EPSC, we recorded CF responses from PCs in slices prepared from *GluR5*$^{-/-}$ mice (Contractor et al., 2000). If GluR5-containing kainate receptors contribute to the non-AMPA response, GYKI 53655 should inhibit a greater fraction of the CF EPSC in animals lacking this subunit. As shown in Figure II-9*B*, application of 100 μM GYKI 53655 inhibited CF EPSCs by 98.3 ± 0.3 % (n = 4) in *GluR5*$^{-/-}$ mice compared to 96.1 ± 0.5 % (n = 4, $p < 0.01$) in wild-type littermates, and the amplitude of the residual current was dramatically reduced in *GluR5*$^{-/-}$ mice (peak current in GYKI @ −65 mV: *GluR5*$^{-/-}$, −74.8 ± 15.6 pA, n = 4; wild-type, −263.0 ± 68.7 pA, n = 4, $p < 0.05$). These data indicate that the CF EPSC is generated by two distinct glutamate receptors, AMPA receptors and kainate receptors, and that GluR5 containing kainate receptors are responsible for the majority of the non-AMPA EPSC at CF synapses.

Discussion

In this study we analyzed CF synaptic currents from mice deficient in EAAC1 and/or EAAT4 and found that both stoichiometric and anion transporter currents were absent in mice lacking EAAT4, but not EAAC1, suggesting that EAAT4 has a specialized role in clearing glutamate released at CF synapses. The inability to detect synaptic currents mediated by EAAC1 suggests that this transporter is present at a much lower

density than EAAT4 near CF synapses. These data are in accordance with the hypothesis that EAAC1 is primarily a metabolic transporter (Rothstein et al., 1996; Sepkuty et al., 2002), rather than one involved in clearing synaptic glutamate. However, because EAAT4 is largely restricted to PCs in the mature brain, EAAC1 may perform a similar role at some excitatory synapses (Diamond, 2001; He et al., 2000), perhaps at synapses that are partially ensheathed by glia (Ventura and Harris, 1999).

CF synaptic currents recorded in the presence of 25 μM NBQX were believed to reflect the activity of glutamate transporters exclusively, with the amount of charge transferred during these responses proportional to the amount of glutamate taken up into PCs. Estimates based on transporter-associated anion currents suggested that at least 22% of the glutamate released at CF synapses is taken up by PCs (Otis et al., 1997), while measurements based on stoichiometric transporter currents suggested that the majority of this glutamate (56 – 230 %) is removed by PCs (Auger and Attwell, 2000). The latter estimate is surprising given the tight ensheathment of PC synapses by Bergmann glial cells (Spacek, 1985), and the higher density of transporters in these membranes (Lehre et al., 1995). However, the putative transporter current recorded in 25 μM NBQX was only partially inhibited by a saturating dose of TBOA, and a residual synaptic current (rEPSC) was observed in *EAAC1*$^{-/-}$ x *EAAT4*$^{-/-}$ mice in the presence of 25 μM NBQX, indicating that the currents recorded previously were not mediated entirely by transporters. These results indicate that the amount of glutamate removed by PCs has been overestimated.

Unfortunately, merely subtracting the rEPSC in TBOA from control will not provide an accurate measure of the charge transferred by glutamate transporters, because TBOA altered the activation of the receptors underlying the rEPSC (see Figure II-4). If the transporter kinetics are similar to the rEPSC, our results indicate that glutamate transporters transfer 43% less charge than previously estimated (Auger and Attwell, 2000). Because transporters contribute proportionally more to the rEPSC when permeant anions are present in the internal solution (see Figure II-2), the error is less (25%) for estimates based on rEPSCs recorded with NO_3^- as the primary internal anion (Otis et al., 1997). However, both estimates are based on the assumption that each CF synapse releases only a single vesicle upon stimulation, while recent results indicate that multivesicular release predominates at CF synapses (Wadiche and Jahr, 2001). Assuming that CFs release on average three vesicles per site, then less than 10% of the glutamate released by the CF is removed by EAAT4; the majority is presumably cleared by diffusion and uptake into Bergmann glial cells (Bergles et al., 1997). Although glutamate transporters are generally more abundant in glial membranes (total transporter density: 5,400 μm^2) (Lehre et al., 1995), EAAT4 is enriched in the region of the spine membrane just outside the synapse (estimated density: 3,600 μm^2) (Dehnes et al., 1998) and has a 10-fold higher affinity than glial transporters (Fairman et al., 1995), suggesting that it should out compete other transporters. These data raise the possibility that this peridendritic region is exposed to a smaller fraction of the glutamate released, perhaps due to a preferential diffusion of glutamate towards the presynaptic side (Lehre and Rusakov, 2002; Spacek, 1980).

Kainate receptors contribute to the excitation of PCs

A CF synaptic current remained in *EAAC1*$^{-/-}$ x *EAAT4*$^{-/-}$ mice in the presence of 25 μM NBQX, that reversed at the same potential as the CF EPSC and was not blocked by TBOA, indicating that it was not mediated by glutamate transporters. Given the large amount of glutamate released at CF synapses (Wadiche and Jahr, 2001) and the slow clearance of this glutamate away from PC AMPA receptors (Barbour et al., 1994), there is concern that a competitive antagonist such as NBQX could be displaced. However, neither the amplitude nor the decay time of rEPSCs were affected by CTZ (200 μM), as would be expected if this current was mediated by unblocked AMPA receptors (Rammes et al., 1998). This residual current was, however, largely blocked by a higher dose of NBQX (100 μM), suggesting that it is mediated by non-NMDA glutamate receptors. By measuring the size of the CF EPSC remaining in the non-competitive AMPA receptor antagonist GYKI 53655 (100 μM) we determined that these receptors mediate ~ 5% of the CF EPSC; although a minor component, this current was ~ –250 pA (mice) to –400 pA (rats) at the resting potential (– 65 mV).

Glutamate receptor currents that are insensitive to GYKI 53655 and blocked by NBQX are thought to be mediated by kainate receptors (Lerma, 2003). Both GluR5 and KA1 kainate receptor subunits are expressed by PCs (Wisden and Seeburg, 1993), and the selective kainate receptor agonist domoate elicits currents in PCs (in GYKI 53655) (Brickley et al., 1999), indicating that functional kainate receptors are formed. A previous study (Brickley et al., 1999) reported that CF EPSCs in PCs from

wild-type mice were completely blocked by 100 μM GYKI 53655, concluding that kainate receptors were restricted to extrasynaptic sites. However, we show here that the portion of the CF EPSC that was insensitive to GYKI 53655 was inhibited by the kainate receptor antagonist LY 382884, at a concentration that does not affect AMPA receptors (Bortolotto et al., 1999), and the size of the current remaining in GYKI 53655 was dramatically reduced in *GluR5*$^{-/-}$ mice. These data suggest that GluR5-containing kainate receptors are responsible for the majority of the GYKI-insensitive CF response. The cause of the discrepancy between our data and that of Brickey et al. (1999) are not known, but small currents at the CF-PC synapses can be obscured by stimulation artifacts (Auger and Attwell, 2000).

At synapses that express both AMPA and kainate receptors, kainate receptor synaptic currents are typically about 10% as large as those mediated by AMPA receptors and exhibit slower rise and decay kinetics (Lerma, 2003). Consistent with these observations, the CF kainate receptor EPSC was much smaller than the AMPA receptor current and had a much slower rise and decay time (under reduced release conditions) (see Figure II-8). The decay time of these currents was ~ 10 ms (decay tau), remarkably similar to the decay of kainate receptor synaptic currents recorded from hippocampal interneurons (Cossart et al., 2002) and for heterologously expressed kainate receptors (Swanson and Heinemann, 1998). Perhaps related to their slower kinetics, kainate receptors appear to be further from saturation than AMPA receptors (Bureau et al., 2000; Kidd and Isaac, 2001). CF EPSCs recorded in GYKI 53655 (or NBQX) exhibited a much smaller PPR than CF EPSCs recorded under

control conditions, and were more sensitive to a reduction in release probability (see Figure II-7*B*). These results suggest that despite the large amount of glutamate released from CFs, PC kainate receptors experience a lower occupancy than AMPA receptors. The small effect of transporter inhibition on CF rEPSCs suggests that this may result from their lower affinity rather than a location remote from release sites (Bureau et al., 2000; Kidd and Isaac, 2001).

Although much smaller in amplitude than AMPA receptor currents, the slower time course of kainate receptor responses allows greater temporal summation of synaptic inputs at some synapses (Frerking and Ohliger-Frerking, 2002). It is unlikely that kainate receptors perform a similar function at CF synapses, because under physiological release conditions the decay of the kainate receptor current was faster than the AMPA receptor current. The small amplitude of the kainate response suggests that these receptors also are not essential for complex spike generation. While the functional significance of these PC kainate receptors remains to be determined, recent results suggest that kainate receptors also may function as metabotropic receptors (Rozas et al., 2003), raising the possibility that these receptors may regulate the efficacy of other inputs onto PCs.

Figure II-1. Generation of mice deficient in neuronal glutamate transporters. *A*, Western blot of cerebellar tissue from wild-type and transporter knockout mice, using anti-EAAC1 and anti-EAAT4 antibodies. EAAC1 protein was not detected in tissue from *EAAC1*$^{-/-}$ and *EAAC1*$^{-/-}$ x *EAAT4*$^{-/-}$ mice, and EAAT4 protein was not detected in *EAAT4*$^{-/-}$ and *EAAC1*$^{-/-}$ x *EAAT4*$^{-/-}$ mice. Immunoblotting with anti-actin antibodies demonstrate that a comparable amount of protein was loaded into each lane. *B*, Immunostaining of cerebellar slices from wild-type and transporter knockout mice. EAAT4 and EAAC1 immunoreactivity was absent in *EAAC1*$^{-/-}$ x *EAAT4*$^{-/-}$ mice. Immunostaining with anti-calbindin antibodies shows that the morphology of Purkinje cells was normal in *EAAC1*$^{-/-}$ x *EAAT4*$^{-/-}$ mice. Scale bar = 50 μm.

Figure II- 1

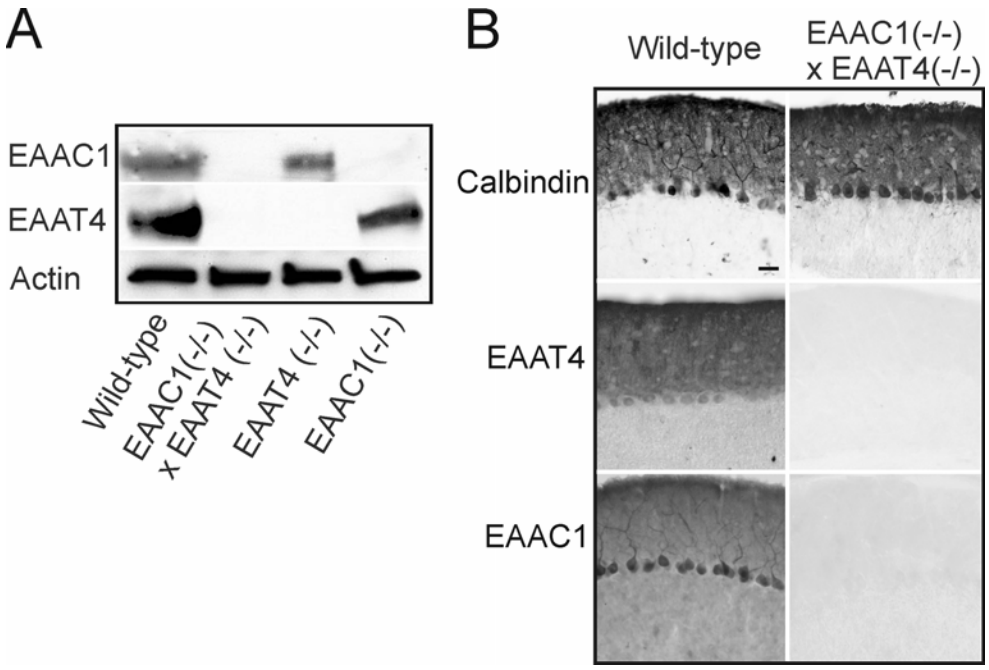
A
EAAC1
EAAT4
Actin
Wild-type
EAAC1(-/-) x EAAT4 (-/-)
EAAT4 (-/-)
EAAC1(-/-)
B
Wild-type
EAAC1(-/-) x EAAT4(-/-)
Calbindin
EAAT4
EAAC1

Figure II-2. Glutamate transporter activation at CF-PC synapses. *A*, A CF EPSC recorded in a PC from a wild-type mouse (P16). The CF response exhibited a sharp stimulation threshold of 10 μA and all-or-none behavior. The holding potential was –10 mV and the internal solution was CsMeS. *B*, The CF EPSC recorded from the cell in *A* after application of 25 μM NBQX, 25 μM GYKI 52466, 10 μM RS-CPP, 5 μM SR-95531, and 20 μM bicuculline to block AMPA, NMDA and $GABA_A$ receptors. This residual current was clearly separated from the stimulus artifact and exhibited the same threshold as the CF EPSC. This response was inhibited by TBOA (200 μM) (*dark trace*). The holding potential was –65 mV. *C*, A CF EPSC recorded with a $CsNO_3$ internal solution in the same antagonists as *B*. This CF response was larger, had slower kinetics, and was inhibited to a greater extent by TBOA (*dark trace*). The holding potential was –65 mV.

Figure II- 2

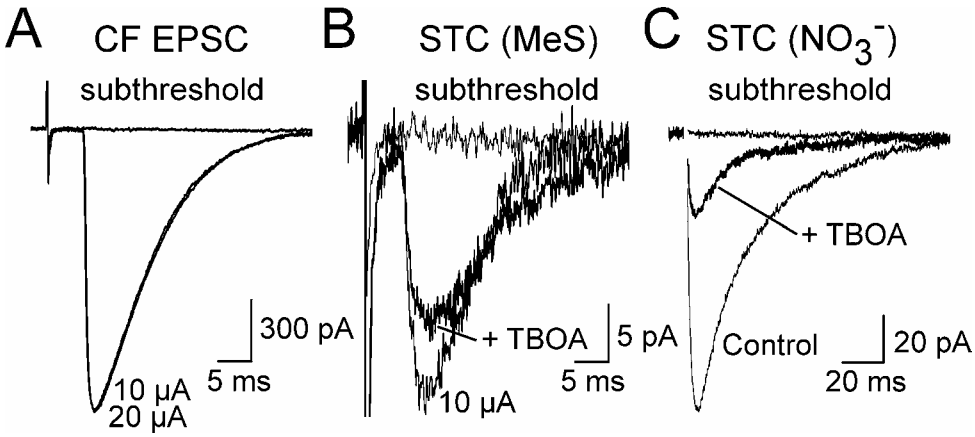
A
CF EPSC
subthreshold
300 pA
5 ms
10 µA
20 µA
B
STC (MeS)
subthreshold
+ TBOA
5 pA
5 ms
10 µA
C
STC (NO_3^-)
subthreshold
+ TBOA
Control
20 pA
20 ms

Figure II-3. Glutamate transporter currents are absent in mice lacking EAAT4. *A*, CF synaptic currents recorded from mice lacking EAAC1, EAAT4 or both EAAC1 and EAAT4 glutamate transporters. Recordings were made with either MeS (*left traces*) or NO_3^- (*right traces*) as the primary internal anion. The dark traces show the response after application of 200 μM TBOA. *B*, Summary of the decay tau of CF synaptic currents from wild-type and transporter knockout mice recorded with either MeS (*open bars*) or NO_3^- (*closed bars*) as the primary internal anion. CF synaptic currents from mice lacking EAAT4 did not exhibit anion-induced slowing, while CF synaptic currents from mice lacking EAAC1 were indistinguishable from wild-type. The numbers in parentheses indicate the number of experiments performed. Comparisons refer to recordings made with NO_3^-. *C*, Summary of the % inhibition of CF synaptic currents by 200 μM TBOA. TBOA inhibition was reduced in mice lacking EAAT4, but unaffected in mice lacking EAAC1. * refers to MeS groups, and *** refers to NO_3^- groups. All currents were recorded in the presence of 25 μM NBQX, 20 μM GYKI 52466, 10 μM RS-CPP, 5 μM SR-95531, and 20 μM bicuculline at a holding potential of –65 mV. (* = $p < 0.05$, *** = $p < 0.001$; NS = not significant)

Figure II- 3

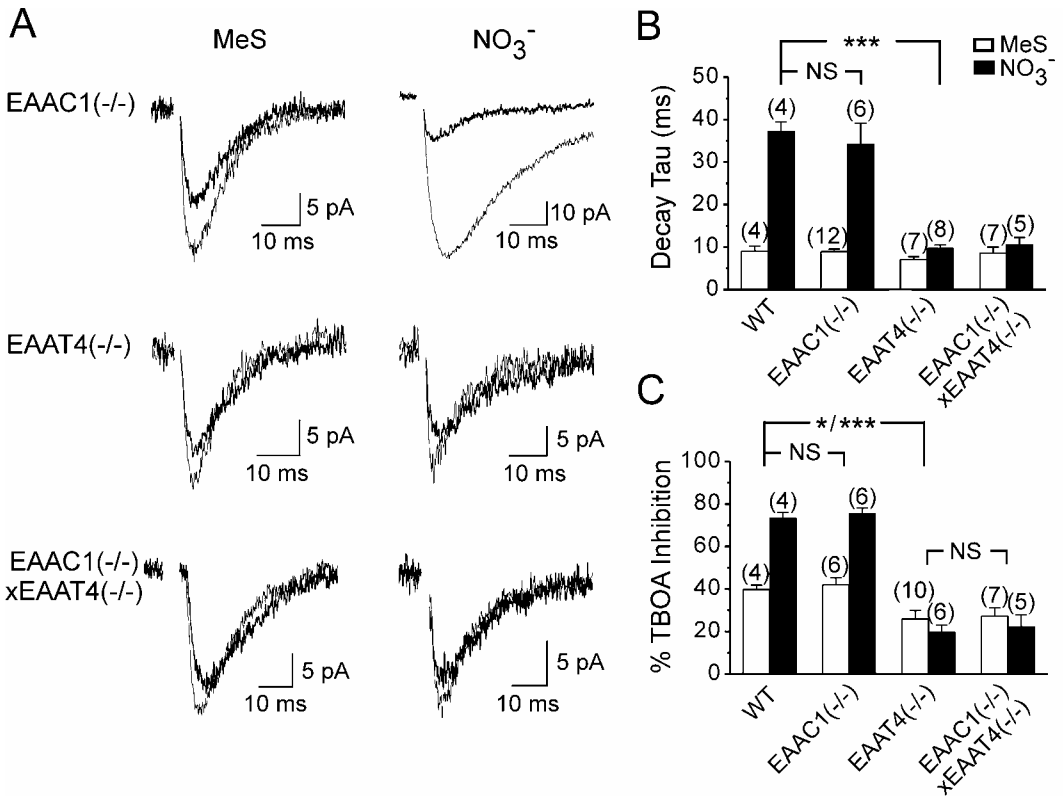
A
MeS
NO3-
EAAC1(-/-)
5 pA
10 ms
10 pA
10 ms
EAAT4(-/-)
5 pA
10 ms
5 pA
10 ms
EAAC1(-/-)
xEAAT4(-/-)
5 pA
10 ms
5 pA
10 ms
B
***
NS
MeS
NO3-
Decay Tau (ms)
50
40
30
20
10
0
(4)
(4)
(6)
(12)
(7)
(8)
(7)
(5)
WT
EAAC1(-/-)
EAAT4(-/-)
EAAC1(-/-)
xEAAT4(-/-)
C
*/***
NS
NS
% TBOA Inhibition
100
80
60
40
20
0
(4)
(4)
(6)
(6)
(10)
(6)
(7)
(5)
WT
EAAC1(-/-)
EAAT4(-/-)
EAAC1(-/-)
xEAAT4(-/-)

Figure II-4. Measurement of the glutamate transporter component of CF rEPSCs. *A*, CF rEPSCs recorded from an *EAAC1*$^{-/-}$ x *EAAT4*$^{-/-}$ mouse under control conditions (*light traces*) and in TBOA (200 μM) (*dark traces*). Below is the summary data showing that TBOA increased the PPR of these responses. (** = $p < 0.01$). Interstimulus interval = 50 ms. ▲= average. *B*, CF rEPSCs recorded from an *EAAC1*$^{-/-}$ x *EAAT4*$^{-/-}$ mouse under control conditions (light traces) and in the presence of TBOA (200 μM) and MCPG (1 mM). Below is the summary data showing that MCPG prevented the change in PPR produced by TBOA (NS = not significant). ▲= average. *C*, CF rEPSCs recorded from a wild-type mouse (*left traces*) or a rat (*right traces*) under control conditions and in the presence of TBOA (200 μM) and MCPG (1 mM). Below is the summary data showing the fractional contribution of transporters to the peak amplitude of the CF rEPSC. All currents were recorded in the presence of 25 μM NBQX, 25 μM GYKI 52466, 10 μM RS-CPP, 5 μM SR-95531, and 20 μM bicuculline at a holding potential of –65 mV. The primary internal anion was MeS for all recordings.

Figure II- 4

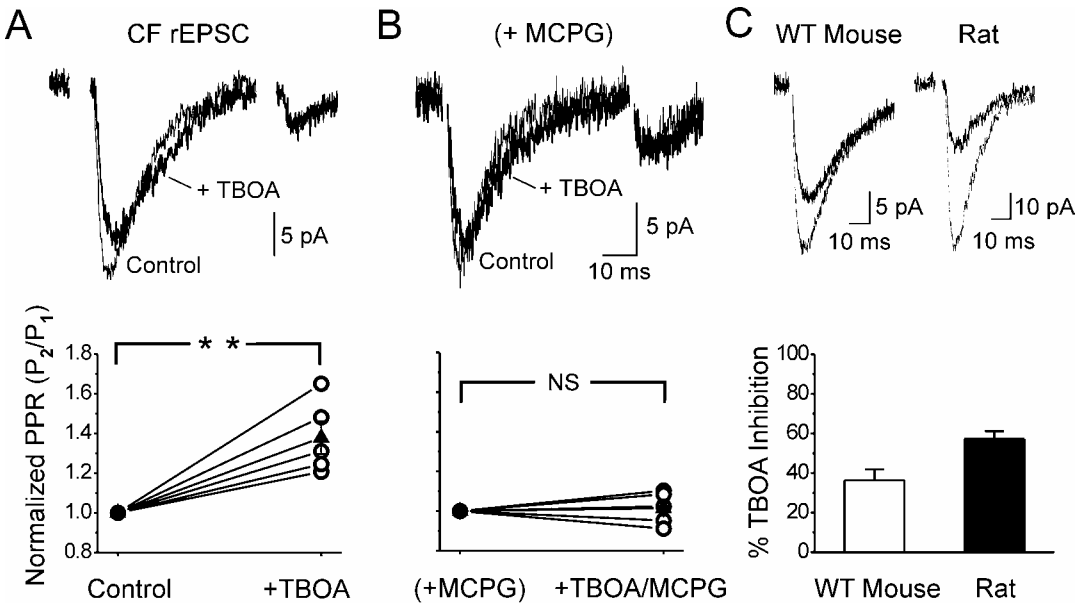
A
CF rEPSC
+ TBOA
5 pA
Control
B
(+ MCPG)
+ TBOA
5 pA
Control
10 ms
C
WT Mouse
Rat
5 pA
10 ms
10 pA
10 ms
Normalized PPR (P2/P1)
1.8
1.6
1.4
1.2
1.0
0.8
* *
Control
+TBOA
NS
(+MCPG)
+TBOA/MCPG
% TBOA Inhibition
100
80
60
40
20
0
WT Mouse
Rat

Figure II-5. The CF rEPSC is mediated by non-AMPA ionotropic glutamate receptors. *A*, CF rEPSCs (*left traces*) and CF EPSCs (*right traces*) recorded at potentials from –65 to 40 mV. *B*, Comparison of the current-to-voltage relationship of CF rEPSCs (○) and CF EPSCs (●). CF rEPSCs were recorded in 25 μM NBQX, and CF EPSCs were recorded in 1 μM NBQX to decrease the size of the responses in order to prevent voltage escape at negative potentials. *C*, CF rEPSCs and CF EPSCs *D* recorded under control conditions (*light traces*) and in the presence of 200 μM cyclothiazide (CTZ) (*dark traces*). The holding potential in *C* was –65 mV and –10 mV in *D*. *E*, CF rEPSCs recorded under control conditions (*light trace*) and in the presence of 100 μM NBQX (*dark trace*). The holding potential was –65 mV. *F*, Summary graph showing the sensitivity of CF rEPSCs to different concentrations of NBQX. All synaptic responses were recorded from PCs in cerebellar slices from *EAAC1*$^{-/-}$ x *EAAT4*$^{-/-}$ mice. The primary anion in the internal solution was MeS for all recordings.

Figure II- 5

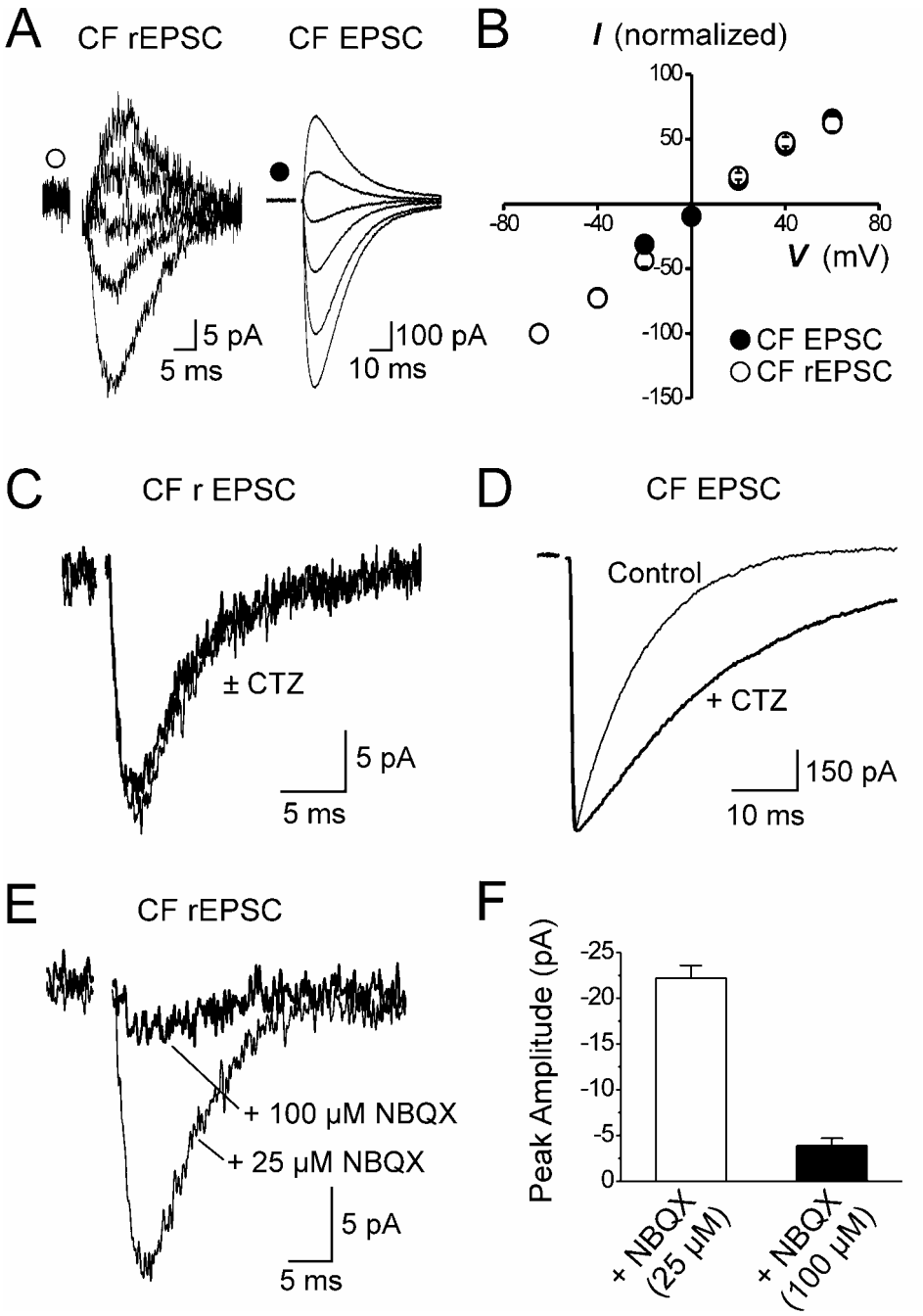
A
CF rEPSC
CF EPSC
5 pA
5 ms
100 pA
10 ms
B
I (normalized)
100
50
-50
-100
-150
-80
-40
40
80
V (mV)
CF EPSC
CF rEPSC
C
CF r EPSC
± CTZ
5 pA
5 ms
D
CF EPSC
Control
+ CTZ
150 pA
10 ms
E
CF rEPSC
+ 100 µM NBQX
+ 25 µM NBQX
5 pA
5 ms
F
Peak Amplitude (pA)
-25
-20
-15
-10
-5
0
+ NBQX (25 µM)
+ NBQX (100 µM)

Figure II-6. Size of the non-AMPA EPSC at CF-PC synapses. *A,* CF EPSCs recorded from a wild-type mouse (*left traces*) or a rat (*right traces*) under control conditions and in the presence of 100 μM GYKI 53655. Below is the summary data showing the % contribution of the non-AMPA current to the CF EPSC and the absolute size of the non-AMPA CF synaptic current in mouse and rat. Percent inhibition was recorded at –10 mV and peak current was measured at –65 mV. *B*, CF EPSCs recorded in 100 μM GYKI 53655 with and without 200 μM CTZ. Below is the summary data showing the effect of CTZ on the decay tau of CF EPSCs recorded in 100 μM GYKI 53655. All recordings were made from PCs in cerebellar slices from rat. NS = not significant.

Figure II- 6

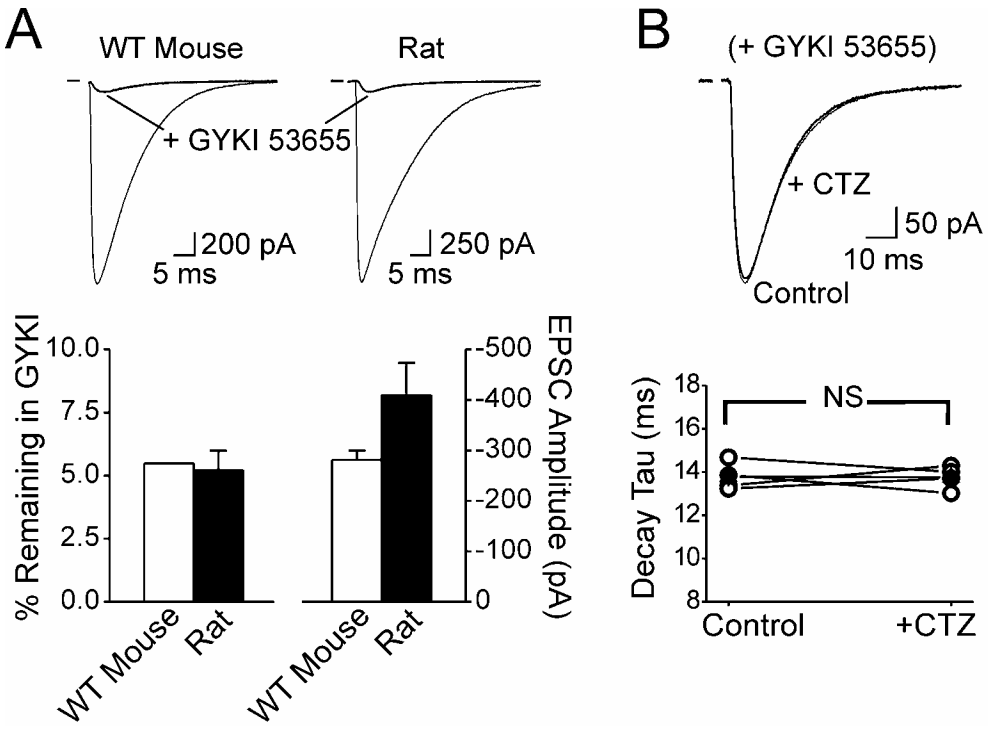
A
WT Mouse
Rat
+ GYKI 53655
200 pA
5 ms
250 pA
5 ms
% Remaining in GYKI
10.0
7.5
5.0
2.5
0.0
EPSC Amplitude (pA)
-500
-400
-300
-200
-100
0
WT Mouse
Rat
WT Mouse
Rat
B
(+ GYKI 53655)
+ CTZ
50 pA
10 ms
Control
Decay Tau (ms)
18
16
14
12
10
8
NS
Control
+CTZ

Figure II-7. Non-AMPA receptors have lower occupancy than AMPA receptors at CF-PC synapses. *A*, Paired-pulse responses of CF EPSCs recorded under control conditions (*left traces*), in the presence of 100 μM GYKI 53655 (*middle traces*), or 25 μM NBQX (*right traces*). Interstimulus interval = 50 ms. Below is the summary data showing that the non-AMPA CF EPSC exhibited a smaller PPR. CF EPSCs in control were recorded at –10 mV, while CF EPSCs in antagonists were recorded at –65 mV. *B*, CF EPSCs (*left traces*) and CF EPSCs in 100 μM GYKI 53655 (*right traces*), recorded in the presence or absence of 5 μM Cd^{2+}. Below is the summary data showing that the non-AMPA CF EPSC was more sensitive to extracellular Cd^{2+}. (*** = $p < 0.001$; NS = not significant).

Figure II- 7

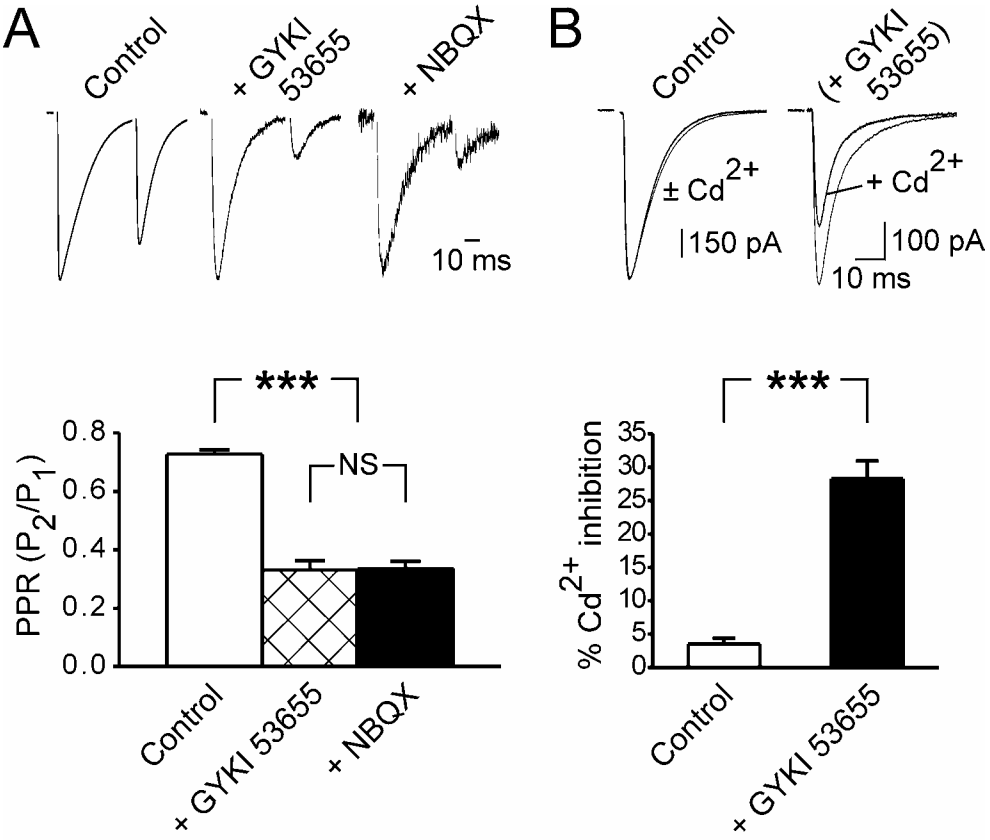
A
Control
+ GYKI 53655
+ NBQX
10 ms
B
Control
(+ GYKI 53655)
± Cd2+
+ Cd2+
150 pA
100 pA
10 ms
***
NS
PPR (P2/P1)
0.8
0.6
0.4
0.2
0.0
Control
+ GYKI 53655
+ NBQX
***
% Cd2+ inhibition
35
30
25
20
15
10
5
0
Control
+ GYKI 53655

Figure II-8. The non-AMPA CF synaptic current has a slow time course. *A*, Overlay of a CF EPSC recorded in 100 μM GYKI 53655 (*dark trace*) scaled to the peak of the CF ESPC recorded under control conditions (*light trace*), illustrating the slower rise time of the non-AMPA current. Inset shows the two responses at a faster time scale. Holding potential = –10 mV. *B*, CF EPSCs recorded under control conditions and in the presence of 12 μM Cd^{2+}. *Red trace* is the response in Cd^{2+} scaled to the control response, showing the faster decay of the CF EPSC when release probability is reduced. *C*, CF EPSCs recorded in the presence of 100 μM GYKI 53655 ± 5 μM Cd^{2}. *Red trace* is the response in Cd^{2+} scaled to the control response, showing that the reduction in release probability did not alter the decay of the non-AMPA EPSC. *D*, Overlay of a CF EPSC recorded in 12 μM Cd^{2+} (*light trace*) and in 100 μM GYKI 53655 (*dark trace*). The response in GYKI has been scaled to the peak of the CF response in 12 μM Cd^{2+}. Holding potential = –10 mV for the CF EPSC, and –65 mV for the response in GYKI.

Figure II- 8

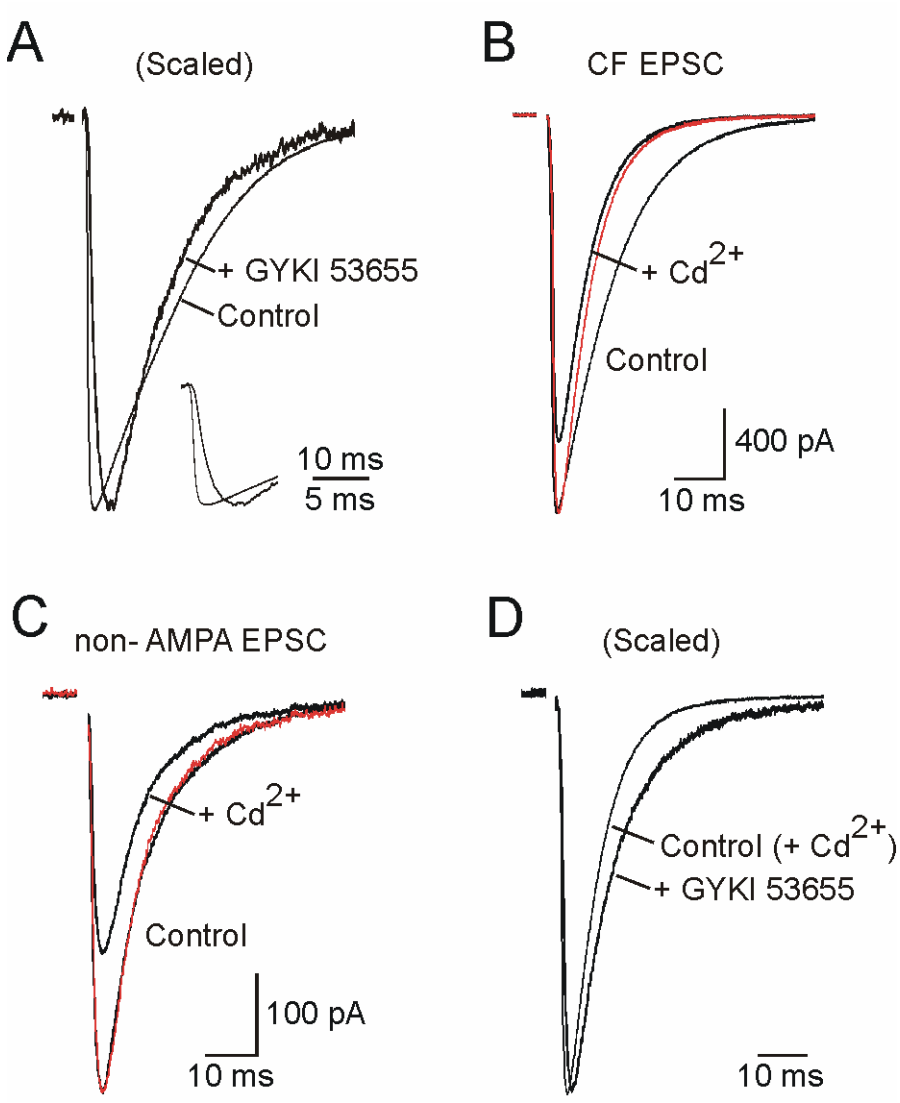
A
(Scaled)
+ GYKI 53655
Control
10 ms
5 ms
B
CF EPSC
+ Cd2+
Control
400 pA
10 ms
C
non- AMPA EPSC
+ Cd2+
Control
100 pA
10 ms
D
(Scaled)
Control (+ Cd2+)
+ GYKI 53655
10 ms

Figure II-9. Kainate receptors are responsible for the non-AMPA CF EPSC. *A*, CF EPSCs recorded in the presence of 100 μM GYKI 53655 were inhibited by the kainate receptor antagonist LY 382884. Holding potential = −65 mV. Graph below plots the sensitivity of this non-AMPA EPSC to LY 382884. *B*, CF EPSCs recorded from wild-type littermates (*left traces*) and *GluR5*$^{-/-}$ mice (*right traces*), under control conditions and in the presence of 100 μM GYKI 53655. Holding potential = −10 mV. The graph below shows the percent contribution of teh non-AMPA current to the CF EPSC and the peak amplitude of the current remaining in GYKI 53655 in these two groups of animals (recorded at –65 mV).

Figure II- 9

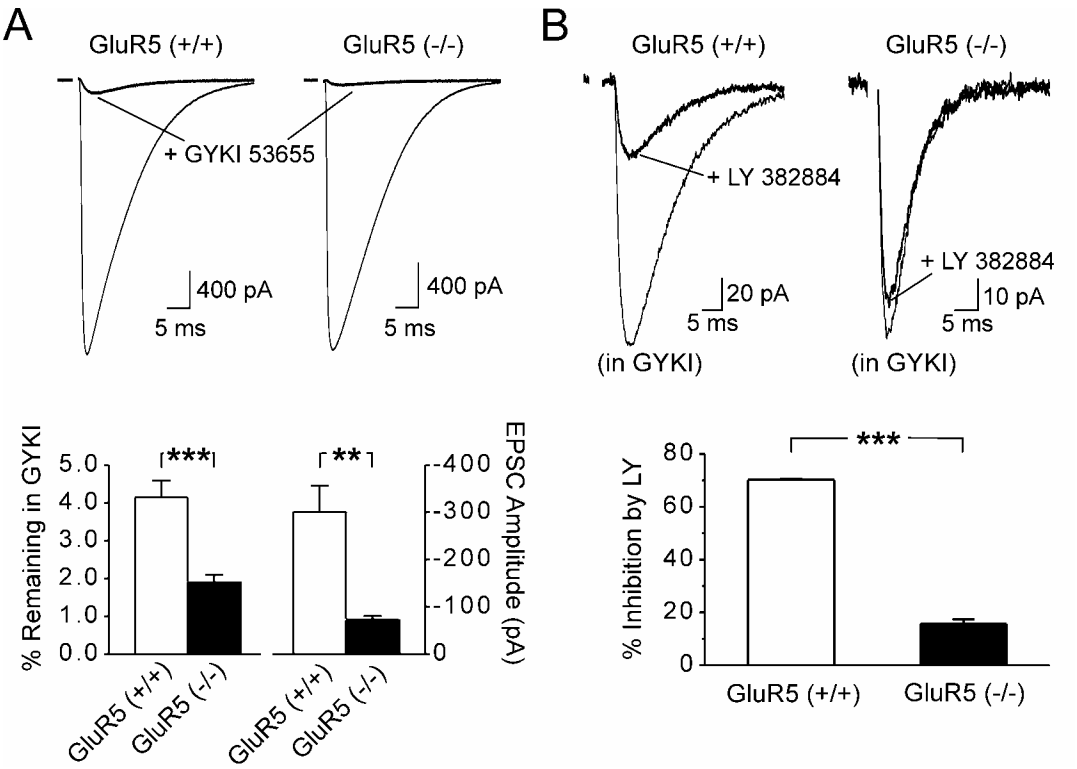
A
GluR5 (+/+)
GluR5 (-/-)
+ GYKI 53655
400 pA
5 ms
400 pA
5 ms
B
GluR5 (+/+)
GluR5 (-/-)
+ LY 382884
20 pA
5 ms
(in GYKI)
+ LY 382884
10 pA
5 ms
(in GYKI)
% Remaining in GYKI
5.0
4.0
3.0
2.0
1.0
0.0
***
**
-400
-300
-200
-100
0
EPSC Amplitude (pA)
GluR5 (+/+)
GluR5 (-/-)
GluR5 (+/+)
GluR5 (-/-)
% Inhibition by LY
80
60
40
20
0
***
GluR5 (+/+)
GluR5 (-/-)

Chapter III

Astrocyte glutamate transporters regulate metabotropic glutamate receptor-mediated excitation of hippocampal interneurons

Introduction

The studies described in **Chapter II** indicate that astroglial transporters are responsible for removing the majority of glutamate at cerebellar climbing fiber-Purkinje cell (CF-PC) synapses; the neuronal transporter EAAT4 contributes to ~10% of total clearance; and EAAC1 contributes a negligible amount. This devision of labor between different transporters presumably reflects a collection of features at CF-PC synapses including the structure of the synapses, the amount of glutamate released, and the types and distribution of glutamate transporters. The CF-PC synapse is unique in that (1) EAAT4 transporters are abundant in PCs at the perisynaptic regions (Dehnes et al., 1998; Tanaka et al., 1997), but they are not expressed by other cell types of the CNS; (2) CF-PC synapses also exhibit a high release probability (~ 2−3 vesicles per synapse, see Wadiche and Jahr, 2001), which is unusually high compared to most other excitatory synapses in the CNS (for review, see Thomson, 2000); and (3), CF-PC synapses are among the most tightly ensheathed synapses in the CNS (Palay and Chan-Palay, 1974; Spacek, 1985). Recent studies indicate that 94% of CF-PC synapses are ensheathed by glial cell membranes (Xu-Friedman et al., 2001), whereas only 58% of spine synapses are associated with astroglial membranes in the hippocampus (Ventura and Harris, 1999); this percentile is comparable to that of

cortical spine synapses as well (Spacek, 1985). The close association of glial cell membranes with CF-PC synapses also brings high concentrations of glial glutamate transporters close to release sites. In summary, although CF-PC synapses provide an unparalleled opportunity to quantitatively measure proportional uptake by neuronal and glial glutamate transporters, the unique properties of these synapses raise the concern that mechanisms of glutamate clearance found here may not be applicable to other more conventional CNS synapses.

Compared to CF-PC synapses, excitatory synapses in the hippocampal are a better representative for studying glutamate clearance at typical CNS synapses. The reasons are the following: (1) hippocampal neurons express EAAC1 but not EAAT4 transporters, a character shared by most CNS synapses; (2) hippocampal synapses exhibit average probability of release; and (3) synapses in the hippocampus are partially ensheathed by astroglial processes, which is another feature shared by most CNS synapses. Therefore, excitatory synapses in the hippocampus are distintly different from CF-PC synapses, raising the question whether neuronal transporters contribute more to synaptic clearance of glutamate when glial transporters are positioned further away from release sites. To study these synapses, however, we and others have not been able to directly measure uptake by neuronal transporters during transmission through isolating synaptic transporter currents from postsynaptic neurons. This is presumably because the amount of synaptically released glutamate is much less than that following a single CF activation, and there are presumably fewer neuronal transporters on the postsynaptic membrane to be activated.

To study glutamate clearance at hippocampal synapses an alternative approach is to examine clearance indirectly by monitoring the occupancy of glutamate receptors during transmission. One potential candidate receptors are the metabotropic glutamate receptors (mGluRs), because they are typically located at perisynaptic regions where glutamate transporters are enriched (Baude et al., 1993; Lujan et al., 1996; Tamaru et al., 2001), and the affinity of mGluRs for glutamate binding is comparable to that of glutamate transporters (see **Introduction**), making them sufficiently sensitive to the ambient glutamate level controlled by transporters. A subtype of mGluRs, mGluR1α, has been shown in cerebellar Purkinje neurons to be located perisynaptically (Baude et al., 1993); and its activation is regulated by postsynaptic transporter activity during parallel fiber-Purkinje neuron transmission (Brasnjo and Otis, 2001; Wadiche and Jahr, 2005).

Hippocampal oriens-lacunosum moleculare (O-LM) interneurons (or oriens alveus, OA-interneurons) in the CA1 region selectively express high levels of mGluR1α (Baude et al., 1993), the same mGluR1 splice variant that is expressed by cerebellar Purkinje neurons. Activation of mGluR1α in Purkinje neurons leads to opening of a non-selective cation channel and the associated current can be used to monitor the extent of mGluR1α activation (Batchelor et al., 1994; Kim et al., 2003). Electronmicroscopy studies have further revealed that in O-LM interneurons, synaptic mGluR1α receptors are predominantly located at perisynaptic regions (Baude et al., 1993; Lujan et al., 1996). In addition, activation of mGluRs by an exogenous agonist elicits an inward current in these neurons (McBain et al., 1994), suggesting that

mGluR1α is similarly coupled to activation of a non-selective cation channel in O-LM interneurons. Nonetheless, unlike in Purkinje neurons, synaptically evoked mGluR currents have not been observed in O-LM interneurons (Gee et al., 2001). Therefore, we aimed to isolate synaptic mGluR currents in O-LM interneurons to examine the differential contributions of transporters to the clearance of glutamate at hippocampal synapses, and the potential impact of glutamate transporters on mGluR-mediated synaptic transmission.

Here we show that mGluR1α-mediated synaptic currents could be evoked in O-LM interneurons if intracellular Ca^{2+} was elevated in these cells prior to stimulation. These synaptic mGluR currents were greatly potentiated by pharmacological inhibition of glutamate transporters, and recordings from mice deficient in glutamate transporters revealed that GLAST and GLT-1, but not EAAC1, were primarily responsible for shielding these perisynaptic receptors. Furthermore, inhibition of these transporters potentiated di-synaptic inhibition of CA1 pyramidal cells, indicating that astroglial glutamate transporters may regulate hippocampal network excitability by regulating mGluR occupancy at interneuron synapses.

Materials and Methods

Glutamate transporter deficient mice. The generation of *EAAC1*$^{-/-}$ mice and *GLAST*$^{-/-}$ mice have been described previously (Peghini et al., 1997; Watase et al., 1998). All comparisons between specific transporter knockout mice and wild-type mice were performed between littermates obtained from heterozygous matings. The

genotype of all experimental animals was determined by PCR.

Slice preparation. Postnatal day 18 to 20 (P18-20) rats and P15-20 mice were deeply anesthetized by halothane and killed by decapitation, in accordance with protocols approved by the Johns Hopkins University Animal Care and Use Committee. Hippocampi were removed and cut into 400 μm slices using a vibratome (Leica, VT1000S) in ice-cold saline solution containing (in mM): 110 choline chloride, 2.5 KCl, 7 $MgSO_4$, 0.5 $CaCl_2$, 1.25 NaH_2PO_4, 25 $NaHCO_3$, 25 glucose, 11.6 Na-ascorbate, and 3.1 Na-pyruvate, saturated with 95% O_2, 5% CO_2. Slices were then incubated at 37° C for 30 minutes in artificial cerebrospinal fluid (ACSF) composed of (in mM): 119 NaCl, 2.5 KCl, 2.5 $CaCl_2$, 1.3 $MgCl_2$, 1 NaH_2PO_4, 26.2 $NaHCO_3$, and 11 glucose, saturated with 95% O_2, 5% CO_2, and then allowed to recover for at least 30 minutes at room temperature before experimentation.

Electrophysiological recordings. During experimentation, slices were superfused with ACSF that was heated to 33-35° C by passing the solution through a feedback controlled in-line heater (Warner Instruments, Hamden, CT) prior to entering the chamber. O-LM interneurons were visualized in stratum oriens using infrared-DIC imaging with a 40x water immersion objective on an upright microscope (Axioskop FS2, Zeiss) equipped with a CCD camera (Sony XC-73). Whole-cell recordings were made under visual control with an internal solution consisting of (in mM): 105 $CsCH_3O_3S$, 20 TEA-Cl, 20 HEPES, 10 EGTA (or 10 BAPTA), 2 Mg-ATP, 0.2 Na-GTP, 1 QX-314, pH 7.3. Excitatory afferents were stimulated using a glass pipette filled with ACSF. Stimuli (20−35 μA) were generated using a constant current

isolated stimulator (Digitimer DS3), and a programmable pulse generator (Master-8, A.M.P. Instruments) was used to trigger a train of pulses (10 pulses @ 100 Hz; 200 μs duration for each pulse). Synaptic currents were recorded with a MultiClamp 700A amplifier (Axon instruments), filtered at 3 kHz, amplified 5x or 10x (Brownlee 440; Brownlee Precision), and then digitized at 10 kHz (Digidata 1322A, Axon instruments). Data were analyzed off-line using pClamp 9 (Axon Instruments) and Origin (OriginLab) software. The action potentials for waveform analysis were elicited by injecting just enough current to induce spontaneous firing. Action potential properties were determined as previously described (Zhang and McBain, 1995). The charge transfer associated with IPSCs recorded from CA1 pyramidal neurons was determined by integrating the charge over a window of 4000 ms, starting 220 ms after the last stimulus artifact. Statistical significance was determined using the student's t-test (paired or unpaired, depending on the experiment), and mean values are expressed ± standard error of the mean (S.E.M.).

Photolysis experiments were performed on an upright microscope (Axioskop FS2) to which the output of an Argon ion laser (Stabilite 2017S, Spectra-Physics) was coupled using a multi-mode quartz fiber optic cable (Oz Optics Ltd.) and a high-speed shutter (NM Laser) using the fluorescence light path. The laser output was tuned to 333.6 – 363.8 nm and had an average output of ~230 mW before entering the fiber. The UV beam was focused to a ~50 μm spot on the preparation using a 40x water immersion objective (Olympus). This spot was centered on the soma of the recorded cell using a second targeting laser (632 nm) and photolysis was induced by opening

the shutter for 1 ms. The caged compound, 4-methoxy-7-nitroindolinyl-L-glutamate (MNI-L-glutamate, 125 μM; Tocris) was dissolved in a HEPES-buffered solution composed of (in mM): 137 NaCl, 2.5 KCl, 2.5 $CaCl_2$, 1.3 $MgCl_2$, 20 HEPES, pH 7.3. Any antagonists included in the bath solution were also included in solutions containing caged compound. Solutions containing MNI-L-glutamate were superfused locally onto the slice through a wide-bore pipette placed near the recording area. Whole cell currents were recorded with an Axopatch 200B amplifier (Axon Instruments), filtered at 2 kHz and digitized at 20 kHz.

Morphological reconstruction and immunocytochemistry. O-LM interneurons were filled with neurobiotin (0.2% weight/volume in intracellular solution; Vector Laboratories, Burlingame, CA) for 30 minutes during recordings and then incubated in oxygenated ACSF for 5-9 hours in ACSF after removal of the recording electrode. Slices were then fixed over night in 4% formaldehyde, 0.2% picric acid in phosphate buffered saline at 4° C, and resectioned @ 80 μm on a vibratome (Leica VT1000S). These sections were processed using avidin-HRP reaction (Elite ABC, Vector Laboratories, Burlingame, CA), developed using 3-3'-diaminobenzidine (DAB, Peroxidase Substrate Kit, Vector Laboratories), and intensified using DAB enhancing solution (Vector Laboratories). Morphological reconstruction was made with the aid of an upright Zeiss microscope and drawing tube.

Results

Isolation of an mGluR1α-mediated synaptic current in O-LM interneurons

To determine if glutamate transporters are essential for clearing glutamate away from mGluRs at excitatory synapses on hippocampal interneurons, we recorded from O-LM interneurons (sometimes referred to as O-A interneurons) in the oriens/alveus region of area CA1. mGluR1α is highly expressed by O-LM interneurons (Baude et al., 1993), and application of *RS*-1-aminocyclopentane-trans-1,3-dicarboxylic acid (*trans*-ACPD), a Group I/II mGluR agonist, elicits an inward current in these cells (McBain et al., 1994).

The ability of mGluRs to induce opening of cation channels in these neurons provides a means to monitor mGluR activity using electrophysiological techniques. Putative O-LM interneurons had large, oval-shaped cell bodies with two prominent dendrites extending parallel to the pyramidal cell layer. Injection of depolarizing current induced a train of action potentials in these neurons that did not exhibit spike frequency adaptation, and each action potential during the train was followed by a large spike after-hyperpolarization (Figure III-1*A*, *inset*). Spontaneous action potentials recorded from these interneurons were 73.5 ± 3.2 mV in amplitude and 1.3 ± 0.1 ms in duration (n = 6). These electrophysiological properties are in accordance with those reported for O-LM interneurons (Zhang and McBain, 1995). Reconstruction of neurobiotin-filled interneurons revealed that they had dendrites that extended parallel to the pyramidal cell layer and axons that projected through the pyramidal cell layer and ramified extensively in stratum lacunosum-moleculare (n =

9/9 cells), morphological features unique to O-LM interneurons (Freund and Buzsáki, 1996).

Although application of *trans*-ACPD elicits an inward current in O-LM interneurons (Gee et al., 2001; McBain et al., 1994), activation of an mGluR current in these cells following synaptic stimulation has not been previously reported. We found that brief, high frequency stimulation in stratum oriens (100 Hz, 10 pulses, 200 μs, 20-35 μA per pulse) elicited a slowly developing inward current in some O-LM interneurons (n = 7/20 cells) (Figure III-1*B*), which persisted when AMPA (15 μM NBQX, 25 μM GYKI 52466), NMDA (10 μM *RS*-CPP, 50 μM MK-801, 20 μM 7-chlorokynurenate) and $GABA_A$ receptors (5 μM SR 95531, 20 μM bicuculline) were blocked (n = 7/7 cells); evoked responses also were not affected by the $GABA_B$ antagonist CGP 55845A (data not shown). However, the low probability of observing this current limited our ability to examine transporter-receptor interactions. In cerebellar Purkinje neurons, mGluR1α–mediated currents are potentiated when the cytosolic concentration of Ca^{2+} is increased (Batchelor and Garthwaite, 1997), suggesting that this manipulation might similarly increase mGluR-mediated currents in O-LM interneurons. As shown in Figure III-1*B*, when O-LM interneurons were briefly depolarized to 0 mV (from –65 mV) just prior to stimulation to allow Ca^{2+} influx through voltage-gated Ca^{2+} channels, the amplitude of the evoked response was larger (– step = –29.8 ± 6.2 pA; + step = –112.2 ± 27.7 pA, n = 11, $p < 0.01$), and the rise time was faster (20–80% rise time: – step = 957 ± 282 ms; + step = 94 ± 9 ms, n = 3, $p < 0.05$), although it was only possible to measure the latter feature accurately

when the stimulus artifact did not obscure the onset of the response (3/11 cells). Using this protocol, slow synaptic currents were observed in 27/28 O-LM interneurons in AMPA, NMDA, and $GABA_A$ receptor antagonists (see above). This synaptic current was inhibited by 92.8 ± 1.1 % (n = 9) by the selective mGluR1α antagonist LY 367385 (50 μM) (Figure III-1*C*), indicating that the response was dependent on activation of mGluR1α. This response was also blocked by SKF 96365 (50 μM) (n = 4/4 cells), an antagonist of receptor-gated cation channels that also inhibits mGluR1α-mediated inward currents in Purkinje neurons (Kim et al., 2003), suggesting that the synaptic currents recorded from O-LM interneurons resulted from activation of non-selective cation channels.

To confirm that the step depolarization facilitated the mGluR1α response by increasing $[Ca^{2+}]_i$ we examined the size of these EPSCs when a high concentration of BAPTA (40 mM) was included in the pipette solution to rapidly chelate free Ca^{2+}. As shown in Figure III-2*A*, responses recorded with this solution were significantly smaller than those recorded with the control solution (peak amplitude: 10 mM BAPTA = –121.2 ± 36.2 pA, n = 8; 40 mM BAPTA = –5.3 ± 4.5 pA, n = 5, $p < 0.01$), suggesting that elevation of $[Ca^{2+}]_i$ was responsible for step-induced potentiation of the mGluR1α EPSC. To examine the dependence of this response on the step parameters and to maximize the amplitude of the mGluR EPSC, we varied both the step duration and the delay between the end of the step and the beginning of the stimulus (Figure III-2*B*, *C*). The slow EPSC was close to its maximal amplitude when a 500 ms depolarization (from –65 to 0 mV) was applied 1 s prior to stimulation; thus,

this protocol was used for eliciting mGluR1 EPSCs in subsequent experiments.

Inhibition of glutamate transporters enhances activation of mGluR1α

Ultrastructural studies indicate that mGluR1α receptors in O-LM interneurons are predominantly localized at the periphery of the postsynaptic density of type 1 excitatory synapses (Baude et al., 1993), in close proximity to ensheathing glial membranes (Spacek, 1985; Ventura and Harris, 1999). Despite the high affinity of mGluR1α ($EC_{50} \cong 10$ μM) (Conn and Pin, 1997) and the amplification of mGluR-mediated currents by second messengers, the amplitude of mGluR1 EPSCs were small compared to responses evoked by exogenous mGluR1 agonists (McBain et al., 1994), suggesting that these receptors may be exposed to only a fraction of the glutamate that is released. To determine if glutamate transporters restrict activation of mGluRs on O-LM interneurons we examined whether glutamate transporter antagonists potentiated these synaptic currents. Application of 300 μM dihydrokainate (DHK), a concentration that results in selective antagonism of GLT-1 (Arriza et al., 1994), caused a ~ 3-fold increase in the amplitude of mGluR1 EPSCs (control: –97.5 ± 31.8 pA; + DHK: –365.0 ± 100.7 pA, n = 8, $p < 0.01$) (Figure III-3*A,B*); a similar effect was seen on the amount of charge transferred during mGluR1 EPSCs (control: $–7.0 \pm 4.0 \times 10^{-11}$ C; + DHK: $20.7 \pm 6.5 \times 10^{-11}$ C, n = 8, $p < 0.001$) (Figure III-3*A,B*). These results indicate that GLT-1, a transporter that is present at a high density in astrocyte membranes (Lehre and Danbolt, 1998), restricts activation of these interneuron receptors. Subsequent application of a saturating dose of

DL-*threo*-*b*-benzyloxyaspartic acid (TBOA, 100 μM), an antagonist that blocks all glutamate transporters, caused a further, more dramatic enhancement of these slow EPSCs (Figure III-3*A,B*). The current enhanced by transporter antagonists was mGluR1-dependent, as the peak amplitudes of the synaptic responses in TBOA were inhibited 94.0 ± 2.2 % (n = 7) by LY 367385 (50 μM) (charge transfer was inhibited by 94.0 ± 2.1 %). As shown in Figure III-3*C*, TBOA dramatically increased the size of mGluR1-mediated EPSCs elicited in response to a given stimulation intensity. Neither DHK nor TBOA induced an increase in holding current in the absence of stimulation (data not shown) (Arnth-Jensen et al., 2002), presumably because NMDA receptors were blocked in these experiments and the mGluR1-associated conductance depends on elevation of $[Ca^{2+}]_i$.

To determine the effect of transporter inhibition on interneuron excitation as a consequence of increased mGluR activation, we made current-clamp recordings from O-LM interneurons and measured their response to a similar stimulus. As shown in Figure III-4, stimulation in the presence of TBOA led to a dramatic depolarization and sustained firing of action potentials that was not visible under control conditions (n = 5/5 cells). This effect was blocked by LY 367385 (50 μM) (n = 2/2 cells), indicating that this powerful excitatory response was dependent on mGluR1.

Astrocyte glutamate transporters shield interneuron mGluRs.

mGluR1 EPSCs were potentiated more by TBOA than by DHK, suggesting that glutamate transporters other than GLT-1 also may be involved in clearing glutamate

away from these receptors. Immunocytochemical localization studies indicate that three distinct transporters could participate in glutamate clearance at these synapses: GLT-1, GLAST, and EAAC1 (Lehre et al., 1995; Rothstein et al., 1994); a splice variant of GLT-1 (termed GLT-1b) also may be expressed, but has pharmacological properties similar to full-length GLT-1 (Utsunomiya-Tate et al., 1997). To determine the relative contribution of GLAST and EAAC1 to clearance at these synapses, we carried out a similar set of experiments in mice deficient in EAAC1 or GLAST, as selective antagonists for these transporters have not yet been developed. If a particular transporter is involved in clearing glutamate away from mGluRs, then the potentiation of mGluR1 EPSCs by DHK should be greater in mice lacking this transporter, because in the absence of this transporter GLT-1 would be expected to contribute proportionally more to uptake. As shown in Figure III-5*A & C*, application of DHK (300 μM) caused a ~ 1-2 fold potentiation of mGluR1 EPSCs in *EAAC1*$^{-/-}$ mice, similar to that observed in wild-type littermates (fold increase, amplitude/charge transfer: *EAAC1*$^{+/+}$: 1.34 ± 0.47/1.78 ± 0.68, n = 5; *EAAC1*$^{-/-}$: 1.60 ± 0.21/0.96 ± 0.31, n = 6, p = 0.32/0.16). In contrast, DHK (300 μM) produced a much greater enhancement of mGluR1 EPSCs in *GLAST*$^{-/-}$ mice than in wild-type littermates (Figure III-5*B*, *C*) (fold increase, amplitude/charge transfer: *GLAST*$^{+/+}$: 1.57 ± 0.28/1.74 ± 0.58, n = 6; *GLAST*$^{-/-}$: 7.25 ± 1.47/6.90 ± 1.07, n = 11, $p < 0.01/0.001$). The size of mGluR1 EPSCs were not significantly different between transporter knockout and wild-type littermates for EAAC1 (peak amplitude/charge transfer: *EAAC1*$^{+/+}$, –113.9 ± 18.2 pA/8.5 ± 1.8 x 10^{-11} C, n = 5; *EAAC1*$^{-/-}$, –77.1 ± 25.9 pA/6.8

± 1.5 x 10^{-11} C, n = 6, p = 0.28/0.48) and GLAST (peak amplitude/charge transfer: *GLAST*$^{+/+}$, –149.7 ± 44.6 pA/11.0 ± 3.3 x 10^{-11} C, n = 6; *GLAST*$^{-/-}$, –111.9 ± 15.4 pA/6.4 ± 0.6 x 10^{-11} C, n = 8, p = 0.45/0.23). These results suggest that GLT-1 and GLAST, but not EAAC1, determine how much glutamate is available to activate mGluR1 receptors in O-LM interneurons.

The effect of DHK was not equivalent to TBOA in *GLAST*$^{-/-}$ mice, raising concerns that in the absence of GLAST another transporter (i.e. EAAC1, or another unidentified transporter) might also be involved in clearance. Alternatively, the discrepancy in potentiation by these two antagonists could be explained by differences in the ability of DHK and TBOA to inhibit GLT-1 (Bergles et al., 2002). To examine the efficacy of GLT-1 antagonism by DHK, we recorded glutamate transporter currents from stratum oriens astrocytes elicited through photolysis of caged L-glutamate (MNI-L-glutamate, 125 μM). As shown in Figure III-6, a brief (1 ms) flash of UV light elicited an inward current in astrocytes that were exposed to MNI-L-glutamate. This current was not observed when MNI-L-glutamate was absent from the superfusing solution or when the UV beam was shuttered, and the response was blocked by TBOA (200 μM), indicating that this current was produced by the electrogenic cycling of glutamate transporters. DHK (300 μM) inhibited the peak amplitude of these responses by 54.3 ± 1.3 % and slowed their decay (tau decay, single exponential fit: control = 14.7 ± 0.8 ms; DHK = 40.9 ± 3.0 ms, n = 10, p < 0.001), similar to effects seen on transporter currents evoked in astrocytes through synaptic release (Bergles and Jahr, 1997). The effects of 300 μM DHK in *EAAC1*$^{-/-}$

mice were similar to those seen in wild-type mice (% inhibition by DHK, 56.8 ± 1.8 %, n = 4, $p = 0.295$) (tau decay in DHK, 53.8 ± 2.6 ms, n = 3, $p < 0.05$) (Figure III-6*A*, *B*). In contrast, DHK produced a greater inhibition of the peak amplitude (82.6 ± 0.7 %, n = 8, $p < 0.001$) and a greater slowing of the decay of transporter currents in *GLAST*$^{-/-}$ mice (tau decay in DHK, 125.3 ± 8.9 ms, n = 8, $p < 0.001$) (Figure III-6*A*, *B*). However, this concentration of DHK (300 μM) did not completely block astrocyte transporter currents. Because only GLT-1 and GLAST are expressed by astrocytes, these results suggest that 300 μM DHK was not sufficient to block all GLT-1 activity, providing an explanation for the differential potentiation of mGluR EPSCs by TBOA and DHK in *GLAST*$^{-/-}$ mice. Increasing the concentration of DHK to 1 mM increased the inhibition of the transporter current to 91.6 ± 0.5 % (n = 4, $p < 0.001$) (Figure III-6*A*, *B*), and increased the potentiation of mGluR EPSCs in *GLAST*$^{-/-}$ mice to the level of that observed with TBOA (Figure III-5*C*), although 1 mM DHK had no greater effect than 300 μM DHK on the amplitude or charge transfer of mGluR EPSCs in wild-type mice (Figure III-5*C*).

Inhibition of glutamate transporters enhances inhibition of CA1 pyramidal neurons

The axons of O-LM interneurons ramify extensively in stratum LM where the distal dendrites of CA1 pyramidal cells are located, and results obtained from paired recordings indicate that GABA released from O-LM interneurons elicits $GABA_A$ receptor-mediated currents in pyramidal neurons (Maccaferri et al., 2000). The ability

of astrocyte glutamate transporters to regulate mGluR-dependent excitation of O-LM interneurons (see Figure III-4) suggested that transporter inhibition might facilitate the release of GABA from these cells. To investigate this possibility, we recorded the response of CA1 pyramidal neurons to the same stratum oriens stimulation used to elicit mGluR responses in interneurons. These experiments were done in the presence of AMPA (15 μM NBQX; 25 μM GYKI 52466), NMDA (10 μM RS-CPP, 50 μM MK 801, 20 μM 7-Chlorokynurenate) and $GABA_B$ receptor (1 μM CGP 55845) antagonists to isolate $GABA_A$ receptor currents, and an internal solution containing a high [Cl^-] to enlarge these responses. As shown in Figure III-7*A*, stimulation in stratum oriens elicited rapid inward currents in pyramidal neurons, the onset of which was partially obscured by the train of stimuli. In the presence of TBOA (100 μM) a burst of IPSCs became visible following stimulation (Figure III-7*B*), which reached its peak amplitude several hundred milliseconds after the end of the stimulus, in accordance with the delayed onset and slow rise of mGluR-mediated currents in O-LM interneurons (see Figure III-1*B*). Note that a depolarizing step was not applied to O-LM interneurons during this experiment. This burst of IPSCs increased the charge transfer in response to stimulation 3.69 ± 0.84-fold (n = 12, $p < 0.001$) (Figure III-7*E*). This increase in IPSC frequency was blocked by LY 367385 (50–100 μM) (0.38 ± 0.24-fold increase, n = 8, $p = 0.602$), indicating that it required activation of mGluR1. In the presence of TBOA, all evoked responses were blocked by SR 95531 (5 μM) (n = 4/4 cells) (Figure III-7*D, E*), ruling out the possibility that the slow component was mediated by mGluRs on pyramidal cells themselves. These results

indicate that inhibition of astrocyte glutamate transporters facilitates the inhibition of CA1 pyramidal neurons by potentiating mGluR1-mediated excitation of O-LM interneurons.

Discussion

In this study we show that an mGluR1-dependent slow inward current can be elicited in hippocampal O-LM interneurons following stimulation of excitatory afferents in stratum oriens. This response was often revealed only when $[Ca^{2+}]_i$ was elevated in interneurons at the time of stimulation, providing an explanation for why this current has not been observed previously (Gee et al., 2001). A similar Ca^{2+} dependence has been reported for postsynaptic mGluR1 activity at parallel fiber-Purkinje neuron synapses in the cerebellum (Batchelor and Garthwaite, 1997), suggesting that mGluR1 could serve as a coincidence detector to monitor presynaptic glutamate release and postsynaptic Ca^{2+} transients in both types of GABAergic neurons.

Regulation of perisynaptic mGluR1 activation by glial glutamate transporters

Inhibition of GLT-1 transporters caused a ~ 2-fold increase in the size of mGluR1 EPSCs in O-LM interneurons, while inhibition of all glutamate transporters caused a much larger potentiation, indicating that binding and/or uptake of glutamate by transporters restricts activation of mGluRs at these synapses. The relatively small enhancement of mGluR1 EPSCs by DHK suggests that GLT-1 is only a minor contributor to this regulation, particularly when considering that the potentiation by

TBOA, and to a lesser extent by DHK, may have been underestimated, as transporter inhibition in TBOA may have decreased glutamate release by simultaneously enhancing activation of presynaptic mGluRs (Scanziani et al., 1998). These results seem at odds with the density of GLT-1 in the hippocampus, which is almost four times more abundant than GLAST (Lehre and Danbolt, 1998). This discrepancy could be explained if the relative densities of GLAST and GLT-1 are different at these particular synapses. It is also possible that the coupling between mGluR1 and cation channels is non-linear, enabling the synaptic current to become disproportionately larger as more mGluRs are activated in TBOA. Nevertheless, the modest effect of DHK suggests that there are sufficient remaining transporters to compensate for the loss of GLT-1. This hypothesis is consistent with the observation that astrocyte transporter currents were inhibited only ~ 50% by 300 μM DHK (see Figure III-6), and that 1 mM DHK did not potentiate mGluR1 EPSCs more than 300 μM DHK in wild-type mice, even though this higher concentration of DHK inhibited astrocyte transporter currents and potentiated mGluR1 EPSCs to a greater extent in *GLAST*$^{-/-}$ mice. Indeed, previous studies have shown that the pool of astrocyte transporters in stratum radiatum is not saturated following high frequency stimulation, even when GLT-1 transporters are blocked with DHK (Diamond and Jahr, 2000). The decrease in expression of GLAST during development (Furuta et al., 1997) suggests that a proportionally larger role will be played by GLT-1 as the animal matures. Together, these results indicate that two astrocyte transporters, GLT-1 and GLAST, restrict activation of mGluR1s at excitatory synapses on O-LM interneurons.

Although immunolocalization studies indicate that GLT-1 is highly expressed by astrocytes (Lehre et al., 1995; Rothstein et al., 1994), *in situ* hybridization (Berger and Hediger, 1998; Schmitt et al., 1996) and immunolocalization studies (Chen et al., 2004) suggest that GLT-1 is also expressed by some CA3 pyramidal neurons. It is unlikely that the GLT-1 transporters contributing to uptake near interneuron mGluR1s reside in neuronal membranes, as O-LM interneurons in area CA1 receive primarily feedback excitation from CA1 pyramidal neurons rather than feed-forward excitation from CA3 pyramidal neurons (Freund and Buzsáki, 1996), immuno-EM studies indicate that GLT-1 is largely located intracellularly in neurons rather than at the plasma membrane (Chen et al., 2004), and glutamate transporter currents have not been observed in hippocampal neurons (Bergles and Jahr, 1998).

Contribution of neuronal transporters to uptake at excitatory synapses

Recent studies suggest that neuronal glutamate transporters shield postsynaptic receptors at cerebellar (Brasnjo and Otis, 2001) and hippocampal (Diamond, 2001) synapses. EAAC1 is expressed by most neurons in the hippocampus (Rothstein et al., 1994), where it is found primarily in the somo-dendritic compartment (He et al., 2000). Although a detailed analysis of EAAC1 expression by interneurons has not been performed, EAAC1 mRNA is observed in stratum oriens interneurons (Berger and Hediger, 1998). Nevertheless, the similar potentiation of mGluR1 responses by DHK in wild-type and *EAAC1*$^{-/-}$ mice suggests that EAAC1 contributes little to clearance near these receptors. Although the amplitude of mGluR1 EPSCs in *GLAST*$^{-/-}$

mice were increased to a similar extent by 300 μM DHK and 100 μM TBOA, these responses were more prolonged in TBOA, as shown by the enhanced charge transfer (see Figure III-5). The K_i of TBOA is ~ 10-fold lower than DHK at EAAT2 (K_i TBOA = 5.7 μM; K_i DHK = 79 μM) (Shimamoto et al., 1998), and unbinds from GLT-1 about 10x more slowly (Bergles et al., 2002). The persistent rise in extracellular glutamate resulting from high frequency stimulation may force displacement of DHK, allowing GLT-1 to participate in clearance. Consistent with this possibility, 1 mM DHK increased the inhibition of astrocyte transporter currents and potentiated mGluR1-mediated EPSCs to a similar extent as TBOA, suggesting that the discrepancy between the potentiation seen by DHK and TBOA in *GLAST*$^{-/-}$ mice is due, in part, to poorer antagonism of GLT-1 by DHK. However, it has been reported that DHK inhibits EAAC1 with a K_i of 1.12 mM (Dowd et al., 1996) (but see Arriza et al., 1994), raising the possibility that inhibition of EAAC1 also may have contributed to the increased potentiation seen in *GLAST*$^{-/-}$ mice in response to 1 mM DHK. Because 1 mM DHK did not produce greater potentiation than 300 μM DHK in wild-type animals, EAAC1, if involved, is likely to be redundant with GLAST. However, when analyzing complex phenomena in knockout animals there is the concern of compensation. Although a global upregulation of GLT-1 or GLAST is not observed in *EAAC1*$^{-/-}$ mice (Peghini et al., 1997), there could be local changes in the distribution or expression of these transporters at a subset of synapses. Notably, there was no significant change in inhibition of astrocyte transporter currents by DHK in *EAAC1*$^{-/-}$ mice (see Figure III-6), suggesting that relative abundance of GLAST and

GLT-1 is unaltered in astrocytes in these mice.

The prominent role for astrocyte transporters in lowering mGluR1 occupancy at these synapses contrasts with parallel fiber-Purkinje neuron synapses in the cerebellum, where postsynaptic transporters appear to contribute significantly to clearance (Brasnjo and Otis, 2001). Purkinje neurons, unlike O-LM interneurons, express high levels of EAAT4, and recent studies indicate that EAAT4 is responsible for the postsynaptic transporter currents recorded from Purkinje neurons (Huang et al., 2004). These studies, and the present results, suggest that EAAC1 contributes little to perisynaptic clearance at these two excitatory synapses. Notably, EAAC1 is expressed by GABAergic interneurons, and glutamate accumulated by these transporters is used for GABA synthesis (Mathews and Diamond, 2003; Rothstein et al., 1996; Sepkuty et al., 2002), suggesting that it may serve as a metabolic transporter, rather than one specialized for removing synaptic glutamate. However, inhibition of postsynaptic transporters (presumably EAAC1) has been shown to slow the decay of evoked NMDA synaptic currents in CA1 pyramidal neurons (Diamond, 2001). Although the association of astroglia with synapses is essential for placing transporters near release sites (Iino et al., 2001; Oliet et al., 2001), the extent of this ensheathment varies dramatically among hippocampal synapses (Ventura and Harris, 1999), raising the possibility that EAAC1 may prevent spillover of transmitter at synapses that are devoid of astroglia.

Implications for neuronal excitability

Glutamate transporter inhibition potentiated mGluR1 activity in interneurons, increased their firing rate, and greatly enhanced the inhibition of CA1 pyramidal neurons. In cultured hippocampal slices, stimulation of mGluR1 and mGluR5 also have been shown to potentiate inhibition of CA3 pyramidal neurons by increasing interneuron excitability (Maccaferri and Dingledine, 2002; Mori and Gerber, 2002), and in acute slices from guinea-pig tetanic stimulation in the presence of AMPA and NMDA receptor antagonists induces a transient increase in IPSPs in CA3 pyramidal neurons (Miles and Poncer, 1993), indicating a prominent role for mGluRs in regulating interneuron activity. Under physiological conditions, even small shifts in the membrane potential of interneurons caused by moderate mGluR1 activity could serve as a mechanism for short-term regulation of local circuit inhibition, because the timing of action potential firing in these cells is highly sensitive to the resting potential (Freund and Buzsáki, 1996). This modulation of O-LM interneuron mGluR1 activity by glutamate transporters may fine tune the inhibition of perforant path inputs to CA1 pyramidal neurons (Kang et al., 1998), providing insight into the potential consequences of transporter dysregulation.

There is accumulating evidence that the activity of GLT-1 and GLAST are tightly regulated through changes in expression, trafficking, phosphorylation, and interactions with accessory proteins (Gegelashvili et al., 1997; Levy et al., 1995). Furthermore, their expression is closely correlated with neuronal activity (Rao et al., 1998), and is disrupted after trauma (Wong et al., 2003), in epilepsy (Danbolt, 2001), and in many neurological diseases. The results presented here suggest that alterations

in transporter activity could profoundly impact the behavior of neuronal networks by regulating the excitability of interneurons, thereby contributing to the abnormal neuronal activity observed in disease states.

Figure III-1. Isolation of slow EPSCs mediated by mGluR1 in O-LM interneurons. *A*, Morphology of an O-LM interneuron that was filled with neurobiotin through the recording electrode. a, alveus; so, stratum oriens; sp, stratum pyramidale; sr, stratum radiatum; lm, lacunosum-moleculare. *Bottom inset* shows a picture of this interneuron (*scale bar* = 200 μm), and the *upper inset* shows the response of this neuron to injection of depolarizing current (300 pA). *B*, *Left*, response of an O-LM interneuron to field stimulation in stratum oriens (*black trace*). The red trace shows the response of this interneuron to the same stimulus when the cell was depolarized (from –65 mV to 0 mV for 500 ms) 1 second prior to stimulation. *Right*, same traces displayed on a faster time scale. *C*, Inhibition of the slow EPSC recorded from an O-LM interneuron by the specific mGluR1 antagonist LY 367385 (50 μM). Responses in *B* & *C* were recorded in AMPA (15 μM NBQX, 25 μM GYKI 52466), NMDA (10 μM *RS*-CPP, 50 μM MK-801, 20 μM 7-chlorokynurenate) and $GABA_A$ receptor (5 μM SR 95531, 20 μM bicuculline) antagonists at a holding potential of –65 mV.

Figure III- 1

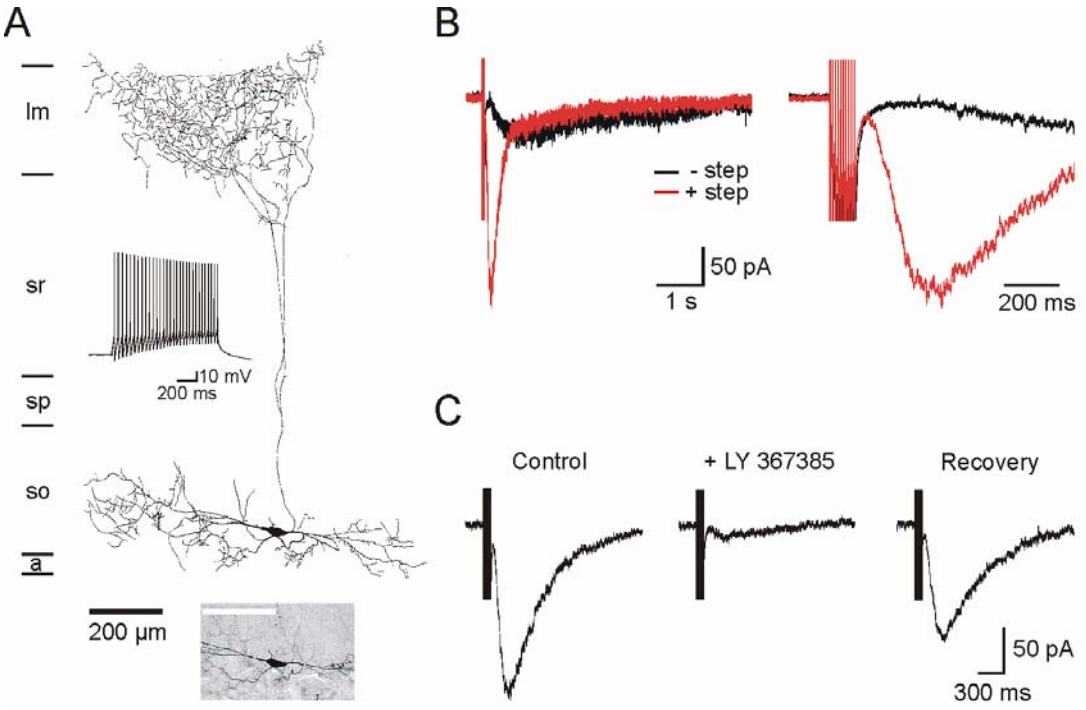
A
lm
sr
sp
so
a
10 mV
200 ms
200 µm
B
- step
+ step
50 pA
1 s
200 ms
C
Control
+ LY 367385
Recovery
50 pA
300 ms

Figure III-2. Ca^{2+} dependence of the mGluR synaptic current. *A*, mGluR1 EPSCs recorded from O-LM interneurons with an internal solution containing 10 mM or 40 mM BAPTA. The grouped data *below* shows the average size of the mGluR1 EPSC recorded under these two conditions. The numbers in parenthesis indicate the number of experiments (** = $p < 0.01$). *B*, mGluR1 EPSCs elicited following depolarizing steps (from –65 mV to 0 mV) of different durations, as indicated. *C*, mGluR1 EPSCs evoked with varying delay (as indicated) after the end of a 500 ms step depolarization to 0 mV.

Figure III- 2

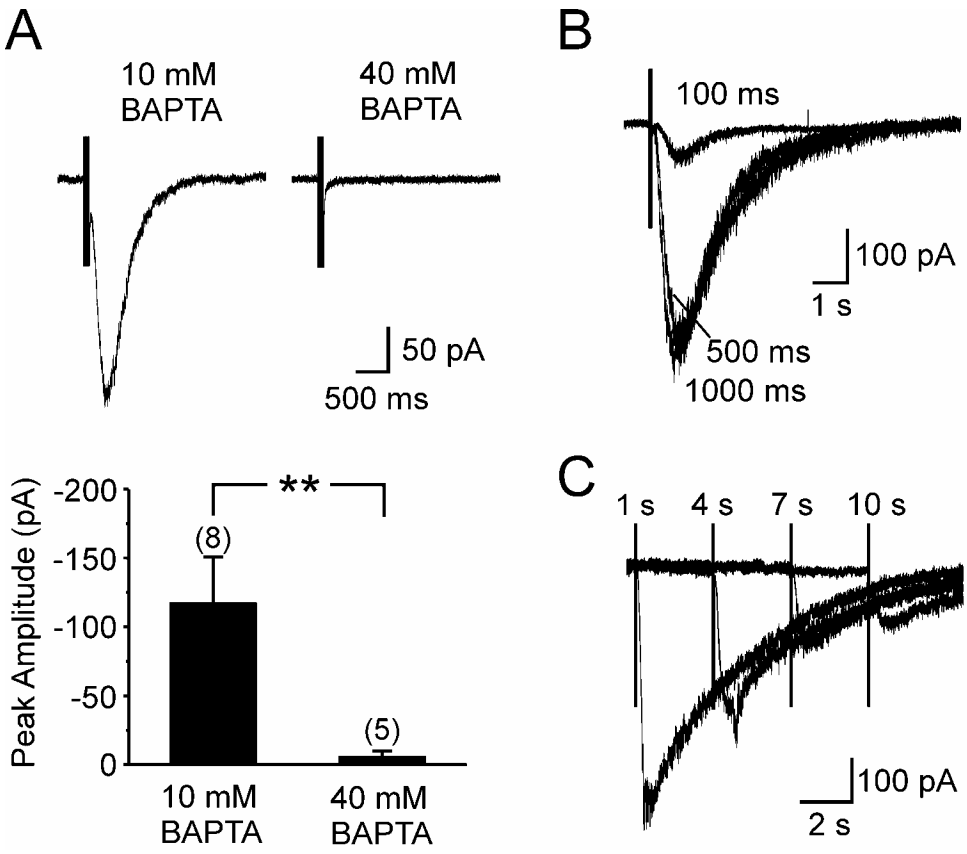
A
10 mM
BAPTA
40 mM
BAPTA
50 pA
500 ms
B
100 ms
100 pA
1 s
500 ms
1000 ms
C
1 s
4 s
7 s
10 s
100 pA
2 s
Peak Amplitude (pA)
-200
-150
-100
-50
0
**
(8)
(5)
10 mM
BAPTA
40 mM
BAPTA

Figure III-3. Inhibition of glutamate transporters potentiates mGluR1 EPSCs. *A*, Evoked mGluR1 EPSCs recorded from O-LM interneurons with (traces labeled #2) or without (traces labeled #1) the step depolarization, under control conditions, in the presence of DHK (300 μM), TBOA (100 μM), or in LY 367385 (50 μM) and TBOA. *B*, Grouped data showing the peak amplitude (open bars) and charge transfer (closed bars) of the mGluR EPSC recorded under these different conditions. Numbers in parenthesis indicate the number of experiments. (** = $p < 0.01$, *** = $p < 0.001$). *C*, Plot of the peak amplitude of evoked AMPA EPSCs (single stimulus, ■) (n = 5−12), mGluR1 EPSCs under control conditions (10 stimuli @ 100 Hz, ○) (n = 5−13), and mGluR EPSCs in the presence of TBOA (10 stimuli @ 100 Hz, ●) (n = 8−13) in response to stimuli of different intensity. When absent, error bars were shorter than the points.

Figure III- 3

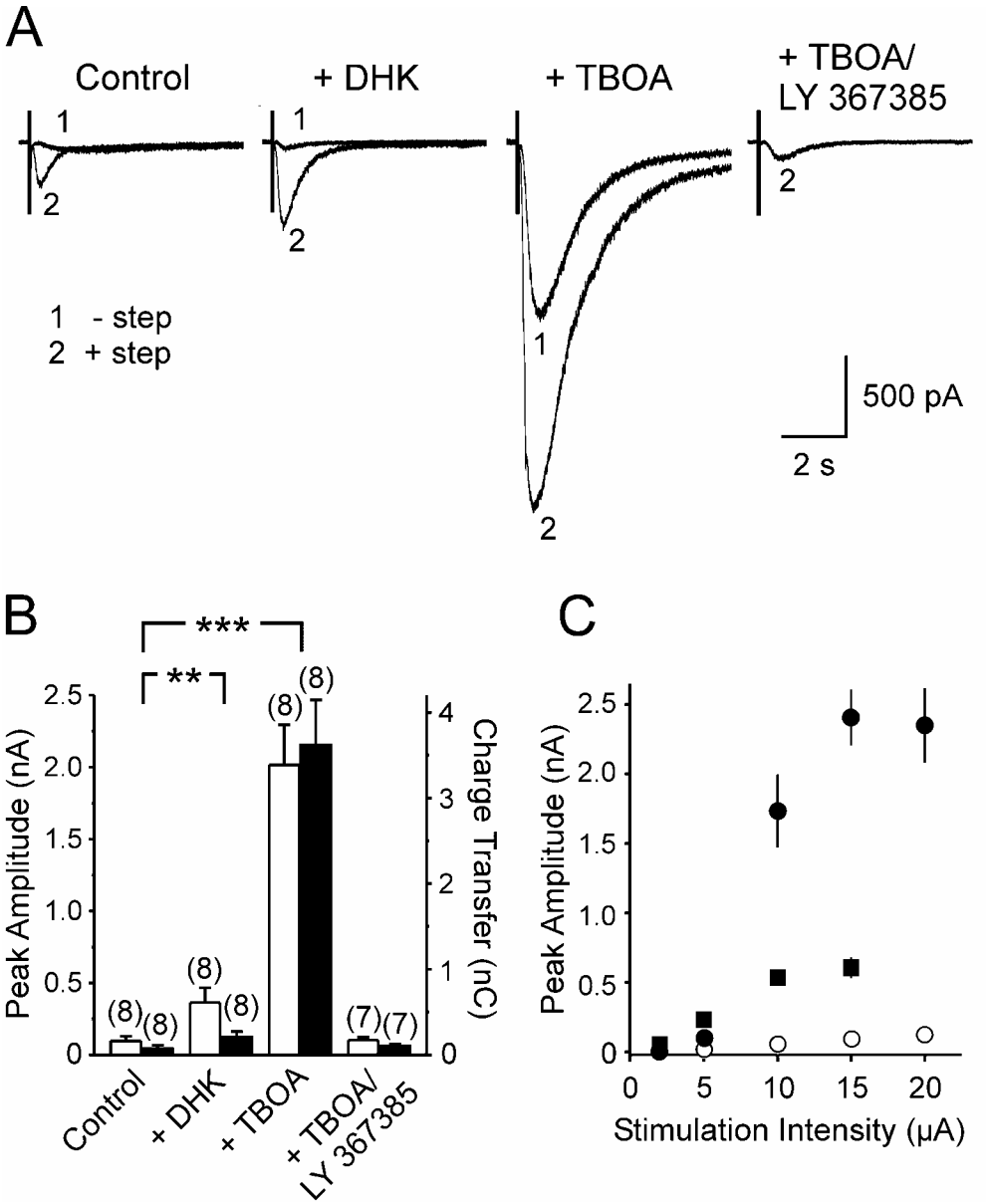
A
Control
+ DHK
+ TBOA
+ TBOA/
LY 367385
1
2
1 - step
2 + step
500 pA
2 s
B
***
**
Peak Amplitude (nA)
Charge Transfer (nC)
(8)
(7)
Control
+ DHK
+ TBOA
+ TBOA/
LY 367385
C
Peak Amplitude (nA)
Stimulation Intensity (µA)

Figure III-4. Inhibition of glutamate transporters potentiates mGluR1-mediated depolarization of O-LM interneurons. Response of an O-LM interneuron to a train of stimuli (*arrow*) following a depolarizing current injection (200 pA) recorded under control conditions (*left trace*), in the presence of TBOA (100 μM, *center trace*), and in the presence of TBOA and LY 367385 (50 μM, *right trace*). Transporter inhibition revealed an mGluR1-mediated response in this O-LM interneuron.

Figure III- 4

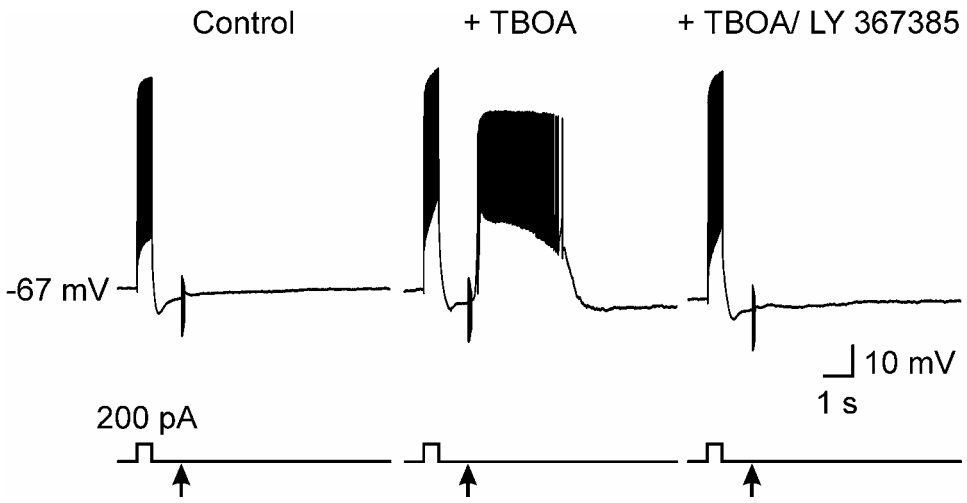

Figure III-5. GLT-1 and GLAST, but not EAAC1 restrict the activation of mGluR1 receptors. *A*, Evoked mGluR1-mediated EPSCs recorded in O-LM interneurons from an *EAAC1*$^{-/-}$ mouse and a wild-type littermate under control conditions and in the presence of DHK (300 μM) or TBOA (100 μM). *B*, The same set of experiments as in *A*, performed on slices from a *GLAST*$^{-/-}$ mouse and a wild-type littermate. The *arrow* highlights the larger effect of DHK (300 μM) observed in the *GLAST*$^{-/-}$ mouse. *C*, Grouped data showing the effects of DHK and TBOA on the peak amplitude (*left*) and charge transfer (*right*) of mGluR1-mediated EPSCs in mice with different genotypes (as indicated). The effect of 1 mM DHK on mGluR1-mediated EPSCs was studied in *GLAST*$^{-/-}$ mice and wild-type littermates. (** = $p < 0.01$, *** = $p < 0.001$). Numbers in parenthesis indicate the number of experiments.

Figure III- 5

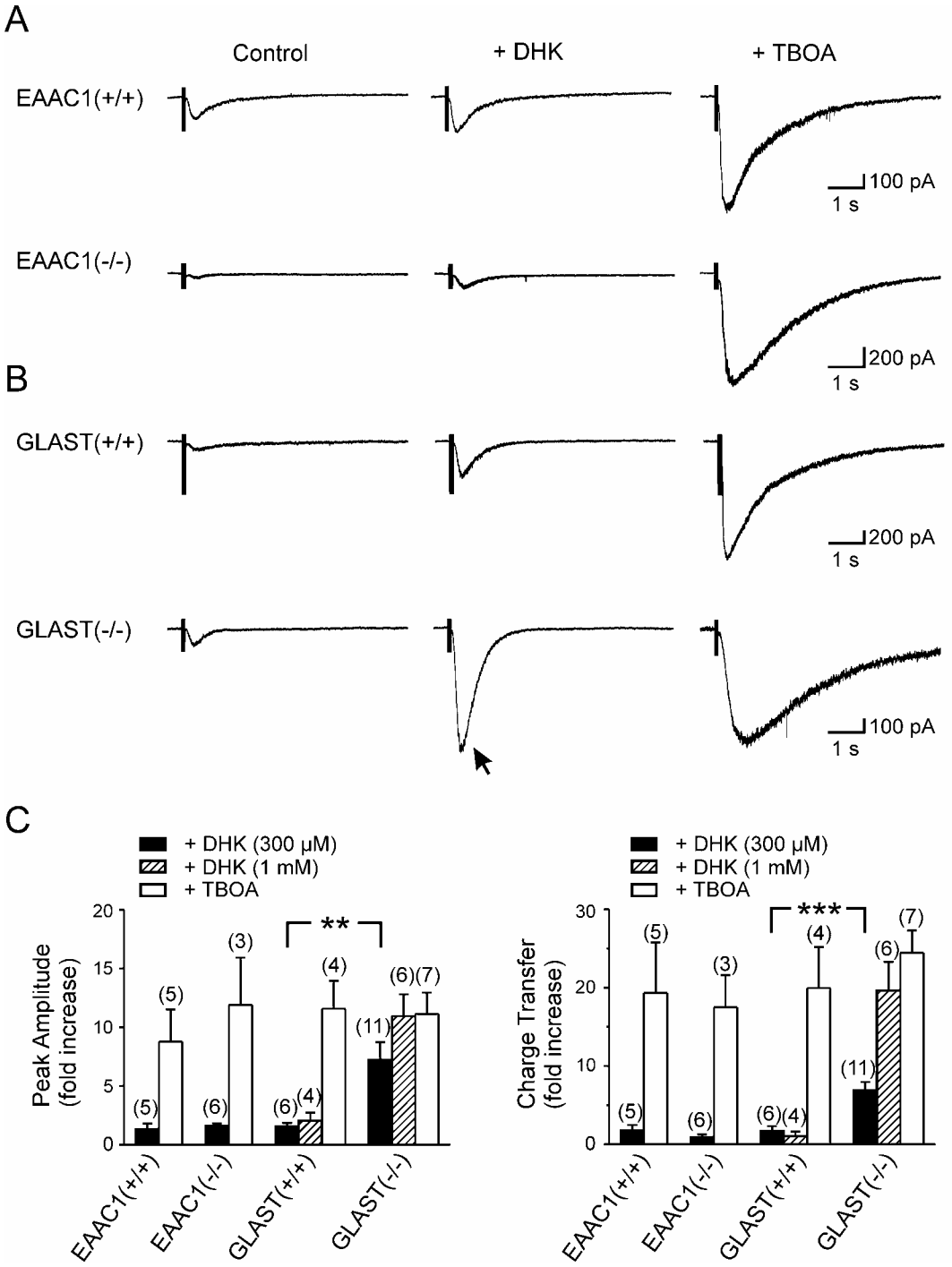
A
Control
+ DHK
+ TBOA
EAAC1(+/+)
100 pA
1 s
EAAC1(-/-)
200 pA
1 s
B
GLAST(+/+)
200 pA
1 s
GLAST(-/-)
100 pA
1 s
C
+ DHK (300 µM)
+ DHK (1 mM)
+ TBOA
Peak Amplitude (fold increase)
**
Charge Transfer (fold increase)
***
EAAC1(+/+)
EAAC1(-/-)
GLAST(+/+)
GLAST(-/-)

Figure III-6. Differential effects of transporter antagonists on astrocyte transporter currents recorded from transporter deficient mice. *A*, Astrocyte transporter currents elicited by UV photolysis of MNI-L-glutamate (125 μM) recorded under control conditions (*black traces*), in the presence of DHK (300 μM, *red traces*; 1 mM, *blue traces*) or TBOA (200 μM) (*green traces*) from mice with different genotypes (as indicated). *B*, Grouped data showing % inhibition of the peak amplitude of these transporter currents by DHK and TBOA in wild-type, *EAAC1*$^{-/-}$, and *GLAST*$^{-/-}$ mice (*** = $p < 0.001$; compared to wild-type). Numbers in parenthesis indicate the number of experiments (ND = not done).

Figure III- 6

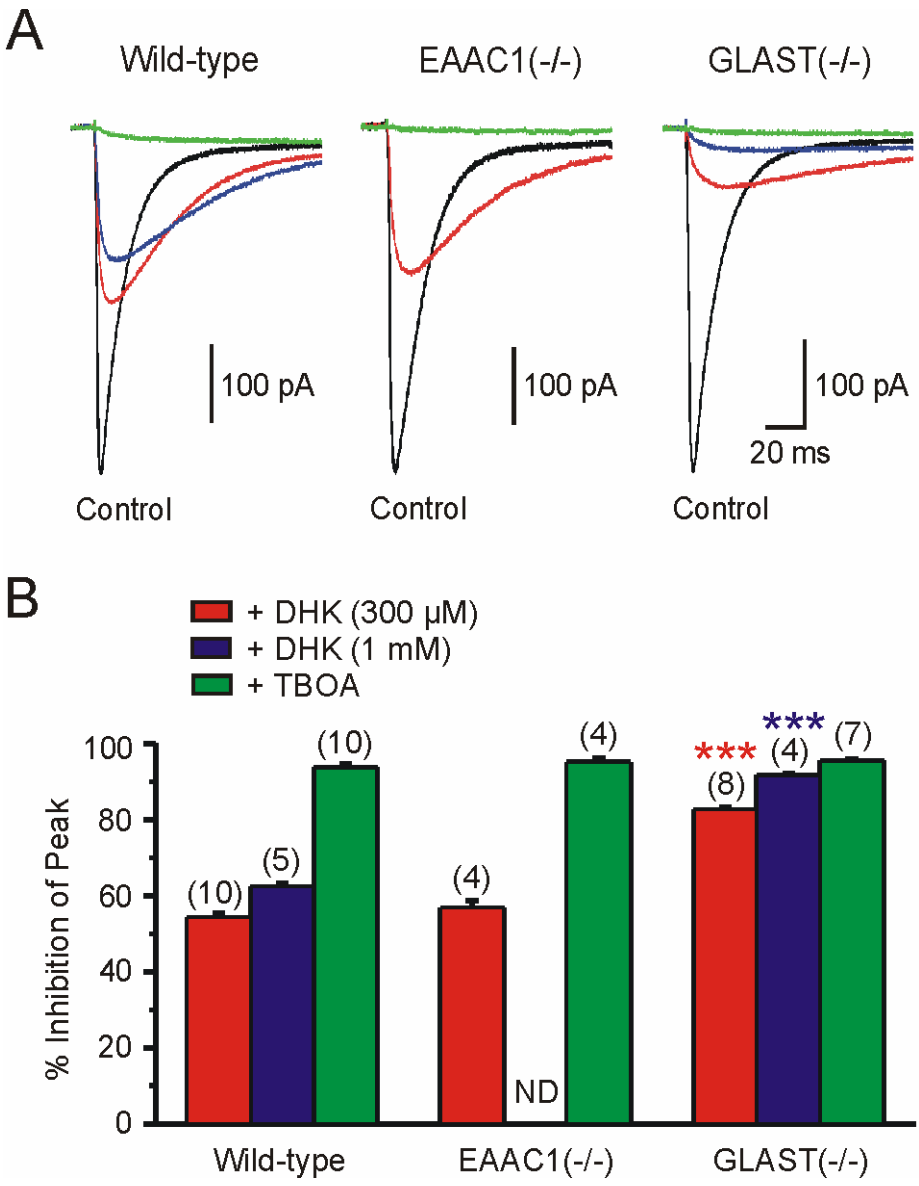
A
Wild-type
EAAC1(-/-)
GLAST(-/-)
100 pA
100 pA
100 pA
20 ms
Control
Control
Control
B
+ DHK (300 µM)
+ DHK (1 mM)
+ TBOA
% Inhibition of Peak
100
80
60
40
20
0
(10)
(5)
(10)
(4)
(4)
ND
(8)
***
***
(4)
(7)
Wild-type
EAAC1(-/-)
GLAST(-/-)

Figure III-7. Inhibition of glutamate transporters induces an mGluR1-dependent delayed burst of IPSCs in CA1 pyramidal cells. *A*, Whole-cell recording from a CA1 pyramidal neuron showing the response to stimulation (10 stimuli @ 100 Hz) in stratum oriens under control conditions. *B*, Response of this cell to the same stimulus in the presence of TBOA (100 μM). *C*, Response of this cell to the same stimulus in the presence of TBOA (100 μM) and the mGluR1 antagonist LY 367385 (100 μM). *D*, Response of this cell to the same stimulus in the presence of TBOA (100 μM) and the $GABA_A$ receptor antagonist SR 95531 (5 μM). *E*, Grouped data showing the charge transfer conveyed by IPSCs recorded from CA1 pyramidal neurons under different conditions, as indicated. The effect of SR 95531 on the burst of IPSCs was analyzed by performing a separate set of experiments (n = 4), in which SR 95531 was applied in the presence of TBOA, but in the absence of LY 367385. (*** = $p < 0.001$; NS = not significant.). Numbers in parenthesis indicate the number of experiments. Recordings were performed using a high Cl^- -based internal solution (Vm = –65 mV) and the ACSF contained 15 μM NBQX, 25 μM GYKI 52466, 10 μM RS-CPP, 50 μM MK-801, 20 μM 7-Chlorokynurenate, and 1 μM CGP 55845.

Figure III- 7

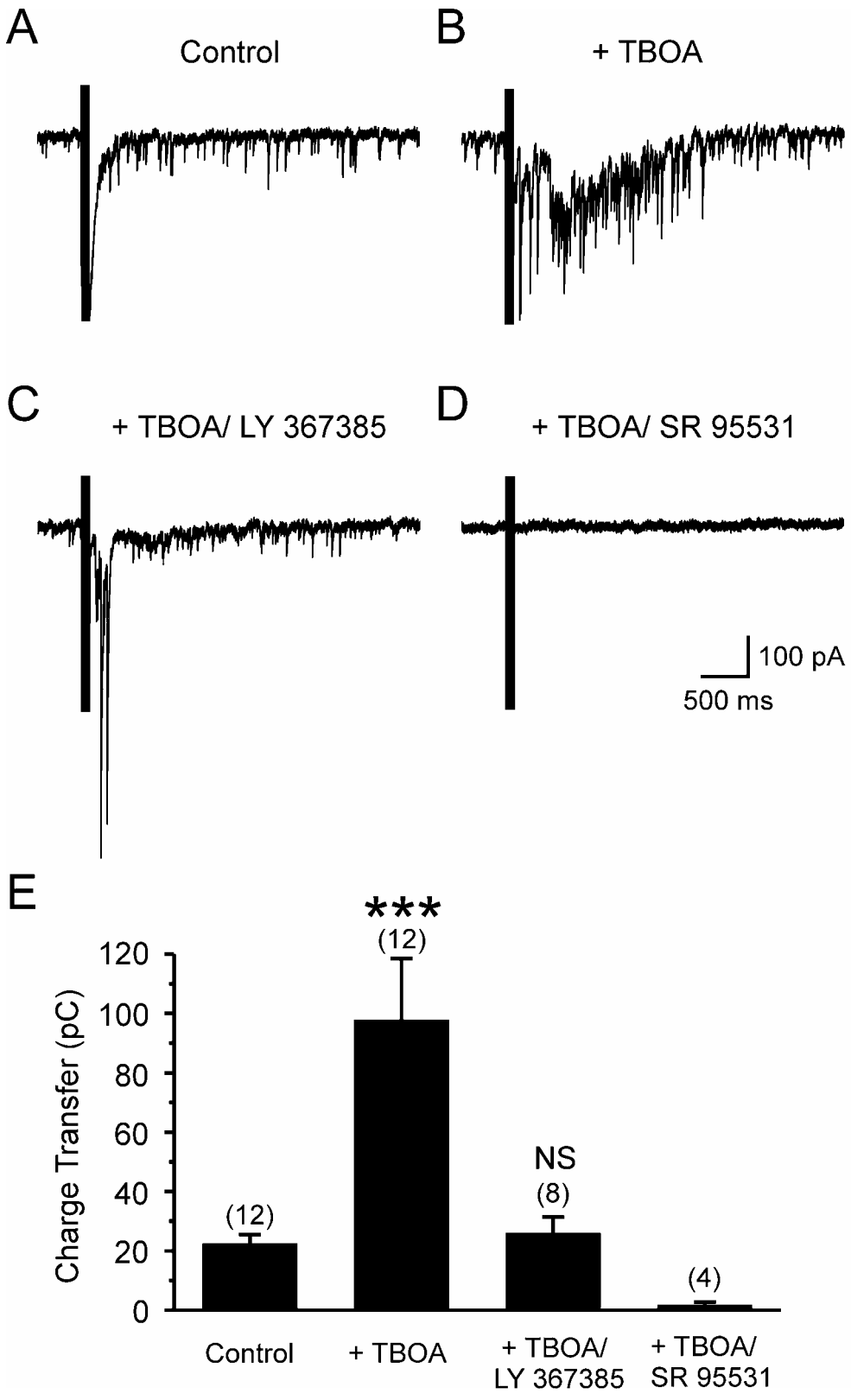
A
Control
B
+ TBOA
C
+ TBOA/ LY 367385
D
+ TBOA/ SR 95531
100 pA
500 ms
E
***
(12)
NS
(8)
(12)
(4)
Charge Transfer (pC)
120
100
80
60
40
20
0
Control
+ TBOA
+ TBOA/
LY 367385
+ TBOA/
SR 95531

Chapter IV

Synthesis and characterization of 4-methoxy-7-nitroindolinyl-D-aspartate, a caged compound for selective activation of glutamate transporters and *N*-methyl-D-aspartate (NMDA) receptors in brain tissue

Introduction

Glutamate transporter activity can be monitored with high temporal fidelity by recording transport-associated charge movements in individual cells. Transporter currents can be elicited from astrocytes in brain slices following stimulation of excitatory afferents (Bergles and Jahr, 1997), by bath application of substrate, by focal application of substrate using pressure, or by photolysis of caged substrates (Huang et al., 2004). The analysis of synaptic transporter currents is complicated by the dependence on nerve terminals for glutamate, while bath application is very slow and lacks spatial precision. Pressure application improves temporal and spatial resolution, but requires positioning of the application pipette within tissue, and responses elicited using this approach exhibit poor stability due to repeated mechanical disruption of surrounding tissue. In contrast, photolysis of caged substrates allows rapid and focal activation of transporters, in a manner free from mechanical artifact.

The D-isomer of aspartate is efficiently transported by high affinity Na^+/K^+ dependent glutamate transporters and is an effective ligand of *N*-methyl-D-aspartate (NMDA) receptors. To facilitate analysis of the regulation of glutamate transporters in

their native membranes we synthesized a photolabile analogue of D-aspartate, 4-methoxy-7-nitroindolinyl -D-aspartate (MNI-D-aspartate) to allow rapid and focal activation of transporters by brief exposure to near UV light.

An ideal caged compound should have the following properties: (1) it must be biologically inert (neither an agonist or antagonist); (2) the compound should be rapidly released upon photolysis (release half-time < 20 microseconds); (3) uncaging should make efficient use of the incident light (exhibit a large extinction coefficient and quantum yield); (4) the caging group by-product should not exhibit activity nor be harmful to cells; and (5) the caged compound must not undergo spontaneous hydrolysis during storage or in physiological buffer. For studies of high affinity receptors such as transporters (K_m range: 4−97 μM) (Arriza et al., 1994) and NMDA receptors (K_m ~ 5 μM) (Olverman et al., 1988), this latter property is particularly important, as this free substrate will alter baseline conditions by causing transporter activation in the absence of light. Our previous studies indicate that MNI-caged L-glutamate (MNI-L-glutamate) is very stable (Matsuzaki et al., 2001), and this knowledge was a prime driving force for the synthesis of MNI-D-aspartate. Although L-glutamate is the primary physiological substrate of glutamate transporters, caged versions of L-glutamate are of limited use for studying the interaction of glutamate receptors and glutamate transporters *in situ*, as the liberated L-glutamate will act on receptors and transporters simultaneously (Canepari et al., 2001). In contrast, D-aspartate offers significant advantages, as it is efficiently transported (Arriza et al., 1994) but it is unlikely to have appreciable activity at AMPA receptors, kainate

receptors, or mGluRs. A previous report described the synthesis of an CNB-caged D-aspartate, and showed that this compound could be used to study the activation kinetics of EAAC1, the primary neuronal glutamate transporter, when heterologously expressed in HEK293 cells (Grewer et al., 2001). However, this caged compound has been reported to be somewhat unstable, a common problem of excitatory amino acids caged with CNB (Pettit et al., 1997), and its activity at glutamate transporters *in situ* has not been examined.

Here we describe the synthesis of a novel caged form of D-aspartate (MNI-D-aspartate), in which the β-carboxylate of D-aspartate is coupled to 4-methoxy-7-nitroindolinyl (MNI) through a photolabile amidic bond (Amit et al., 1976), and examine the responses triggered in neurons and glial cells in acute brain slices upon photolysis. MNI-D-aspartate is stable in solution, can be photolyzed rapidly, and is biologically inert. Upon brief exposure to near-UV light, this compound reliably evoked glutamate transporter currents in astrocytes, Bergmann glial cells, and Purkinje cells, as well as NMDA receptor currents in pyramidal neurons; however, it did not evoke AMPA/kainate or metabotropic glutamate receptor currents. Thus, MNI-D-aspartate can be used to activate glutamate transporters and NMDA receptors in native membranes, and reveal the interactions between receptors and transporters at excitatory synapses in acute brain slices.

Materials and Methods

Synthesis of MNI-D-aspartate:

General Remarks. Silica gel 60 (mesh 63-200 micron) was used for flash chromatography. A Beckman System Gold fitted with Hamilton PRP-1 columns (4.1 x 250 mm, or 20.1 x 250 mm) was used for HPLC. ^{1}H and ^{13}C NMR were measured on a Varian Mercury 300.

Synthesis. N-(*tert*-Butoxycarbonyl)-D-aspartic acid α-*tert*-butyl ester (**2**) was prepared according to a published procedure (Li et al., 2001).

4-Methoxyindolinyl N-(tert-butoxycarbonyl)-D-aspartic acid α-tert-butyl ester (3). N-(*tert*-Butoxycarbonyl)-D-aspartic acid α-*tert*-butyl ester (356 mg, 1.23 mmol), 1,3-dicyclohexylcarbodiimide (254 mg, 1.23 mmol), and 4-dimethylaminopyridine (150 mg, 1.23 mmol) were added to a solution of 4-methoxyindoline (142 mg, 0.95 mmol), synthesized as described previously (Matsuzaki et al., 2001), in dichloromethane (7 ml). The reaction mixture was stirred at room temperature for 20 hours, then it was filtered, diluted with CH_2Cl_2, washed with saturated $NaHCO_3$ solution, 0.5N HCl and brine. The organic layer was dried ($MgSO_4$) and evaporated to dryness. The crude product was purified by flash column chromatography (ethyl acetate/hexane 1:3) to yield product **3** as white solid (357 mg, 0.85 mmol, 89%). ^{1}H NMR ($CDCl_3$) δ 7.8 (1H, d, *J*=8.1 Hz), 7.15 (1H, t, *J*=8.1 Hz), 6.58 (1H, d, *J*=8.1 Hz), 5.82 (1H, d, *J*=8.9 Hz), 4.48 (1H, m), 4.04 (2H, t, *J*=8.2 Hz), 3.83 (3H, s), 3.1 (3H, m), 2.83 (1H, dd, *J* = 4.0, 16.8 Hz), 1.45 (9H, s), 1.44 (9H, s); ^{13}C NMR ($CDCl_3$) δ 170.6, 168.6, 156.0, 155.9, 144.1, 129.1, 118.5, 110.2, 106.4, 82.1, 79.8, 55.6, 50.9, 48.7, 38.7, 28.7, 28.3, 25.5; IR (neat) 3440, 3040, 2980, 2938, 1740, 1710, 1660, 1610, 1490, 1465, 1415, 1365, 1340, 1150, 1060, 840 cm^{-1}; MS (ESI) *m/z* 421.2 ($M+H^{+}$).

4-Methoxy-7-nitroindolinyl N-(tert-butoxycarbonyl)-D-tert-butyl-aspartic acid (4).

To a solution of **3** (357 mg, 0.85 mmol) and silver nitrate (0.287 g, 1.7 mmol) in acetonitrile (10 ml) was added a solution of acetyl chloride (0.133 g , 1.7 mmol) in acetonitrile (5 ml). The reaction mixture was filtered; the filtrate was diluted with ethyl acetate and washed with saturated solution of sodium bicarbonate. The solvent was removed by rotary evaporation, leaving a dark orange oil, which was purified over silica gel using ethyl acetate/hexane (1:2) to yield 251 mg (0.54 mmol, 64%) of product **5**. ^{1}H NMR ($CDCl_3$) δ 7.74 (1H, d, *J*=9.0 Hz), 6.63 (1H, d, *J*=9.0 Hz), 5.67 (1H, broad d, *J*=8.1 Hz), 4.44 (1H, m), 4.22 (2H, t, *J*=8.1 Hz), 3.90 (3H, s), 3.16 (1H, dd, *J* = 4.1, 16.5 Hz), 3.07 (2H, t, *J*=8.1 Hz), 2.97 (1H, dd, *J* = 4.1, 16.5 Hz), 1.47 (9H, s), 1.42 (9H, s); ^{13}C NMR ($CDCl_3$) δ 170.0, 169.1, 158.8, 155.8, 136.4, 135.4, 125.5, 122.8, 106.5, 82.4, 79.8, 56.1, 51.1, 49.0, 37.7, 28.6, 28.1, 26.5; IR (neat) 3420, 3050, 2980, 2930, 1740, 1710, 1680, 1610, 1590, 1530, 1490, 1450, 1390, 1365, 1340, 1270, 1250, 1230, 1150, 1080, 1050, 890, 750, 700 cm^{-1}; MS (ESI) *m/z* 488.2 ($M+Na^{+}$).

4-Methoxy-7-nitroindolinyl-D-aspartic acid (1). TFA (0.7 ml) was slowly added to a solution of compound **4** (113 mg, 0.24 mmol) in dichloromethane (3 ml). The reaction mixture was stirred at room temperature for 20 hours, then the solvent was removed and the crude material was purified by preparative HPLC (isocratic elution with 20% CH_3CN in H_2O) to yield 37 mg (0.12 mmol, 50%) of product **1**. ^{1}H NMR (D_2O) δ 7.78 (1H, d, *J*=9.3 Hz), 6.88 (1H, d, *J*=9.3 Hz), 4.43 (1H, t, *J*=5.0 Hz), 4.29 (2H, t, *J*=8.0 Hz), 3.94 (3H, s), 3.39 (2H, m), 3.08 (2H, t, *J*=8.0 Hz); ^{13}C NMR (D_2O) δ

171.0, 169.2, 159.5, 135.0, 134.3, 125.7, 123.9, 108.3, 56.3, 50.5, 49.7, 34.9, 26.1; MS *m/z* 307.8 ($M\text{-}H^+$).

Quantum Yield. The quantum yield for uncaging MNI-D-aspartate was measured by comparing the time of photolysis with the filtered (280-400 nm) output of a 500 W medium pressure Hg lamp of an equimolar solution (250 μM) of MNI-L-glutamate and MNI-D-aspartate in HEPES ACSF. Inosine was used as an inert internal standard (Ellis-Davies and Kaplan, 1994). The path-length of the cuvette was 0.1 mm.

Slice preparation and Electrophysiology:

Slice Preparation. Hippocampal slices were prepared from 12-17 day-old Sprague-Dawley rats in accordance with a protocol approved by the Animal Care and Use Committee at Johns Hopkins University. Rats were deeply anesthetized with halothane and decapitated, the hippocampi were dissected free, mounted in agar blocks, cut in 400 μm thick transverse sections using a vibratome (VT1000S, Leica), in oxygenated ice-cold artificial cerebrospinal fluid (ACSF) containing (in mM): NaCl 119, KCl 2.5, $CaCl_2$ 2.5, $MgCl_2$ 1.3, NaH_2PO_4 1, $NaHCO_3$ 26.2 and D-Glucose 11. Slices were allowed to recover on a gauze net submerged in ACSF at 37^{o}C for 30 minutes and kept at room temperature thereafter. For cerebellar slices, 250 μm thick parasagittal sections were prepared. Brain slices were used within 7 hours of preparation.

Whole Cell Recording. Brain slices that had recovered for at least one hour were transferred to a Lucite chamber with a coverslip bottom and continuously superfused with oxygenated ACSF. Individual cells (astrocytes, CA1 pyramidal neurons,

Bergmann glial cells, or Purkinje neurons) were visualized through a 40x water immersion objective (Olympus LUMPlanFl, NA = 0.8) using an upright microscope (Axioskop FS2, Zeiss) equipped with infrared-Nomarski optics and a CCD camera (Sony XC-73). Recording electrodes were pulled from glass capillary tubing and had a combined resistance of 1.5-3.0 MΩ when filled with the internal solution. For astrocytes and Bergmann glial cells, the internal solution contained (in mM): KCH_3O_3S (KMeS) 120, EGTA 10, HEPES 20, $MgCl_2$ 1, Na_2ATP 2, NaGTP 0.2; the pH was 7.3. For neuronal recordings the internal solution contained (in mM): $CsCH_3O_3S$ (CsMeS) 105, TEA-Cl 20, EGTA 10, HEPES 20, $MgCl_2$ 1, QX-314 1, Na_2ATP 2, NaGTP 0.2; the pH was 7.3. To record transporter associated anion currents from Purkinje neurons, the internal solution contained (in mM): $CsNO_3$ 100, TEA-Cl 20, EGTA 10, HEPES 20, $MgCl_2$ 1, QX-314 1, Na_2ATP 2, NaGTP 0.2; the pH was 7.3. With these solutions the series resistance during recordings was <10 MΩ, and was left uncompensated. Unless stated otherwise, holding potentials have not been corrected for the junction potential. Whole-cell currents were amplified using an Axopatch 200B (Axon Instruments), filtered at 2-5 kHz and sampled at 10-20 kHz. A 0.5-5 mV step was applied at the beginning of each trace to measure both the membrane and access resistances. Perforated patch recordings were performed in the cell attached patch mode by including Amphotericin-B (120 μg/ml) in the KMeS internal solution.

Solution Application. Caged compounds were dissolved in HEPES buffered saline (HEPES ACSF) containing (in mM): NaCl 137, KCl 2.5, $CaCl_2$ 2.5, $MgCl_2$ 1.3,

HEPES 20; the pH was 7.3. Solutions containing caged compounds were applied to the slice using a wide bore (tip diameter 50-100 μm) pipette connected to a manifold fed by four 10 ml reservoirs. Solutions were switched by alternately opening and closing valves attached to each reservoir. Antagonists were used to block voltage-gated Na^+ channels (tetrodotoxin; TTX, 1 μM), AMPA/kainate receptors (2,3-dioxo-6-nitro-1,2,3,4-tetrahydrobenzo[f]quinoxaline-7-sulfonamide disodium salt; NBQX, 10 μM), NMDA receptors ((RS)-3-(2-carboxypiperazin-4-yl)-propyl-1-phosphonic acid; R,S-CPP, 10 μM; and (5R,10S)-(+)-5-methyl-10,11-dihydro-5H-dibenzo[a,d]cyclo-hepten-5,10-imine hydrogen maleate; MK-801, 50 μM), and $GABA_A$ receptors (6-imino-3-(4-methoxyphenyl)-1(6H)-pyridazinebutanoic acid dihydrobromide; SR-95531, 5 μM). In some experiments, group I mGluRs were blocked with LY367385 (100 μM). Glutamate transporters were inhibited using DL-threo-β-benzyloxyaspartic acid (TBOA, 100-200 μM). The specific blockers used in each experiment are indicated in the figure legends. For each experiment, the caged compound solution contained the same concentration of antagonists present in the bath solution. In some experiments, D-aspartate (500 μM dissolved in HEPES ACSF) was applied locally through a small tip pipette (~1 μm diameter) using a picospritzer (Pressure System IIe, Toohey Company); a 5-10 ms pulse of 15-20 psi was used to eject the solution. All appropriate blockers were included in the puffer pipette solution.

Photolysis of Caged Compounds: For photolysis, an argon ion laser (Stabilite 2017-AR, Spectra-Physics) providing ~ 230 mW or 380 mW of multi-line UV light

(333.6-363.8 nm) was coupled to the microscope through a multi-mode quartz fiber optic cable (Oz Optics Ltd.). The output of the fiber optic was collimated using a quartz lens, projected through the fluorescence port of a Zeiss Axioskop FS2 microscope, and focused to a ~50 μm spot using a 40x water immersion objective (Olympus LUMPlanFl) , or to a ~100 μm spot using a 20x water immersion objective (Olympus UMPlanFl). The UV spot was centered on the soma of astrocytes or pyramidal cells or on the dendritic arbor of the Purkinje cells, using a targeting laser (633 nm HeNe). To control the length of exposure, a computer controlled programmable pulse generator (Master 8, AMP Instruments) was used to trigger a high-speed laser shutter (NM laser) placed between the laser head and the fiber launch. Photolysis was achieved by opening the shutter for 1 ms. In some experiments, the intensity of the laser was varied using the aperture on the laser head. The output intensity for each aperture was measured using a power meter. A laser intensity (at the output) of 230 mW was used for recordings from astrocytes, Bergmann glial cells and pyramidal neurons (40x objective), corresponding to a total light energy of 29 mJ/cm^2. An intensity of 380 mW was used for recordings from Purkinje neurons (20x objective), corresponding to a total light energy of 48 mJ/cm^2. These values reflect the laser power prior to entering the fiber optic; the energy reaching the cell is likely to be considerably less due to loss at the fiber launch, the microscope lenses, and the intervening tissue.

Chemicals Used for Photolysis Experiments: MNI-L-glutamate, NBQX, R,S-CPP, MK-801, LY367385, SR-95531, and TBOA were purchased from Tocris. D-aspartate

was purchased from Sigma. TTX and QX-314 (N-(2,6-dimethylphenyl carbamoylmethyl) triethylammonium chloride) were purchased from Alomone Labs.

Data Analysis and Statistics: Data were analyzed off-line using Clampfit (Axon Instruments) and Origin (Microcal) software. For experiments on astrocytes, only cells in which the amplitude of the response to a –5 mV step changed by less than 25% during the course of an experiment were analyzed. All values are represented as mean ± standard error of the mean. The Student's t-test (paired or unpaired, as appropriate) was used for statistical comparison; $p < 0.05$ was considered significant. The rise time of responses were calculated from 10−90% of the peak the response, and the tau decay was measured using a single exponential least squares fit. Half decay refers to the time required for the response to decay to 50% of the peak amplitude.

Results

Synthesis and quantum yield of MNI-D-aspartate.

The steps involved in the synthesis of MNI-D-aspartate are outlined in Figure IV-1. The requisitely protected D-aspartate was synthesized in the same manner as reported previously for L-aspartate (Li et al., 2001) in a yield of 73%. The beta carboxylate was coupled to 4-methoxyindoline (Matsuzaki et al., 2001) using standard DCCD/DMAP conditions to give **3** in a yield of 89%. The essential nitro functionality was introduced into intermediate **3** using silver nitrate and acetyl chloride (Norman and Radda, 1961) to give 7-nitro indoline **4**, along with the undesired 5-nitro isomer. The yield of **4** after flash chromatography was 64% (the 7 and 5 nitro isomers could easily be separated at this stage, unlike MNI-L-glutamate). The BOC and *tert*-butyl protecting groups were removed by treatment of **4** with TFA to give the target caged D-aspartate, **1**, in a yield of 50% after HPLC purification. HPLC purification of MNI-D-aspartate was essential to remove free D-aspartate.

Quantum yield of photolysis.

The quantum yield of uncaging of MNI-D-aspartate was determined by direct comparison with MNI-L-glutamate. Both caged compounds have the same extinction coefficient, so analysis of the irradiation of an equimolar solution of both compounds, to test the relative extent of photolysis, yields the quantum of MNI-D-aspartate uncaging. We found that when a solution containing 0.25 mM of each compound was irradiated (total OD = 0.215, to ensure uniform photolysis), the quantum yield was

0.09 ± 0.01 (n = 3), slightly faster than MNI-L-glutamate (Matsuzaki et al., 2001).

Photolysis of MNI-D-aspartate triggers glutamate transporter currents in astrocytes.

Glutamate transporters are present at a high density in the membranes of astrocytes in the hippocampus (Lehre and Danbolt, 1998), and application of L-glutamate through pressure or photolysis in brain slices induces an inward current in astrocytes that is blocked by glutamate transporter antagonists (Bergles and Jahr, 1997; Huang et al., 2004). To determine whether photolysis of MNI-D-aspartate is also capable of eliciting glutamate transporter currents *in situ*, we made whole-cell voltage-clamp recordings from astrocytes in the CA1 region of hippocampus and measured their response to UV light in the presence of MNI-D-aspartate. When the ACSF contained antagonists of AMPA, NMDA, and $GABA_A$ receptors, as well as TTX (see **Methods**) to block possible indirect effects resulting from excitation of surrounding neurons, brief (1 ms) exposure to laser UV light produced a rapidly activating, transient inward current in astrocytes (Figure IV-2*A*), that was only observed when the superfusing solution contained MNI-D-aspartate (125 μM). These currents had a slightly faster rise time than responses elicited by photolysis of 125 μM MNI-L-glutamate (rise time: MNI-D-aspartate, 3.1 ± 0.2 ms; MNI-L-glutamate, 3.5 ± 0.2 ms, $p < 0.001$) but slightly slower decay kinetics (decay tau: MNI-D-aspartate, 16.9 ± 0.9 ms, n = 11; MNI-L-glutamate, 15.4 ± 0.6 ms, $p < 0.05$, n = 11) (Figure IV-2*B*) (Huang et al., 2004). The peak amplitude of these responses was reduced by 94.5 ± 0.6 % (n = 4) by

TBOA (200 μM), a selective antagonist of glutamate transporters (Shigeri et al., 2001; Shimamoto et al., 1998) (Figure IV-2*C*). These currents reflect the movement of charges that are directly coupled to the flux of glutamate, as they were recorded with an internal solution (KMeS) which does not reveal the glutamate transporter-associated anion conductance (Bergles et al., 2002). Increasing the temperature from room temperature (22−24° C) to near physiological temperature (34−36° C) increased the amplitude of these responses by 34.1 ± 6.2 % ($P < 0.01$) and decreased the rise time by 10.0 ± 3.5 % ($P < 0.05$) and the decay time by 29.9 ± 2.6 % ($n = 5$, $p < 0.001$) (Figure IV-2*D*), in accordance with the high temperature dependence exhibited by glutamate transporters (Bergles and Jahr, 1998; Wadiche et al., 1995). However, the charge transfer induced by these currents was similar at higher temperature (5.0 ± 3.2 % increase, $p = 0.099$, $n = 5$), suggesting that a comparable amount of D-aspartate was transported at both temperatures. These results indicate that laser induced photolysis of MNI-D-aspartate releases the free amino acid, which is then removed by glutamate transporters in astrocyte membranes.

By varying the intensity of UV light it was possible to control the amount of D-aspartate liberated. As shown in Figure IV-3*A*, the peak amplitude of astrocyte transporter currents increased monotonically with increasing laser power, suggesting that glutamate transporters were operating in a linear range of their dose-response curve under these conditions. As expected from the concentration dependence of binding, the rise times of glutamate transporter currents became faster as the laser intensity was increased, from 2.1 ± 0.1 ms at 50% laser power to 1.7 ± 0.1 ms ($n = 3$,

$p < 0.01$) at 100% (relative) power (230 mW at laser output; 50 μm spot illumination), similar to concentration-dependent effects on transporter currents observed in outside-out patches removed from astrocytes (Bergles and Jahr, 1997). However, unlike responses recorded from patches, photolysis-induced glutamate transporter currents recorded *in situ* became more prolonged as more D-aspartate was released (half decay time: 50% relative intensity, 22.8 ± 4.1 ms; 100% relative intensity, 27.2 ± 4.5 ms, n = 3, $p < 0.01$), suggesting that clearance from within the tissue is delayed as more D-aspartate is liberated, or that additional GLAST transporters, which exhibit a lower affinity and slower transport rate for D-aspartate (*17*), are recruited at higher laser intensities.

In addition to the transient response, glutamate transporter currents recorded from astrocytes exhibited a slowly decaying "tail current" that required several seconds to return to baseline (Figure IV-3*B*), similar to transporter currents evoked in astrocytes through synaptic release (Bergles and Jahr, 1997). The amplitude of this prolonged inward current was ~ 2% of the peak, and this proportion remained fixed at all laser intensities (Figure IV-3*B*). This tail current is unlikely to have resulted from activation of voltage-gated channels in surrounding neurons, as UV illumination under these conditions did not elicit a response from surrounding neurons (see Figure IV-7). These results suggest that the photolysis induced tail current occurs as a direct result of glutamate transporter activation.

Physiological properties and aqueous stability of MNI-D-aspartate.

An ideal caged substrate of glutamate transporters should not act as a substrate or an antagonist, and should be stable in aqueous solution. To determine whether our new caged compound is a substrate for glutamate transporters we measured the response of astrocytes to a high concentration of MNI-D-aspartate. Although perfusion of free D-aspartate (500 μM) induced an inward current of –134.7 ± 41.0 pA (n = 4), application of 500 μM MNI-D-aspartate did not elicit a consistent response (–15.2 ± 11.3 pA, n = 6, $p > 0.05$), indicating that the caged compound is not a substrate for glutamate transporters. Although MNI-D-aspartate did not activate glutamate transporters, it could act as an antagonist, similar to the aspartate analogues TBOA and THA (Shimamoto et al., 1998). This is a significant concern because other caged neurotransmitters (e.g., 4-methoxycarbonyl-7-nitroindolinyl-caged-GABA and -glycine) have been demonstrated to have antagonistic properties at their respective receptors (Canepari et al., 2001). To determine whether MNI-D-aspartate is an antagonist of glutamate transporters, we examined the effect of the caged compound on responses evoked through local pressure application of D-aspartate (500 μM). As shown in Figure IV-4*A*, application of MNI-D-aspartate (500 μM) did not significantly change the amplitude, charge transfer, or time course of transporter currents induced by D-aspartate, indicating that the caged compound is not a glutamate transporter antagonist. To assess the stability of the caged compound, a 500 μM solution of MNI-D-aspartate was prepared in HEPES-ACSF (pH 7.3), stored at 4^{o} C in the dark, and applied to astrocytes 2 and 4 days later. This solution produced a

change in holding current of 10.0 ± 18.8 pA (n = 6) at 2 days and –8.7 ± 3.3 pA (n = 3) at 4 days, indicating that this compound is highly stable in aqueous solution. The amplitude of glutamate transporter currents induced by photolysis of MNI-D-aspartate was dependent on the concentration of MNI-D-aspartate, the relative locations of the superfusion pipette, the cell, and the illumination area, as well as the depth of the cell within the slice. For a given configuration, the peak amplitude of the transporter current was stable for ~30 minutes with repeated uncaging (Figure IV-4*B*), but became more prolonged over time (half decay time was increased by 26.5 ± 5.9 % after 30 min, n = 4, $p < 0.001$).

Glutamate transporter currents evoked in Bergmann glial cells through photolysis of MNI-D-aspartate.

Astroglial cells throughout the CNS express glutamate transporters (Danbolt, 2001), but the types of transporters expressed and their density vary among cells in different brain regions. Bergmann glial cells contribute to the clearance of glutamate released at climbing fiber and parallel fiber terminals in the molecular layer of the cerebellum (Bergles et al., 1997; Clark and Barbour, 1997; Lehre et al., 1995; Rothstein et al., 1994). To determine if MNI-D-aspartate can also be used to activate glutamate transporters in Bergmann glial cells, we made whole cell recordings from these cells in acute cerebellar slices and measured their response to uncaging of MNI-D-aspartate. As shown in Figure IV-5*A*, an inward current was triggered in Bergmann glial cells by the same uncaging conditions that were used to elicit glutamate transporter currents in

astrocytes (125 μM MNI-D-aspartate, 1 ms UV exposure), and this current was similarly inhibited by TBOA (200 μM) . Responses elicited from Bergmann glial cells were smaller on average than responses recorded from astrocytes (Bergmann glia: 63.2 ± 7.3 pA, n = 7; Astrocytes: 454.5 ± 84.9 pA, n = 4, $p < 0.01$) and were inhibited less by TBOA (% inhibition: Bergmann glia, 81.5 ± 1.1 %, n = 7, $p < 0.01$) (Figure IV-5*B*). These data are consistent with the lower affinity of TBOA for GLAST (Shimamoto et al., 1998), the primary glutamate transporter expressed by Bergmann glia (Lehre et al., 1995; Rothstein et al., 1994), than GLT-1, the primary glutamate transporter expressed by astrocytes (Lehre and Danbolt, 1998). Bergmann glial responses also exhibited slower rise and decay kinetics than transporter currents recorded from astrocytes, perhaps reflecting both the lower affinity of GLAST for D-aspartate (Arriza et al., 1994) and the lower density of transporters expressed by Bergmann glial cells (Lehre and Danbolt, 1998).

Glutamate transporter currents evoked in Purkinje cells through photolysis of MNI-D-aspartate.

The previous results indicate that MNI-D-aspartate can be used to probe transporter activity in astroglial cells. To determine whether this compound is also suitable for monitoring glutamate transporter activity in neurons, we examined photolysis-induced responses in cerebellar Purkinje neurons. Purkinje neurons express EAAT4, a glutamate transporter that exhibits a 10-fold higher affinity for glutamate, cycles 5-10 times more slowly than other glutamate transporters, and exhibits a high permeability

to anions (Fairman et al., 1995). This transporter contributes to uptake at parallel fiber and climbing fiber synapses, and currents produced by EAAT4 cycling have been recorded in response to synaptic (Auger and Attwell, 2000; Huang et al., 2004; Otis et al., 1997) and photorelease of L-glutamate (Brasnjo and Otis, 2004; Canepari et al., 2001), and have been used to estimate the amount of glutamate released at climbing fiber synapses (Auger and Attwell, 2000; Huang et al., 2004; Otis et al., 1997). To determine if photolysis of MNI-D-aspartate is able to elicit detectible glutamate transporter currents in Purkinje neurons, we measured the response of these neurons to photolysis of 500 μM MNI-D-aspartate in the presence of ionotropic glutamate and $GABA_A$ receptor antagonists, and TTX (see **Methods**). When the UV illumination (~ 100 μm diameter spot) was centered in the molecular layer over Purkinje cell dendrites, an inward current of –89.6 ± 25.9 pA (range: –41.1 to –172.6 pA, n = 6) was elicited following a 1 ms exposure to UV light (Figure IV-6*A*). These currents exhibited a rise time of 4.0 ± 0.6 ms and a half decay time of 54.8 ± 3.8 ms (n = 6; CsMeS-based internal solution), and were inhibited by 86.3 ± 0.13 % (n = 3) by 200 μM TBOA. These transporter currents were much smaller than the currents recorded from astrocytes or Bergmann glia under comparable conditions (see Figures 2 & 5), consistent with the lower density of transporters in Purkinje neurons (Dehnes et al., 1998). Charge movements associated with glutamate transport are enhanced in the presence of anions such as nitrate (NO_3^-) and thiocyanate (SCN^-), which permeate these transporters in a manner uncoupled from the flux of glutamate (Wadiche et al., 1995). Photolysis-induced transporter currents recorded from Purkinje neurons

recorded with a $CsNO_3$-based internal solution were larger ($CsNO_3^-$: –634.4 ± 62.5 pA, $p < 0.001$) and exhibited slower rise times ($CsNO_3^-$: 13.1 ± 0.8 ms, n = 8, $p < 0.001$) than responses recorded with a CsMeS-based internal solution (Figure IV-6*B*, *C*), consistent with previous observations (Auger and Attwell, 2000; Huang et al., 2004).

Purkinje neurons also express mGluR1, a metabotropic glutamate receptor that triggers release of calcium from internal stores and opens non-selective cation channels in the plasma membrane (Canepari et al., 2001; Kim et al., 2003). Photorelease of L-glutamate has been shown to elicit inward currents mediated by mGluRs in these neurons (Canepari et al., 2001). To determine whether the D-aspartate liberated by photolysis activates mGluRs we compared the response of Purkinje neurons to photolysis of MNI-D-aspartate (500 μM) and MNI-L-glutamate (500 μM). In the presence of TBOA (and antagonists of AMPA, NMDA, and $GABA_A$ receptors, and TTX), photolysis of MNI-L-glutamate produced a large (–500 to –1600 pA), slowly activating inward current in Purkinje neurons (Figure IV-6*D*) that was inhibited by 93.5 ± 2.4 % (n = 3) by the mGluR1 antagonist LY 367385 (100 μM) (Figure IV-6*E*). This slow inward current was not observed in response to photolysis of MNI-D-aspartate (n = 7/7 cells) (Figure IV-6*D*, *F*), even when uptake was blocked with TBOA, indicating that the released D-aspartate does not activate mGluR1. Notably, a small (~10 pA) rapidly activating inward current was observed in response to photolysis of MNI-L-glutamate (in the presence of 25 μM NBQX and TBOA), but not MNI-D-aspartate (see Figure IV-6*D*,*E*), presumably due to the activation of

kainate receptors (Huang et al., 2004).

NMDA receptor activation following photolysis of MNI-D-aspartate.

Ionotropic glutamate receptors exhibit striking differences in affinity and stereoselectivity for aspartate; NMDA receptors have a similar affinity for D- and L-aspartate (D-aspartate, 10 μM; L-aspartate, 11 μM) (Olverman et al., 1988), while AMPA receptors have an extremely low affinity for both L- and D-aspartate (Patneau and Mayer, 1990). To determine if MNI-D-aspartate can also be used to selectively activate NMDA receptors in neurons, we measured the response of CA1 pyramidal neurons to photolysis of MNI-D-aspartate. In the absence of antagonists of glutamate receptors or transporters, photolysis of MNI-D-aspartate produced an inward current when pyramidal neurons were held at –30 mV (Figure IV-7*A*). The current-to-voltage relationship of this response reversed at 0 mV and contained an area of negative slope conductance, characteristic of responses mediated by NMDA receptors (Figure IV-7*B*). These currents were blocked by R,S-CPP (10 μM) and MK-801 (50 μM), indicating that the D-aspartate released by photolysis of MNI-D-aspartate results in selective activation of NMDA receptors in CA1 pyramidal neurons (Figure IV-7*B*). Transporter currents were not observed in these neurons, presumably due to the low level of expression of EAAC1 (Bergles and Jahr, 1998; Danbolt, 2001). MNI-D-aspartate (500 μM) did not induce an outward current in neurons held at 25 mV (n = 6), indicating that there was little free D-aspartate in the solution and that MNI-caged D-aspartate does not activate NMDA receptors. To address whether MNI-D-aspartate acts as an

inhibitor, we measured D-aspartate evoked NMDA receptor currents in the presence or absence of MNI-D-aspartate. As shown in Figures 7C and 7D, MNI-D-aspartate (500 μM) did not alter the amplitude or kinetics of NMDA receptor currents evoked through focal application of D-aspartate (500 μM) (n = 6). These data indicate that MNI-D-aspartate is neither an agonist nor antagonist of NMDA receptors, yet can be rapidly photolyzed by UV light to release free D-aspartate that can activate NMDA receptors in neuronal membranes.

Discussion

Glutamate transporters expressed in neuronal and glial membranes set the level of ambient glutamate, shape the activation of receptors at synapses, and help maintain synapse specificity (Danbolt, 2001; Huang and Bergles, 2004). Despite the importance of these transporters in regulating glutamate dynamics under physiological and pathological conditions, we know little about how their activity is regulated *in vivo*. Studies of glutamate transporters in heterologous systems have yielded conflicting results (Dowd and Robinson, 1996; Gonzalez and Robinson, 2004; Trotti et al., 2001), highlighting the importance of studying these processes in their native membranes. Yet, few studies have examined the regulation of transporters in brain tissue, due to the challenges inherent in working with intact preparations. To enable such analysis, we have developed a novel caged analogue of D-aspartate (MNI-D-aspartate), because D-aspartate is efficiently transported by glutamate transporters (Arriza et al., 1994) but has a low affinity for many glutamate receptors. We found that MNI-D-aspartate is neither an agonist nor an antagonist of glutamate transporters, and is stable in aqueous solution for a period of days (in the dark at 4° C), yet can be photolyzed to release D-aspartate upon exposure to near-UV light. Photolysis of this compound elicited transient glutamate transporter currents in astrocytes, Bergmann glia, and Purkinje neurons in acute brain slices, but did not activate AMPA/kainate receptors or mGluRs. Thus, the combination of MNI-D-aspartate photolysis and electrophysiological monitoring of glutamate transporter currents represents a promising approach for examining the interaction

between receptors and transporters at synapses in semi-intact tissue.

Photorelease of D-aspartate reveals a high density of transporters in astrocyte membranes

Laser induced photolysis of MNI-D-aspartate in hippocampal slices triggered an inward current in astrocytes. Because these currents were recorded in the absence of anions that exhibit a high permeability through glutamate transporters (Wadiche et al., 1995), they reflect the net influx of two positive charges that accompany each molecule of glutamate (Levy et al., 1998; Zerangue and Kavanaugh, 1996). Thus, a movement of 33.6 pC of charge (see Figure IV-2) corresponds to the transport of 10.5 x 10^7 molecules of D-aspartate, and activation of an equal number of transporters, if it is assumed that the transporters complete a single cycle following brief photolysis (Bergles and Jahr, 1997); this assumption is based on the slow cycling time of astrocyte glutamate transporters (time constant: 35 ms) (Bergles and Jahr, 1998) and EAAT2 (time constant: 137 ms) (Wadiche and Kavanaugh, 1998) when transporting D-aspartate, as compared to the decay of the photolysis-induced transporter current (time constant: 17 ms). It is likely that this measurement underestimates the total number of transporters activated in a single cell, as some of the charge associated with transport is lost through the low resistance astrocyte membrane (Bergles and Jahr, 1997; Dzubay and Jahr, 1999). It is possible that activation of glutamate transporters on a neighboring astrocyte could have contributed to the currents recorded from single astrocytes; however, previous studies suggest that the high resting conductance of the

astrocyte membrane limits current spread through the astrocyte syncytium (Bergles and Jahr, 1997). The slow time course of these transporter currents suggests that the peak concentration of D-aspartate achieved during the 1 ms pulse was sub-saturating (Bergles et al., 2002). Together, these data indicate that a high density of functional glutamate transporters are expressed by astrocytes in this region, consistent with previous immunogold density measurements (Lehre and Danbolt, 1998), and functional assays (Bergles and Jahr, 1997; Diamond and Jahr, 2000). By comparison, glutamate transporter currents recorded from Purkinje neurons under similar conditions (50 μm spot, 125 μM MNI-D-aspartate) were more than 100-fold smaller. In order to maximize the transporter current from Purkinje neurons, we increased the area of illumination and the concentration of MNI-D-aspartate. Photolyic release of D-aspartate under these conditions resulted in the movement of ~ 8.4 pC of charge (see Figure IV-6), reflecting the activation of 2.6×10^7 transporters in these neurons, if it is assumed that the only one cycle of transport is completed due to slow transport of D-aspartate by EAAT4 (Fairman et al., 1995). Although these results indicate that there are fewer EAAT4 transporters in the membranes of Purkinje neurons (Dehnes et al., 1998; Lehre and Danbolt, 1998), these transporters may reach a high density near synapses, particularly in parasagittal zones that are enriched in EAAT4 (Dehnes et al., 1998). Somewhat surprisingly, glutamate transporter currents recorded from Bergmann glial cells were ~10 fold smaller than those recorded from astrocytes. This may reflect the ~2-fold lower density of glutamate transporters in Bergmann glial cell membranes (Lehre and Danbolt, 1998), and the smaller membrane area of individual

Bergmann glial cells.

Glutamate transport raises extracellular K^+

In astrocyte recordings, photolysis of either MNI-D-aspartate or MNI-L-glutamate (Huang et al., 2004) produced a fast transient current that decayed in ~ 30 ms, and a small tail current that decayed over several seconds. This biphasic waveform is similar to glutamate transporter currents recorded from astrocytes (Bergles and Jahr, 1997) and Bergmann glial cells (Clark and Barbour, 1997) following electrically evoked release of glutamate from nerve terminals. It was initially proposed that the slowly decaying component of the synaptic transporter current resulted from the release of K^+ from axons following stimulation (Bergles and Jahr, 1997); because astrocytes exhibit a very high resting conductance to K^+, release of K^+ during axonal repolarization may shift the K^+ equilibrium potential and depolarize the astrocyte membrane. Indeed, the slow decay of the tail current is consistent with the slow clearance of K^+ from the extracellular space (Aitken and Somjen, 1986). Glutamate transporters counter transport one K^+ ion to complete the transport cycle (Kanner and Bendahan, 1982), suggesting that transporter activity alone may contribute to the accumulation of K^+. In support of this conclusion, the tail current was observed following photolysis of MNI-D-aspartate when all neuronal activity was blocked. Furthermore, the amplitude of this current was the same proportion (~ 2%) of the peak amplitude over a wide range of light intensities, as expected if the tail current occurs as a consequence of transporter activity. The tail current depolarized astrocytes

by ~1 mV in response to intense UV illumination (500 μM MNI-D-aspartate; data not shown), suggesting that glutamate transporter activity increased the extracellular concentration of K^+ by about 100 μM, assuming that the astrocyte membrane behaves like a perfect K^+ electrode. These results suggest that glutamate transporters may contribute to the rise in extracellular K^+ during periods of intense coordinated activity. By comparison, the tail current observed in astrocytes following electrical stimulation of axons was ~10% of the peak amplitude of the transporter current (Bergles and Jahr, 1997), indicating that the majority of the tail current recorded under these conditions results from the release of K^+ from axons rather than by transporters.

Comparison of CNB-D-aspartate and MNI-D-aspartate

A prior study examined the kinetics of transporter-associated anion currents in EAAC1-expressing HEK293 cells following photolysis of CNB-D-aspartate (Grewer et al., 2001), a compound that has an approximately two-fold higher quantum yield than that of MNI-D-aspartate (MNI-D-aspartate: 0.09; α-CNB-D-aspartate: 0.19). In these cells, D-aspartate-induced transporter currents exhibited a slower rise time than currents evoked by photolysis of CNB-L-glutamate, and lacked discrete peak and steady-state components (Grewer et al., 2001). In contrast, astrocyte transporter currents induced by photolysis of MNI-D-aspartate exhibited rise and decay kinetics that were comparable to responses evoked by MNI-L-glutamate (see Figure IV-2*B*). These results are consistent with the similar kinetics of GLT-1 transporter currents induced by L-glutamate and D-aspartate (Bergles et al., 2002). Notably, EAAT2

(GLT-1) exhibits a higher affinity for D-aspartate than for L-glutamate (K_m: D-aspartate, 13 μM; L-glutamate, 18 μM), while EAAT3 (EAAC1) exhibits a lower affinity for D-aspartate (K_m: D-aspartate, 47 μM; L-glutamate, 28 μM)(Arriza et al., 1994). As suggested by Grewer et al. (Grewer et al., 2001), the slower kinetics of EAAC1 currents in response to D-aspartate may indicate that binding of D-aspartate was rate limiting in their experiments. However, their study examined transporter associated anion currents, which do not always mimic the movement of coupled charges (Bergles et al., 2002). In addition, the duration of the responses triggered by CNB-D-aspartate (> 120 ms), and the distinct steady-state component of the EAAC1 transporter current, indicate that transporters were exposed to D-aspartate for a longer time in their experiments, which may accentuate kinetic differences among substrates. Carboxylic acids caged by esterification with the CNB chromophore have been shown to undergo (spontaneous) hydrolysis in physiological buffers (Grewer et al., 2001; Pettit et al., 1997). In contrast, we were unable to detect free D-aspartate in solutions of MNI-D-aspartate, indicating that this compound may be more suitable for analysis of high affinity receptors and transporters *in situ*.

D-aspartate accumulation and operation of transporters in exchange mode

Although the rise times of astrocyte transporter currents to photorelease of D-aspartate and L-glutamate were similar, the decay of responses to D-aspartate was slightly slower (see Figure IV-2*B*). Furthermore, the decay time of D-aspartate induced transporter currents became longer over time with repeated stimulation, an

effect that was less apparent when L-glutamate was photoreleased. Transporters can, under certain conditions, operate in an exchange mode during which the movement of substrate into the cell is followed by the movement of this or another substrate back out (Dunlop, 2001; Kanner and Bendahan, 1982). Such activity can prolong transporter currents and slow the clearance of substrate (Isaacson and Nicoll, 1993), and may contribute to the relatively low efficiency of glutamate transporters (Bergles et al., 2002; Otis and Jahr, 1998; Wadiche and Kavanaugh, 1998). Because D-aspartate is not metabolized, it is possible that the prolongation of the transporter currents results from accumulation and subsequent release of D-aspartate by homoexchange.

Cerebellar Purkinje neurons are the only neurons in the brain where glutamate transporter currents have been resolved. These neurons express EAAT4, a glutamate transporter that exhibits a high conductance to anions (Fairman et al., 1995). Transporter currents mediated by EAAT4 have been recorded from Purkinje neurons in response to synaptic stimulation (Auger and Attwell, 2000; Huang et al., 2004; Otis et al., 1997) and photorelease of glutamate (Brasnjo and Otis, 2004; Canepari et al., 2001). Photorelease of L-glutamate elicits a complex response resulting from the activation of AMPA, kainate, and mGluRs, in addition to glutamate transporters (Canepari et al., 2001); in contrast, we found that photolysis of MNI-D-aspartate reliably evoked a small inward current in these neurons that was selectively mediated by glutamate transporters, as this D-aspartate induced current was larger when recorded with a NO_3^-–based internal solution and was blocked by TBOA. Purkinje

cell transporter currents decayed in two phases, an initial rapid decay (to 27.2 ± 1.2 % of peak in 16.8 ± 1.6 ms, n = 6), and a slower phase that became prominent at higher laser intensities, similar to responses observed in Purkinje neurons with 7-nitroindolinyl (NI)-caged L-glutamate when glutamate receptors were blocked (Canepari et al., 2001). The slower phase of decay was also enhanced when Cs^+ rather than K^+ was used as the primary internal cation (data not shown). Because internal Cs^+ does not support transporter cycling as well as K^+ (Barbour et al., 1991; Bergles et al., 2002), internal solutions with this cation may allow a greater fraction of the transporters to operate in exchange mode (Kanner and Bendahan, 1982). Thus, although internal Cs^+ and TEA will increase membrane resistance and improve voltage-clamp in whole-cell recordings, they may significantly disrupt transporter cycling and alter baseline synaptic currents.

MNI-D-aspartate as a tool for activating NMDA receptors in brain slices

Unlike AMPA receptors, NMDA receptors exhibit little stereoselectivity for aspartate isomers, and exhibit an affinity for aspartate that is comparable to L-glutamate (Olverman et al., 1988). We found that photolysis of MNI-D-aspartate triggered NMDA receptor-mediated currents, but not AMPA-, kainate- or mGluR-mediated currents, in hippocampal CA1 pyramidal neurons. These currents were comparable in both kinetics and amplitude to NMDA receptor mediated currents evoked through release of glutamate at Schaffer collateral-commissural synapses (Arnth-Jensen et al., 2002; Diamond, 2001). MNI-D-aspartate did not act as an antagonist of NMDA

receptors, and was stable in physiological saline. A photolabile analogue of NMDA (β-DNB NMDA) has been developed as a tool for investigating the kinetics of NMDA receptors (Gee et al., 1999). However, because NMDA is not a substrate for glutamate transporters, clearance of NMDA within the slice is dependent on diffusion alone. As a result, photorelease of NMDA is likely to produce long-duration NMDA receptor-mediated currents, limiting temporal resolution and causing substantial receptor desensitization. The properties of MNI-D-aspartate described here suggest that it may be more suitable than caged analogues of NMDA for examining NMDA receptor function in brain slices.

Figure IV-1. Synthesis and structure of MNI-D-aspartate.

Figure IV- 1

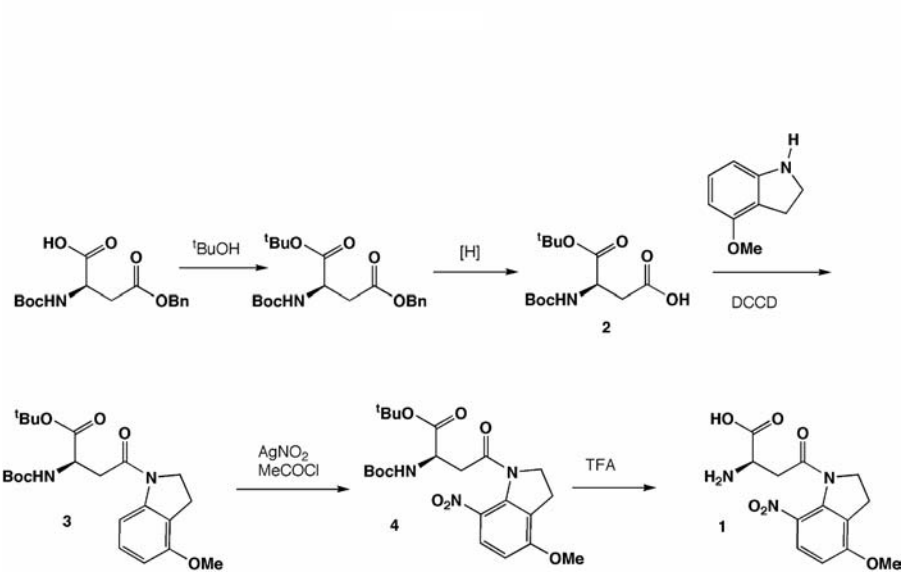
HO
O
O
BocHN
OBn
tBuOH
tBuO
O
O
BocHN
OBn
[H]
tBuO
O
O
BocHN
OH
2
H
N
OMe
DCCD
tBuO
O
O
BocHN
N
3
OMe
AgNO2
MeCOCl
tBuO
O
O
BocHN
N
O2N
4
OMe
TFA
HO
O
O
H2N
N
O2N
1
OMe

Figure IV-2. Photolysis of MNI-D-aspartate activates glutamate transporter currents in hippocampal astrocytes. *A*, A transient inward current was elicited in an astrocyte by a 1 ms flash of UV laser light in the presence but not in the absence of MNI-D-aspartate (MNI-D-Asp, 125 μM). The trace above shows the duration of UV exposure. *B*, The response elicited by photolysis of MNI-D-aspartate (MNI-D-Asp, 125 μM, *red trace*) exhibited similar kinetics to the response elicited by photolysis of MNI-L-glutamate (MNI-L-Glu, 125 μM). *C*, The current evoked by photolysis of MNI-D-aspartate was reversibly inhibited by TBOA (200 μM). *D*, The glutamate transporter current evoked in astrocytes by photolysis of MNI-D-aspartate exhibited a larger peak amplitude and faster decay at near physiological temperature. (R.T., room temperature). All recordings were made from astrocytes located in stratum radiatum of area CA1, in the presence of TTX (1 μM), R,S-CPP (10 μM), MK-801 (50 μM) and NBQX (10 μM). Astrocytes were voltage-clamped at –80 mV with a KMeS-based internal solution.

Figure IV- 2

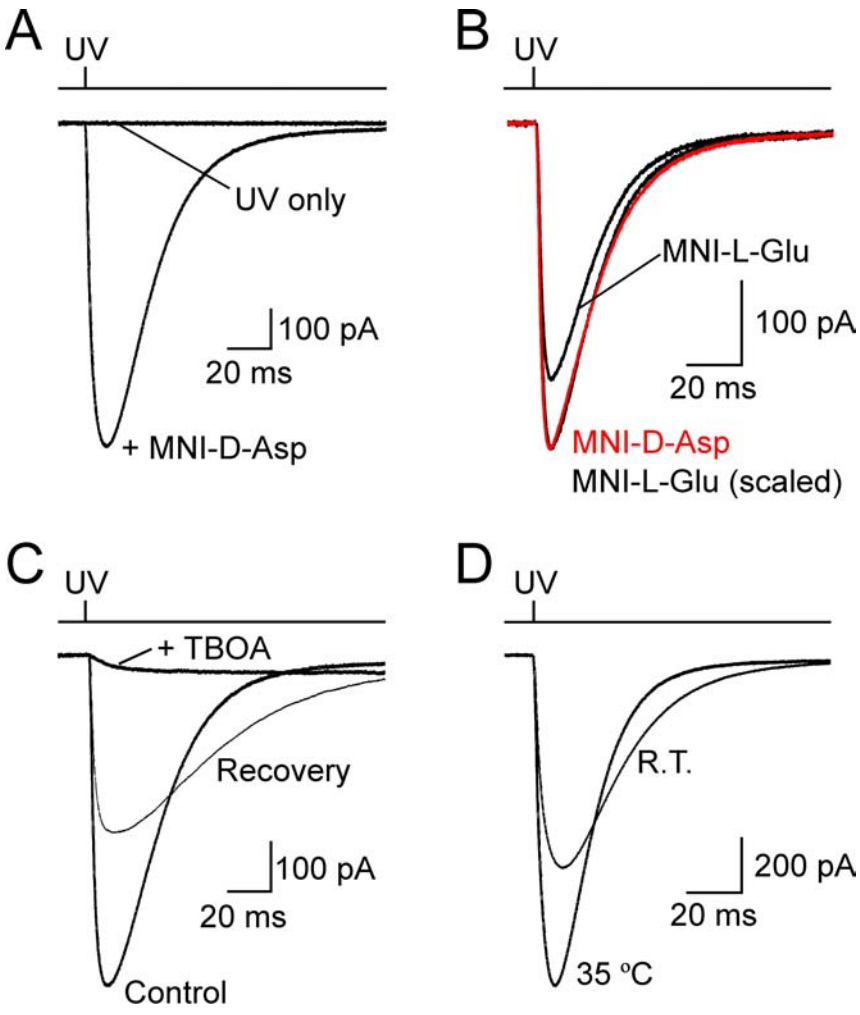
A
UV
UV only
100 pA
20 ms
+ MNI-D-Asp
B
UV
MNI-L-Glu
100 pA
20 ms
MNI-D-Asp
MNI-L-Glu (scaled)
C
UV
+ TBOA
Recovery
100 pA
20 ms
Control
D
UV
R.T.
200 pA
20 ms
35 °C

Figure IV-3. Photolysis evoked glutamate transporter currents recorded at different UV light intensities. *A*, *Left*, Glutamate transporter currents induced in a hippocampal astrocyte by uncaging MNI-D-aspartate (125 μM) with a range of UV light intensities. *Right*, Grouped data showing the relationship between light intensity and the normalized peak amplitude of the evoked transporter current (n = 3). *B*, *Left*, A single response recorded from an astrocyte in response to MNI-D-aspartate photolysis illustrating the discrete peak and tail currents. *Right*, Grouped data showing the relative amplitude of the tail current (% of peak) at different UV light intensities. The tail current was measured by averaging the current 500-600 ms after the flash (n = 3). All recordings were made from astrocytes located in stratum radiatum of area CA1, in the presence of TTX (1 μM), R,S-CPP (10 μM), MK-801 (50 μM) and NBQX (10 μM). Astrocytes were voltage-clamped at –80 mV with a KMeS-based internal solution.

Figure IV- 3

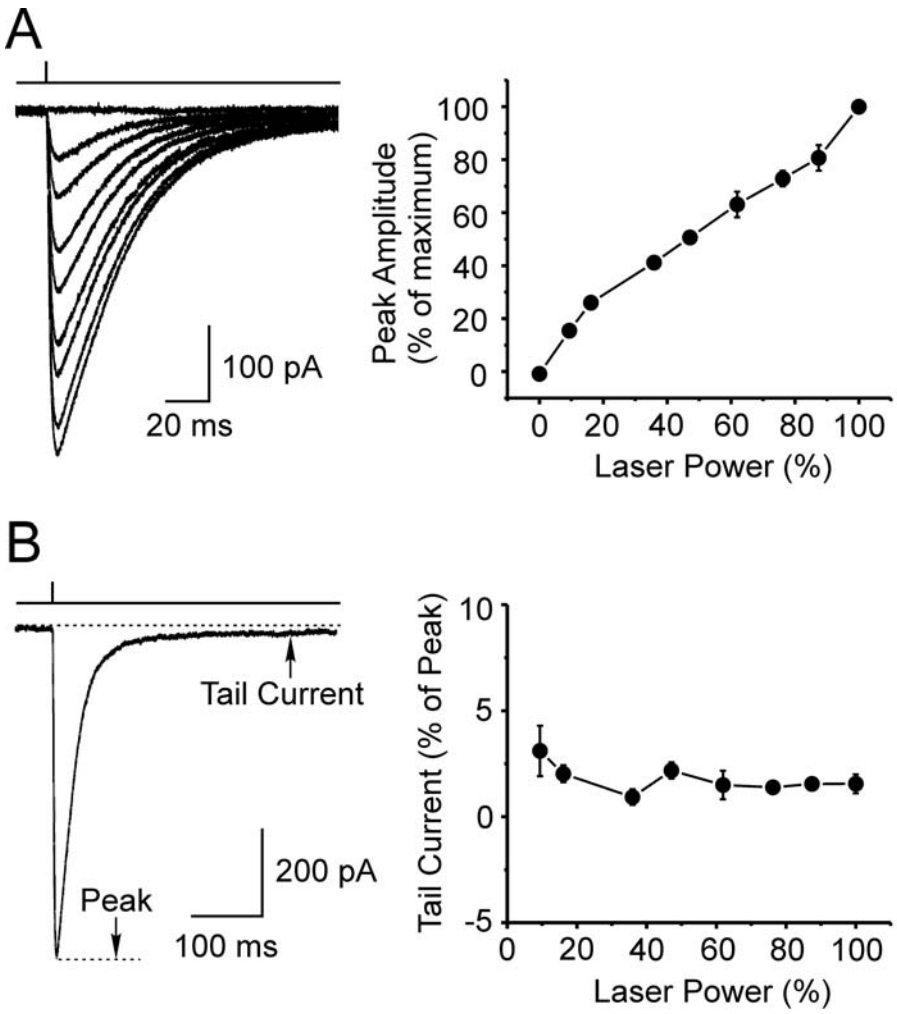
A
100 pA
20 ms
Peak Amplitude
(% of maximum)
100
80
60
40
20
0
0 20 40 60 80 100
Laser Power (%)
B
Tail Current
Peak
200 pA
100 ms
Tail Current (% of Peak)
10
5
0
-5
0 20 40 60 80 100
Laser Power (%)

Figure IV-4. MNI-D-aspartate does not antagonize glutamate transporters. *A*, *Left*, Glutamate transporter currents evoked in a hippocampal astrocyte by local pressure application of D-aspartate (500 μM; pressure pulse: 5-10 ms at 15-20 psi), in the absence and presence of MNI-D-aspartate (MNI-D-Asp, 500 μM). A 1 ms UV flash was applied at the end of the recording to demonstrate the presence of the caged compound. *Right*, Grouped data showing the change in peak amplitude, charge transfer, 10−90% rise time and half decay time of transporter currents elicited through pressure application of D-aspartate recorded in the absence and presence of MNI-D-aspartate (n = 4). *B*, *Left*, Peak amplitude of glutamate transporter currents recorded from an astrocyte over a period of 25 minutes in a perforated-patch recording configuration ([MNI-D-aspartate] = 125 μM). Three representative traces are shown in the inset to illustrate the time course of the transporter currents over the duration of the recording. *Right*, Grouped data showing normalized peak amplitudes over the 25 minute recording period for four experiments. All recordings were made from astrocytes located in stratum radiatum of area CA1, in the presence of TTX (1 μM), R,S-CPP (10 μM), MK-801 (50 μM) and NBQX (10 μM). Astrocytes were voltage-clamped at –80 mV with a KMeS-based internal solution.

Figure IV- 4

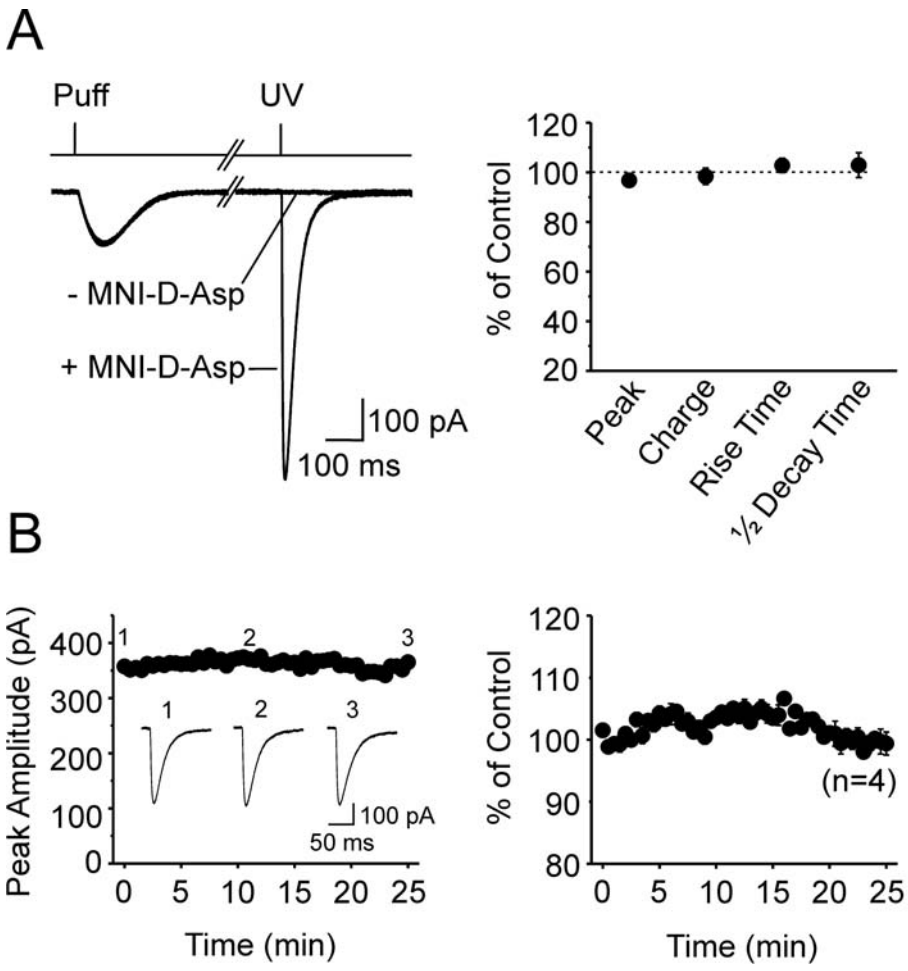
A
Puff
UV
- MNI-D-Asp
+ MNI-D-Asp
100 pA
100 ms
% of Control
120
100
80
60
40
20
Peak
Charge
Rise Time
½ Decay Time
B
Peak Amplitude (pA)
400
300
200
100
0
1
2
3
100 pA
50 ms
0 5 10 15 20 25
Time (min)
% of Control
120
110
100
90
80
(n=4)
0 5 10 15 20 25
Time (min)

Figure IV-5. **Photolysis of MNI-D-aspartate elicits glutamate transporter currents in Bergmann glia of the cerebellum.** *A*, Inward currents recorded from a Bergmann glial cell in response to photolysis of MNI-D-aspartate (125 μM), were inhibited by the glutamate transporter antagonist TBOA (200 μM). SR 95531 (5 μM), R,S-CPP (10 μM) and NBQX (10 μM) were present throughout the experiment. *B*, Grouped data comparing the peak amplitudes and % inhibition by TBOA of responses recorded in Bergmann glia and hippocampal astrocytes in response to photolysis of MNI-D-aspartate. Numbers in parenthesis indicate the number of experiments. Transporter currents in each case were recorded with a 40x objective using 125 μM MNI-D-aspartate. Astrocytes and Bergmann glia were voltage-clamped at –80 mV with a KMeS-based internal solution. ** $p < 0.01$; *** $p < 0.001$.

Figure IV- 5

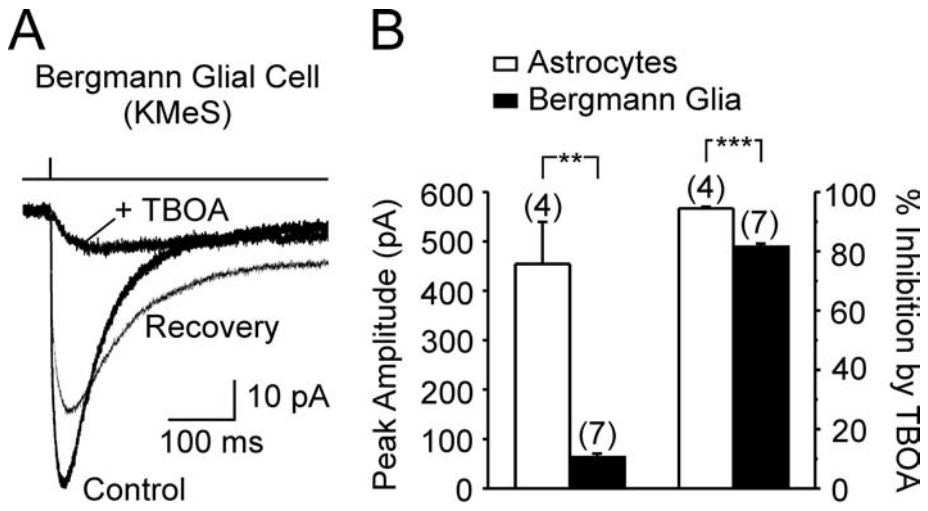
A
Bergmann Glial Cell
(KMeS)
+ TBOA
Recovery
10 pA
100 ms
Control
B
Astrocytes
Bergmann Glia
**
***
(4)
(7)
(4)
(7)
Peak Amplitude (pA)
600
500
400
300
200
100
0
100
80
60
40
20
0
% Inhibition by TBOA

Figure IV-6. Glutamate transporter currents evoked in Purkinje neurons through photolysis of MNI-D-aspartate. *A*, Inward currents recorded from a Purkinje neuron to photolysis of MNI-D-aspartate (500 μM), in the absence and presence of TBOA (200 μM). CsMeS-based internal solution. *B*, Same experiment as in *A* except that the recording was made with a $CsNO_3$-based internal solution. *C*, Grouped data showing the peak amplitude and 10−90% rise time of glutamate transporter currents recorded in Purkinje neurons using two different internal solutions. Numbers in parenthesis indicate the number of experiments. *** $p < 0.001$. *D*, Comparison of the response of a Purkinje neuron to photolysis of MNI-L-glutamate (500 μM) and MNI-D-aspartate (MNI-D-Asp, 500 μM) in the presence of TBOA (100 μM). *E*, Response of a Purkinje neuron to photolysis of MNI-L-glutamate (MNI-L-Glu, 500 μM) recorded in the absence or presence of the mGluR1 selective antagonist LY 367385 (100 μM). *F*, A glutamate transporter current recorded from the cell shown in *D* in response to photolysis of MNI-D-aspartate. All currents were recorded at –65 mV in the presence of SR 95531 (5 μM), picrotoxin (100 μM), R,S-CPP (10 μM) and NBQX (15 μM).

Figure IV- 6

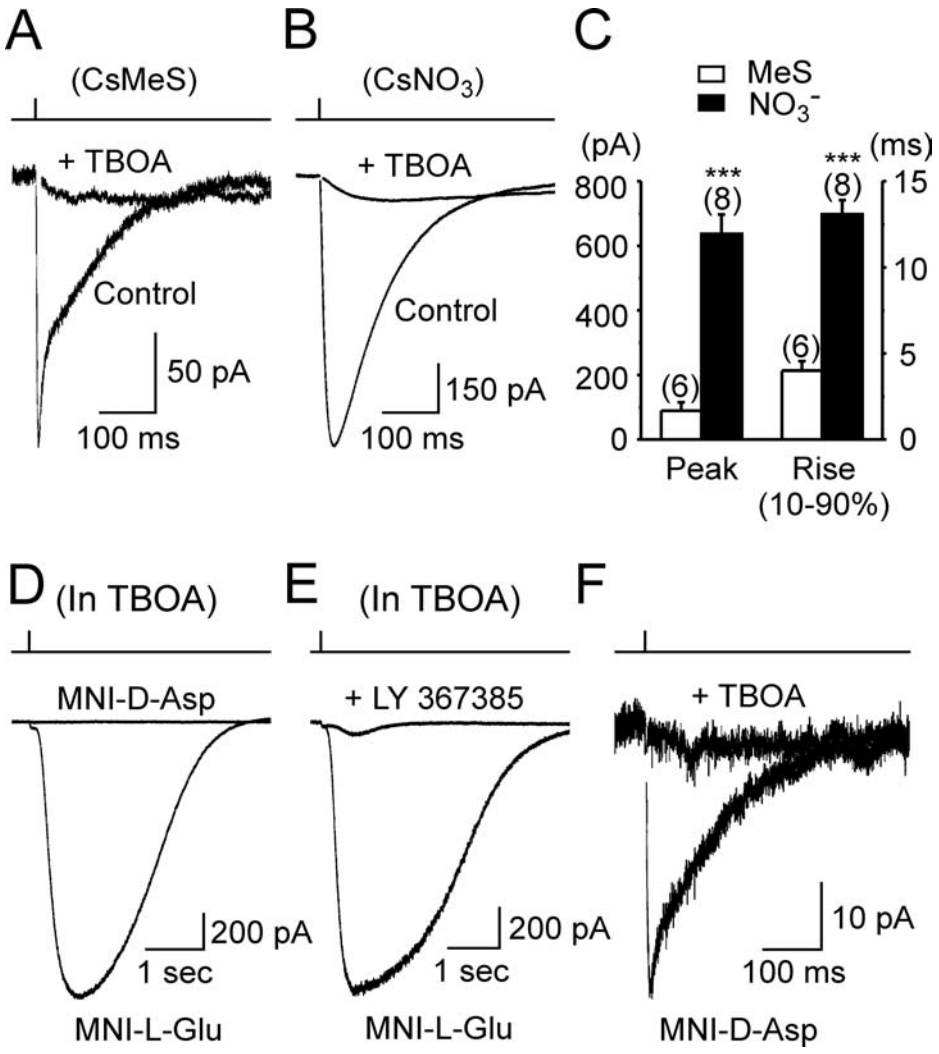
A
(CsMeS)
+ TBOA
Control
50 pA
100 ms
B
(CsNO3)
+ TBOA
Control
150 pA
100 ms
C
MeS
NO3-
(pA)
800
600
400
200
0
(ms)
15
10
5
0
***
(8)
(6)
Peak
Rise
(10-90%)
D (In TBOA)
MNI-D-Asp
200 pA
1 sec
MNI-L-Glu
E (In TBOA)
+ LY 367385
200 pA
1 sec
MNI-L-Glu
F
+ TBOA
10 pA
100 ms
MNI-D-Asp

Figure IV-7. Photolysis of MNI-D-aspartate elicits NMDA receptor-mediated currents in hippocampal CA1 pyramidal neurons. *A*, Response of a pyramidal neuron to photolytic release of D-aspartate recorded at different holding potentials (as indicated). The ACSF contained 1 μM TTX, and responses were recorded with a CsMeS-based internal solution. *B*, Plot of the current-voltage relationship of currents recorded from CA1 pyramidal neurons in response to photolysis of MNI-D-aspartate under control conditions (closed circles) or in the presence of R,S-CPP (10 μM) and MK-801 (50 μM) (open squares). Peak amplitudes were normalized to the value recorded at V_m = –30 mV (n = 3). *C*, NMDA receptor currents recorded at V_m = 25 mV in response to local pressure application of 500 μM D-aspartate in the presence or absence of MNI-D-aspartate (500 μM). A 1 ms UV flash was applied at the end of the recording to demonstrate the presence of the caged compound. *D*, Grouped data showing the change in peak amplitude, charge transfer, 10−90% rise time and half decay time of transporter currents elicited through pressure application of D-aspartate, recorded in the absence and presence of 500 μM MNI-D-aspartate (n = 6).

Figure IV- 7

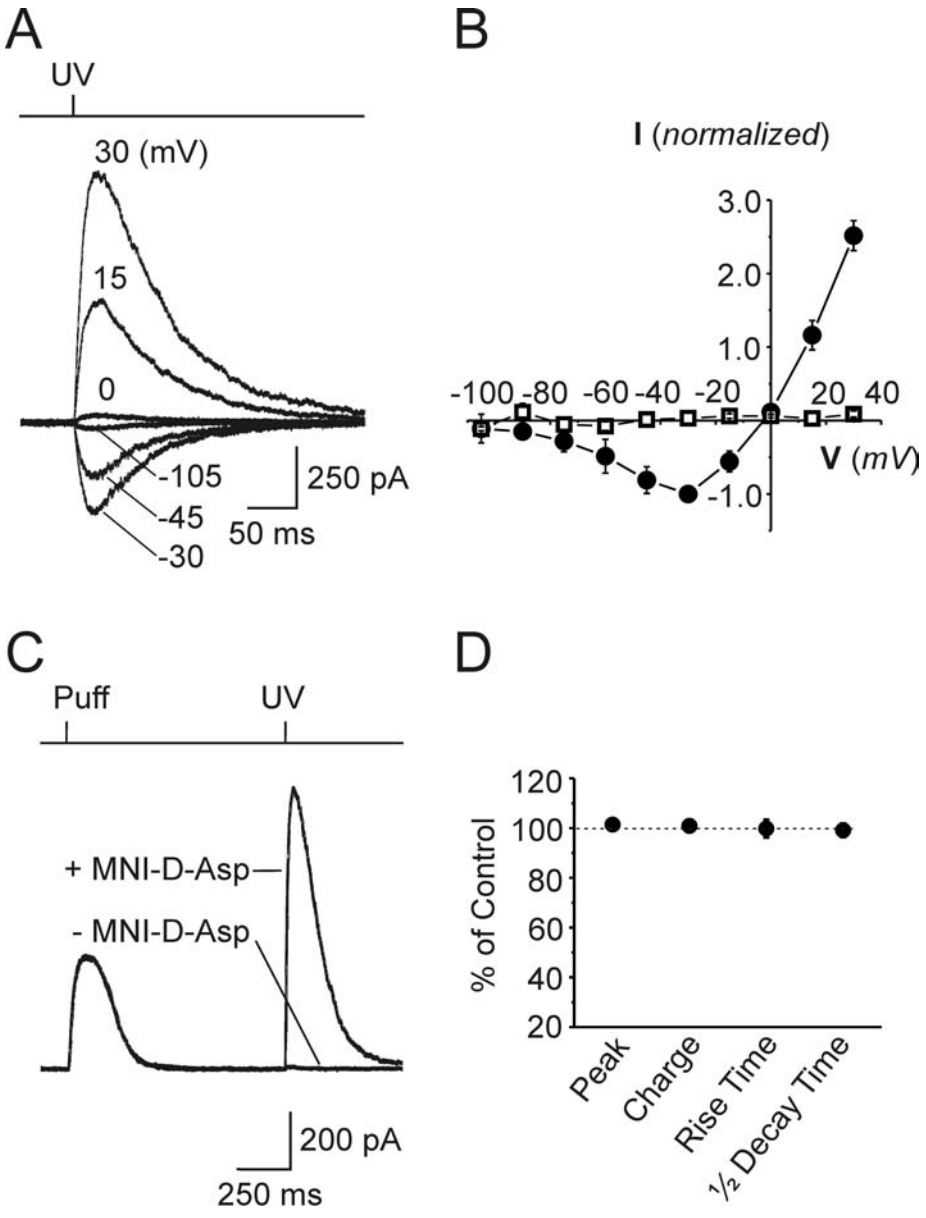
A
UV
30 (mV)
15
0
-105
-45
-30
250 pA
50 ms
B
I (normalized)
3.0
2.0
1.0
-100 -80 -60 -40 -20 20 40
-1.0
V (mV)
C
Puff
UV
+ MNI-D-Asp
- MNI-D-Asp
200 pA
250 ms
D
% of Control
120
100
80
60
40
20
Peak
Charge
Rise Time
½ Decay Time

Chapter V

GLT-1 function in hippocampal CA3 pyramidal neurons

Introduction

The studies described in **Chapters II** and **III** suggest that glutamate transporters GLT-1 and GLAST are responsible for removing the majority of glutamate at excitatory synapses, whereas neuronal transporters EAAC1 and EAAT4 contribute minimally. GLT-1 and GLAST are the quantitatively dominant transporters in the brain, and they are almost exclusively expressed by glial cells. However, there has been a long-standing debate on the putative expression of GLT-1 protein in a subpopulation of neurons in the normal adult brain. GLT-1 mRNA has been detected in a selective population of neurons in multiple regions of the normal adult brain (Berger and Hediger, 1998; Schmitt et al., 1996; Torp et al., 1994; Torp et al., 1997), and GLT-1 protein has been found in neurons in the retina (Euler and Wassle, 1995; Rauen and Kanner, 1994; Rauen et al., 1996), transiently during development (Northington et al., 1998), in cell cultures (Chen et al., 2002) and in pathological brain tissue (Martin et al., 1997). Based on these observations, it was speculated that GLT-1 protein may also exist in certain neurons, perhaps at nerve terminals for synaptic recycling of glutamate. However, immunohistological studies using a variety of GLT-1 antibodies initially failed to reveal neuronal GLT-1 expression *in vivo* in the normal adult brain (for review, see Danbolt, 2001). It was concluded that either GLT-1 is expressed in much lower levels in neurons than in astroglial cells, or that the GLT-1

protein present in neurons is a novel isoform not recognized by currently available antibodies. Two recent studies have re-evaluated the expression of GLT-1 by neurons in the hippocampus. Initial results suggested that GLT-1b, a carboxy-terminal splice variant (Utsunomiya-Tate et al., 1997), was found in nerve terminals (Chen et al., 2002). However, this labeling was subsequently shown to be artifactual, as a similar pattern of labeling was observed in tissue taken from GLT-1 knockout mice (Chen et al., 2004). Nonetheless, further examination using peroxidase-enhanced immuno-EM suggests that full-length GLT-1 is present in a subset of nerve terminals in area CA1 that presumably arise from CA3 Schaffer collateral-commissural fibers (Chen et al., 2004). Further analysis is required to obtain information about the precise localization and quantification, as well as functional demonstration of this GLT-1 expression.

To facilitate the study of regional distribution of GLT-1 *in vivo*, we developed GLT-1-BAC-eGFP reporter mouse in collaboration with the laboratory of Dr. Jeffrey Rothstein. This transgenic mouse has the eGFP gene downstream of GLT-1 promoter and therefore is expressed whenever and wherever the GLT-1 promoter is activated. Because the BAC DNA used for this expression construct includes the complete sequence of GLT-1 promoter, it is thought to contain all regulatory cis elements required for faithful control by endogenous transcriptional regulation machinery. As shown in Figure V-1*A*, eGFP signal was present throughout the brain, as expected for GLT-1 promoter activity. In the hippocampus, eGFP signal level was high in stratum radiatum and low in pyramidal cell layers, consistent with the predominant glial expression of GLT-1. In addition, eGFP signal was also detected in CA3 pyramidal

cell layer (Figure V-1*A*, *arrows*), reminiscent of previous observations of GLT-1 mRNA expression in CA3 pyramidal neurons (Berger and Hediger, 1998; Schmitt et al., 1996; Torp et al., 1997). Measurements of eGFP intensity by confocal microscopy in the adult hippocampus revealed high GLT-1 promoter activity in astroglial cells, low but significant promoter activity in CA3 pyramidal neurons, and undetectable promoter activity in CA1 pyramidal neurons (Figure V-1*B*). These results suggest that GLT-1 promoter activity is strictly regulated in different populations of cells, and that GLT-1 protein may be expressed by CA3 pyramidal neurons.

To examine whether there is functional GLT-1 expressed on the plasma membrane of CA3 pyramidal neurons, we aimed to isolate and characterize glutamate transporter currents in these neurons. We used MNI-D-aspartate, a caged form of transporter substrate (for synthesis and characterization see **Chapter IV**), to allow rapid and focal activation of transporters by brief exposure to near UV light. Photolysis of MNI-D-aspartate by 1 ms flash of near UV light reliably elicited an inward current in CA3, but not CA1, pyramidal neurons. The current was inhibited by selective glutamate transporter antagonists and exhibited a current-to-voltage (I-V) relationship characteristic of glutamate transporter currents. The current was also inhibited by a GLT-1-selective antagonist and was absent in GLT-1 knockout mouse selectively, suggesting that the photolysis-evoked current was solely mediated by GLT-1. Functional mapping of the subcellular distribution of the transporter current suggests that GLT-1 is present on both apical and basal dendrites of CA3 pyramidal neurons.

Materials and Methods

Glutamate transporter deficient mice. The generation of *GLT-1*$^{-/-}$ mice, *EAAC1*$^{-/-}$ mice and *GLAST*$^{-/-}$ mice have been described previously (Peghini et al., 1997; Tanaka et al., 1997; Watase et al., 1998). All comparisons between specific transporter knockout mice and wild-type mice were performed between littermates obtained from heterozygous matings. The genotype of all experimental animals was determined by PCR.

Slice Preparation. Hippocampal slices were prepared in similar ways as described in **Chapter III**. Slices were prepared from postnatal day 18 to 20 (P18-20) rats in ice-cold saline solution containing (in mM): choline chloride 110, KCl 2.5, $MgSO_4$ 7, $CaCl_2$ 0.5, NaH_2PO_4 1.25, choline bicarbonate 25, D-glucose 25, kynurenic acid 1, saturated with 95% O_2, 5% CO_2. Slices were incubated in ACSF for 30 min at 37°C, and then allowed to recover for at least 30 min at room temperature before experimentation. Brain slices were used within 7 hours of preparation.

Whole Cell Recording. Brain slices that had recovered for at least one hour were transferred to a Lucite chamber with a coverslip bottom and continuously superfused with oxygenated ACSF. Individual cells (CA1 and CA3 pyramidal neurons) were visualized through a 40x water immersion objective (Olympus LUMPlanFl, NA = 0.8) using an upright microscope (Axioskop FS2, Zeiss) equipped with infrared-Nomarski optics and a CCD camera (Sony XC-73). Recording electrodes were pulled from glass capillary tubing and had a combined resistance of 1.5-3.0 MΩ when filled with the internal solution. To record the coupled transporter current in CA3 pyramidal neurons,

the internal solution contained (in mM): KCH_3O_3S (KMeS) 120, EGTA 10, HEPES 20, $MgCl_2$ 1, Na_2ATP 2, NaGTP 0.2; the pH was 7.3. To record transporter associated anion currents from pyramidal neurons, the internal solution contained (in mM): KSCN 130, EGTA 10, HEPES 20, $MgCl_2$ 1, Na_2ATP 2, NaGTP 0.2; the pH was 7.3; to record the current-voltage relationship of the transporter anion current, KSCN was substituted with $CsNO_3$ 103, and TEA-Cl 20 was included. With these solutions the series resistance during recordings was <10 MΩ, and was left uncompensated. Unless stated otherwise, holding potentials have not been corrected for the junction potential. Whole-cell currents were amplified using an Axopatch 200B (Axon Instruments), filtered at 2-5 kHz and sampled at 10-20 kHz. A 0.5-5 mV step was applied at the beginning of each trace to measure both the membrane and access resistances.

Solution Application. Caged compounds were dissolved in HEPES buffered saline (HEPES ACSF) containing (in mM): NaCl 137, KCl 2.5, $CaCl_2$ 2.5, $MgCl_2$ 1.3, HEPES 20; the pH was 7.3. Solutions containing caged compounds were applied to the slice using a wide bore (tip diameter 50-100 μm) pipette connected to a manifold fed by four 10 ml reservoirs. Solutions were switched by alternately opening and closing valves attached to each reservoir. Antagonists were used to block voltage-gated Na^+ channels (tetrodotoxin; TTX, 1 μM), AMPA/kainate receptors (2,3-dioxo-6-nitro-1,2,3,4-tetrahydrobenzo[f] quinoxaline-7-sulfonamide disodium salt; NBQX, 10 μM), NMDA receptors ((RS)-3-(2-carboxypiperazin-4-yl)-propyl-1 -phosphonic acid; R,S-CPP, 10 μM; (5R,10S)-(+)-5-methyl-10,11-dihydro-5H-dibenzo[a,d]cyclo-hepten-5,10-imine hydrogen maleate; MK-801, 50 μM; and

5,7-dichlorokynurenic acid, 50 μM), and $GABA_A$ receptors (6-imino-3-(4-methoxyphenyl)-1(6H)- pyridazinebutanoic acid dihydrobromide; SR-95531, 5 μM). All appropriate blockers were included in the puffer pipette solution. Glutamate transporters were inhibited using DL-threo-β-benzyloxyaspartic acid (TBOA, 100-200 μM). GLT-1 was selectively inhibited by WAY 213613 (10 μM). The specific blockers used in each experiment are indicated in the figure legends. For experiments mapping the subcellular distribution of transporters in CA3 pyramidal neurons, the Alexa dye 647 (100 μM) was included in the recording pipette; the CMNB-caged fluorescein (500-1000 μM) was dissolved in dH_2O and locally perfused following MNI-D-aspartate application.

Photolysis of Caged Compounds. For photolysis, an argon ion laser (Stabilite 2017-AR, Spectra-Physics) providing ~ 380 mW of multi-line UV light (333.6-363.8 nm) was coupled to the microscope through a multi-mode quartz fiber optic cable (Oz Optics Ltd.). The output of the fiber optic was collimated using a quartz lens, projected through the fluorescence port of a Zeiss Axioskop FS2 microscope, and focused to a ~100 μm spot using a 20x water immersion objective (Olympus UMPlanFl) to cover the soma and proximal dendrites of pyramidal neurons, or to a ~33 μm spot using a 60x water immersion objective (Olympus LUMPlanFl) to cover a restricted region on the soma or dendritic arbor. The UV spot was centered on the soma or dendritic arbor of pyramidal neurons, using a targeting laser (633 nm HeNe). To control the length of exposure, a computer controlled programmable pulse generator (Master 8, AMP Instruments) was used to trigger a high-speed laser shutter

(NM laser) placed between the laser head and the fiber launch. Photolysis was achieved by opening the shutter for 1 ms. In some experiments, the intensity of the laser was varied using the aperture on the laser head. The output intensity for each aperture was measured using a power meter. A laser intensity (at the output) of 380 mW was used for recordings from hippocampal CA3 pyramidal neurons (20x objective), corresponding to a total light energy of 48 mJ/cm^2. These values reflect the laser power prior to entering the fiber optic; the energy reaching the cell is likely to be considerably less due to loss at the fiber launch, the microscope lenses, and the intervening tissue.

Chemicals Used for Photolysis Experiments. NBQX, R,S-CPP, MK-801, 5,7-dichlorokynurenic acid, SR-95531, and TBOA were purchased from Tocris. D-aspartate was purchased from Sigma. TTX was purchased from Alomone Labs. Alexa dye 647 and the CMNB-caged fluorescein were purchased from Molecular Probes (Invitrogen).

Data Analysis and Statistics. Data were analyzed off-line using Clampfit (Axon Instruments) and Origin (Microcal) software. All values are represented as mean ± standard error of the mean. The Student's t-test (paired or unpaired, as appropriate) was used for statistical comparison; $p < 0.05$ was considered significant.

Results

Photolysis of MNI-D-aspartate elicits glutamate transporter currents in CA3 but not CA1 pyramidal neurons.

To maximize the probability of detecting glutamate transporter currents in CA3 neurons, we used a 20x objective to create a wide UV spot of ~ 100 μm to cover the soma and proximal dendrites of CA3 neurons; and used a SCN^--based internal solution (see **Methods**) to amplify the anion conductance associated with glutamate transport. Whole-cell voltage-clamp recordings were made from hippocampal CA3 pyramidal neurons, and their response to photolysis of MNI-D-aspartate (500 μM) was measured in the presence of AMPA, NMDA, and $GABA_A$ receptor antagonists, as well as TTX (see **Methods**). Brief (1 ms) exposure to UV light produced a rapidly activating, transient inward current in these neurons, which was only observed when the superfusing solution contained MNI-D-aspartate (Figure V-2*A*). The peak amplitude of these responses was −7.7 ± 0.9 pA (n = 6) when a MeS-based internal solution was used to reveal the coupled charge movement; when MeS was replaced with SCN^- (see **Methods**), the photolysis-evoked response was much larger (−44.8 ± 9.5 pA, n = 8, $p < 0.01$), suggesting that transporter associated anion conductance was activated by uncaging of MNI-D-aspartate. The peak amplitude of the photolysis-evoked anion current was reduced by 81 ± 2 % (n = 7) by TBOA (200 μM) (Figure V-2*A*), confirming that the anion conductance resulted from the activation of glutamate transporters. Using responses recorded by MeS-based internal solution, the charge transfer induced by photolysis was calculated to be ~ 0.9 pC, which

corresponds to the transport of 2.8 x 10^6 molecules of D-aspartate based on the stoichiometry of glutamate transporters (net influx of two positive charges per glutamate molecule), and activation of an equal number of transporters, if it is assumed that the transporters complete a single cycle following brief photolysis (Bergles and Jahr, 1997). Measurement of the current-voltage (I-V) relationship of these responses using a $CsNO_3$-based internal solution revealed that the photolysis-evoked current continuously decreased as the membrane potential was depolarized, but the current was not reversed even at +40 mV (Figure V-2*B*). This is consistent with the behavior of Na^+-dependent glutamate transport; as the membrane potential approaches the equilibrium potential for Na^+, Na^+-dependent glutamate binding is reduced, but glutamate transport is not reversed (Levy et al., 1998). These results indicate that functional glutamate transporters are present on the membrane of hippocampal CA3 pyramidal neurons.

In contrast, photolysis of MNI-D-aspartate under similar conditions revealed no such current in CA1 pyramidal neurons (SCN^--based internal solution; peak amplitude at −65 mV: −8.8 ± 1.9 pA, n = 7, $p < 0.01$ compared to CA3 pyramidal neurons) (Figure V-3*A*). There was a small and sustained current evoked in the presence but not absence of MNI-D-aspartate, but it was not likely to be mediated by glutamate transporters, as it persisted in the presence of TBOA (200 μM) (Figure V-3*A*). A similar residual current was also observed in EAAC1 knockout mice, and the peak amplitude was not significantly different from the wild-type littermates (*EAAC1*$^{-/-}$: −5.2 ± 0.7 pA, n = 5; *EAAC1*$^{+/+}$: −5.5 ± 0.9 pA, n = 3, $p = 0.369$),

suggesting that it is not mediated by EAAC1 either (Figure V-3*B*). Theses results are consistent with the observation that GLT-1 promoter activity was present in CA3 but not CA1 pyramidal neurons as revealed in the GLT-1-BAC-eGFP reporter mice (Figure V-1*B*). Thus, expression of eGFP in these mice reflects the activity of the GLT-1 protein.

GLT-1 glutamate transporters mediate the photolysis-evoked currents in CA3 pyramidal neurons.

The response to photolysis of MNI-D-aspartate (500 μM) was measured in CA3 pyramidal neurons in the absence and presence of WAY 213613, a newly developed selective antagonist of GLT-1 that exhibits more than 40x higher affinity for GLT-1 than GLAST and EAAC1 (provided by J. Dunlop, Wyeth Research). The peak amplitude was reduced by 77.3 ± 2.5 (n = 3) by WAY 213613 (10 μM), suggesting that GLT-1 mediates the transporter current in CA3 pyramidal neurons. Furthermore, measurements of photolysis-evoked transporter currents in selective glutamate transporter knockout mice showed that the current was only absent in *GLT-1*$^{-/-}$ mice (Figure V-4*A*) (peak amplitude in *GLT-1*$^{+/+}$: −49.2 ± 5.8 pA, n = 6; *GLT-1*$^{-/-}$: −5.3 ± 0.5 pA, n = 5, $p < 0.001$), and the currents in GLAST and EAAC1 knockout mice were not significantly different from those of their wild-type littermates (*GLAST*$^{+/+}$: −55.1 ± 5.6 pA, n = 5; *GLAST*$^{-/-}$: −55.6 ± 5.9 pA, n = 5, $p = 0.475$; *EAAC1*$^{+/+}$: −51.2 ± 5.9 pA, n = 5; *EAAC1*$^{-/-}$: −47.4 ± 5.3 pA, n = 5, $p = 0.323$) (Figure V-4*B*). These results indicate that the photolysis-evoked glutamate transporter currents in CA3

pyramidal neurons are mediated by GLT-1.

Distribution of GLT-1 transporters in CA3 pyramidal neurons.

The above experiments reveal that glutamate transporter activity is present in the soma and proximal dendrites of CA3 pyramidal neurons. To obtain further insights about the potential function of GLT-1 in CA3 neurons during synaptic transmission, we next examined whether there is preferential regional localization of these transporters. CA3 pyramidal neurons receive three main excitatory inputs, which are segregated into different layers along the dendritic arbor (Shepherd, 2004). The most proximal portion of the apical dendrites of CA3 neurons receive mossy fiber (MF) inputs from dentate granule cells; the most distal portion of their apical dendrites receives perforant path inputs from the entorinal cortex; and the middle portion of the apical dendrites as well as the basal dendrites receive associational/ commissural inputs from other CA3 pyramidal neurons (Shepherd, 2004). Using a 60x objective to focus the laser UV light onto a ~33 μm spot, we were able to selectively activate different portions of the dendritic arbor, and record corresponding glutamate transporter currents. To determine the size and position of the uncaging spot in relation to the dendritic arbor of the recorded neuron, a CMNB-caged fluorescein was included in the superfusing solution (see **Methods**), and a fluorescent dye Alexa 647 (red) was included in the recording pipette to reveal the soma and processes. At the positions where MNI-D-aspartate is photolyzed, the CMNB-caged fluorescein is also photolyzed by the same UV light. The released fluorescein emits green fluorescent

light upon excitation with 488 nm light from argon ion laser, and thus reveals the uncaging spot. MNI-D-aspartate and the caged fluorescein were applied sequentially to avoid potential interference of the two either during photolysis or in activating glutamate transporters.

As shown in Figure V-5*A*, *B*, photolysis of MNI-D-aspartate (500 μM) evoked transporter currents throughout the apical and basal dendrites, producing the largest peak amplitude at the soma. These results suggest that GLT-1 may be most abundant in the soma and proximal dendrites of CA3 neurons. However, it was not possible to determine whether GLT-1 is also present at more distal parts of CA3 neuron apical dendrites or at the axon terminals. This is mainly because K^+-based internal solution was used in these recordings to facilitate transporter cycling, which on the other hand makes the cell leaky and causes significant spatial filtering of the current signals; therefore transporter currents are rapidly attenuated as the current source moves away from the recording electrode (soma). Nonetheless, transporter currents evoked from the proximal dendrites of CA3 pyramidal neurons indicate that GLT-1 may exist in the vicinity of MF and commissural fiber inputs to participate in synaptic clearance.

Discussion

In this series of experiments we show that photolysis of MNI-D-aspartate elicited glutamate transporter currents in hippocampal CA3 but not CA1 pyramidal neurons. The photolysis-evoked transporter current was mediated by GLT-1, and could be

evoked at the soma as well as the apical and basal dendrites of CA3 pyramidal neurons.

Functional GLT-1 expression in hippocampal CA3 pyramidal neurons

To our knowledge these data represent the first demonstration of functional GLT-1 expression in neurons *in situ*. Our ability to detect these rather small currents was facilited by the photolysis approach. Compared to other methods for eliciting transporter currents, photolysis has the advantage of being able to activate a large number of transporters in a highly synchronous manner. In **Chapter IV**, we showed that uncaging of MNI-D-aspartate (125 μM) for the duration of 1 ms could activate 10.5 x 10^7 transporters on a single astrocyte. When recording from hippocampal pyramidal neurons, we further augmented the photolysis capacity by increasing the concentration of MNI-D-aspartate to 500 μM and the laser power from ~230 mW to ~380 mW. Recordings from astrocytes under these conditions revealed that transporter currents are greatly potentiated in both peak amplitude and charge transfer (data not shown), suggesting that an even larger number of transporters can be activated when the concentration of caged compound and the laser power are increased. Under these improved conditions, we could isolate the coupled transporter currents from CA3 pyramidal neurons and calculate the number of activated transporters to be ~ 2.8 x 10^6. The photolysis-evoked currents in CA3 pyramidal neurons are much smaller in peak amplitude and charge transfer compared to those recorded in astrocytes and Purkinje neurons under similar conditions (Huang et al.,

2005). These data are consistent with previous studies showing comparatively low levels of GLT-1 immunoreactivity in neurons (for review, see Danbolt, 2001), and the observation that in the GLT1-BAC-eGFP reporter mouse, GLT-1 promoter activity, although detectable in CA3 neurons, is much lower compared to that in the surrounding astrocytes (Figure V-1*B*).

When occurrs close to synapses, glutamate uptake by a limited number of transporters may still influence the occupancy of receptors during transmission. We estimated that ~ 2.8 x 10^6 transporters are activated by photolysis in CA3 pyramidal neurons from illuminating the soma and proximal dendrites. If it is assumed that these transporters are concentrated at the MF postsynaptic region, and that each CA3 neuron receives ~ 210 active release sites from MF terminals (Chicurel and Harris, 1992; von Kitzing et al., 1994), then on average there would be ~ 1.3 x 10^4 transporters for each MF release site. This is significant compared to ~ 4,000 glutamate molecules released per vesicle. One other example is shown by neuronal transporter EAAC1. Transporter currents mediated by EAAC1 is under the detection limit *in situ* (Figure V-3), and yet inhibition of EAAC1 postsynaptically potentiates the activation of extrasynaptic NMDA receptors (Diamond, 2001). Therefore by being preferentially positioned at synapses, a limited number of neuronal transporters could be effective in regulating the activation of peri- or extrasynaptic receptors during transmission.

Putative function of GLT-1 in CA3 pyramidal neurons

Compared to EAAT4, the other neuronal glutamate transporter whose activation and function at Purkinje neuron synapses have been extensively studied, GLT-1 has (1) a lower affinity (Arriza et al., 1994; Fairman et al., 1995), (2) a smaller anion conductance (Fairman et al., 1995; Wadiche et al., 1995), and (3) a faster turnover rate (Bergles et al., 2002; Otis and Jahr, 1998). Consequently, (1) for a given number of transporters, GLT-1 will be a less potent buffer than EAAT4 in reducing the concentration of ambient glutamate. (2) EAAT4 transporters have significant anion (Cl^-) influx accompanying glutamate transport under physiological conditions, which may neutralize charge accumulation at the inside of the membrane and facilitate glutamate uptake. In contrast, the anion conductance associated with GLT-1 activity is much smaller, which may render GLT-1 less effective in transport glutamate beyond the first cycle. (3) But GLT-1 has a faster turnover rate, which presumably will make them more responsive than EAAT4 to high-frequency release of glutamate. In summary, the characteristic features of GLT-1 indicate that at excitatory synapses, GLT-1 may impact transmission very differently than EAAT4.

CA3 pyramidal neurons receive different excitatory inputs that are segregated into layers along the dendritic arbor. Our current studies revealed that GLT-1 mediated transporter currents can be evoked at the proximal and middle portions of CA3 pyramidal neuron apical dendrites as well as the basal dendrites, indicating that GLT-1 is present where mossy fibers and associational axons terminate. Within the scope of synaptic transmission, there are several possibilities to be tested. First, the mossy fiber-CA3 synapse is a large complex synapse where the presynaptic expansion is

penetrated by large thorny spines of the postsynaptic membrane, forming multiple active zones in between (Chicurel and Harris, 1992). The pre- and postsynaptic membranes are further joined together by puncta adherentia junctions that are highly developed at this synapse (Amaral and Dent, 1981; Commons and Milner, 1995), leaving little chance for glial processes to get to the vicinity of release sites. If GLT-1 is present on the postsynaptic neuronal membrane, it would be the primary mechanism to remove synaptic glutamate and thereby influence receptor occupancy during transmission. It has been shown at this synapse that excitatory transmission can be potentiated if diffusion is compromised in the extracellular space (Min et al., 1998). These findings suggest that postsynaptic receptors at this synapse are not saturated normally, and their activation closely follows the spatial and temporal concentration profile of glutamate around the synaptic cleft. In addition to postsynaptic receptors, there are high-affinity mGluRs present on mossy fiber terminals (Shigemoto et al., 1997), whose activity modulates presynaptic release (Manzoni et al., 1995); these receptors are also sensitive to the ambient concentration of glutamate (Min et al., 1998), and thus represent another candidate target for GLT-1 regulation during transmission. Second, CA3 pyramidal neurons are extensively interconnected with each other via excitatory synapses formed by re-current collaterals (Shepherd, 2004). GLT-1 located at these synapses may regulate the recurrent excitation of CA3 neurons and fine-tune the excitability of the local CA3 network by limiting receptor occupancy at these synapses. Third, if present on CA3 neuron axon terminals, GLT-1 may also contribute to glutamate clearance at Schaffer

collateral synapses. It has been long debated whether GLT-1 exists on the presynaptic membrane of excitatory synapses to recycle released glutamate (for review, see Danbolt, 2001); and recent studies reveal that full-length GLT-1 is present in a subset of nerve terminals in area CA1 that presumably arise from CA3 pyramidal neurons (Chen et al., 2004). From our studies it is not conclusive whether GLT-1 is present at the axon terminals of CA3 neurons. Generation of neuronal-specific GLT-1 knockout mice or mice expressing tagged GLT-1 in CA3 pyramidal neurons selectively may be powerful tools to address this question conclusively (see below).

Developing tools for studying GLT-1 function in CA3 pyramidal neurons

To obtain direct evidence of the existence of GLT-1 on the synaptic membranes of CA3 neurons, immuno-EM studies may be necessary. Recent studies using peroxidase-enhanced immuno-EM suggest that GLT-1 is present in some axon terminals at CA1 radiatum region of the hippocampus. To confirm that GLT-1 is located in the Schaffer collateral terminals that originate from CA3 pyramidal neurons, it would be informative to examine the axonal expression in CA3-specific GLT-1 knockout mice. The strategy would be to generate a knock-in mouse line with two lox-P sites flanking the endogenous GLT-1 gene; and cross the mouse with a transgenic mouse line expressing Cre recombinase selectively in neurons (Hirasawa et al., 2001). This approach is currently being developed in our collaborator Dr. Jeffrey Rothstein's laboratory. To overcome the high background of astroglial GLT-1 immunoreactivity for immuno-EM studies, it is necessary to selectively label GLT-1

in CA3 pyramidal neurons. One strategy is to make a knock-in mouse line with GLT-1-"tag" fusion protein replacing the endogenous GLT-1, meanwhile having two lox-P sites flanking a "stop" codon inserted between GLT-1 and "tag". When this mouse line is crossed with the neuronal-Cre transgenic mouse, GLT-1 but not the fusion protein GLT-1-"tag" will be expressed in non-neuronal cells; whereas fusion protein will only be expressed in Cre-expressing neurons, presumably CA3 pyramidal neurons in the hippocampus.

Our efforts to understand the putative function of neuronal GLT-1 during transmission have been hindered largely by a lack of means to selectively manipulate neuronal GLT-1. The currently available GLT-1 selective antagonists dihydrokainate (DHK) and WAY 213613 do not distinguish between neuronal and glial GLT-1 transporters. We have tried to selectively inhibit GLT-1 from the postsynaptic neuron by depleting intracellular K^+ to inhibit transporter turn-over; or by including a high concentration of glutamate transporter antagonist (TBOA, 10 mM) in the recording pipette. However, neither of these manipulations led to the inhibition of glutamate transporter currents induced by photolysis of MNI-D-aspartate (data not shown). Finally, membrane depolarization to near Na^+ equilibrium potential prohibits Na^+ binding; because Na^+ binding is a prerequisite for subsequent glutamate binding, this manipulation blocks glutamate transport (Levy et al., 1998). We also observed that the transporter current is much reduced at depolarized potentials (Figure V-2*B*), suggesting that membrane depolarization may be a promising approach to inhibit transporters. Other than electrophysiology, virus-mediated antisense or RNAi

knockdown of neuronal GLT-1, as well as neuronal-specific GLT-1 knockout mice are powerful tools to enable single-cell examination of GLT-1 function in CA3 pyramidal neurons. These tools are currently being developed in collaboration with the laboratory of Dr. Jeffrey Rothstein.

Figure V-1. Hippocampal CA3 pyramidal neurons exhibit GLT-1 promoter activity in young adult mice. *A*, Saggital sections of the whole brain (*top*) and the hippocampus (*bottom*) of a BAC-GLT1-eGFP transgenic mouse at the age of postnatal day 17. The fluorescence of GLT-1 promoter-driven eGFP was observed using wide-field fluorescence microscope. In the hippocampus (*bottom*), expression of eGFP is largely restricted to astroglial cells; CA1 pyramidal cell layer and the dentate gyrus granule cell layer are negative for the eGFP signal (*asterisks*); CA3 pyramidal cell layer is weakly fluorescent (*arrows*). Scale bars = 2 mm (*top*), 200 μm (*bottom*). *B*, High magnification confocal images of the CA3 and CA1 regions showing eGFP fluorescence and NeuN immunoreactivity. In the CA3 region, eGFP fluorescence was detected in astroglial cells (*a*, *arrow head*) and pyramidal neurons (*a&b*, *asterisks*). Interneurons, as indicated by weak NeuN immunoreactivity (*b*, *arrows*), do not exhibit eGFP fluorescence (*a*, *arrows*). In the CA1 region, eGFP fluorescence was detected in astrocytes (*c*, *arrow head*) but not pyramidal neurons (*c&d*, *asterisks*). Scale bars = 20 μm (*a*−*d*). This figure was kindly provided by Dr. Melissa Regan in the laboratory of Dr. Jeffrey Rothstein.

Figure V- 1

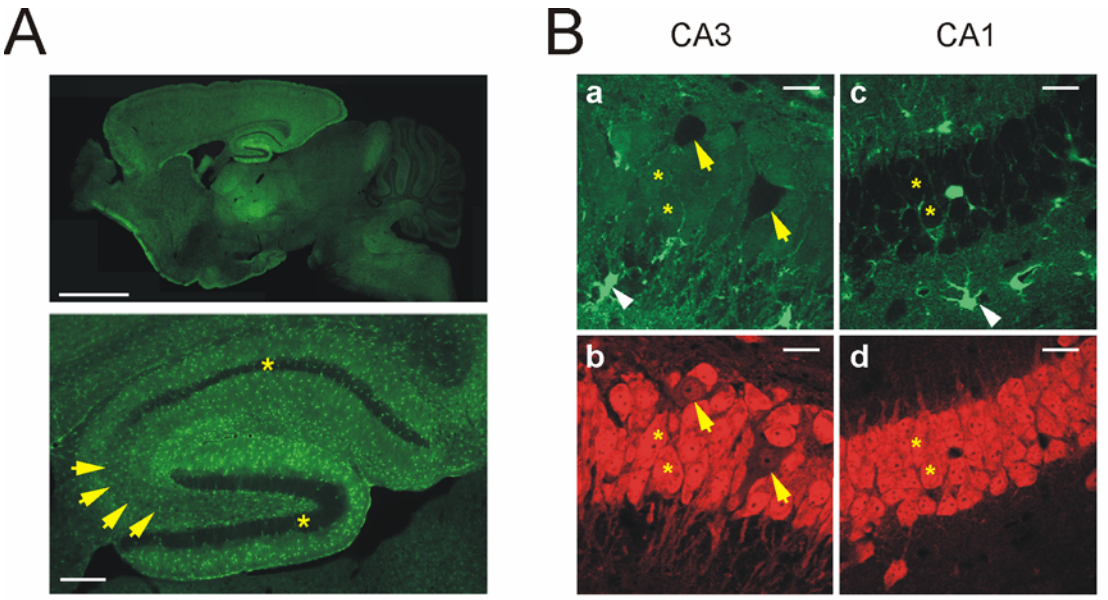

Figure V-2. Glutamate transporter-mediated currents can be elicited in CA3 pyramidal neurons by photolysis of MNI-D-aspartate. *A*, A transient inward current was elicited in a CA3 pyramidal neuron of an adult rat by a 1 ms flash of UV laser light in the presence but not absence of MNI-D-aspartate (MNI-D-Asp, 500 μM) (*left*). The response was inhibited by application of 200 μM TBOA. The trace above shows the duration of UV exposure. The neuron was held at −65 mV using a KSCN-based internal solution. *Right*, Summary of the peak amplitude of the evoked currents in the absence and presence of TBOA. (*** = $p < 0.001$). *B*, Current-Voltage (I-V) relationship of the photolysis-evoked responses. The evoked currents were recorded at different membrane potentials changing from −80 mV to +40 mV. $CsNO_3$-based internal saline was used. Notice that the currents were not reversed at +40 mV. Numbers in parentheses indicate the numbers of recordings. All responses were recorded in the presence of AMPA, NMDA and $GABA_A$ receptor antagonists as well as TTX (see **Methods**).

Figure V- 2

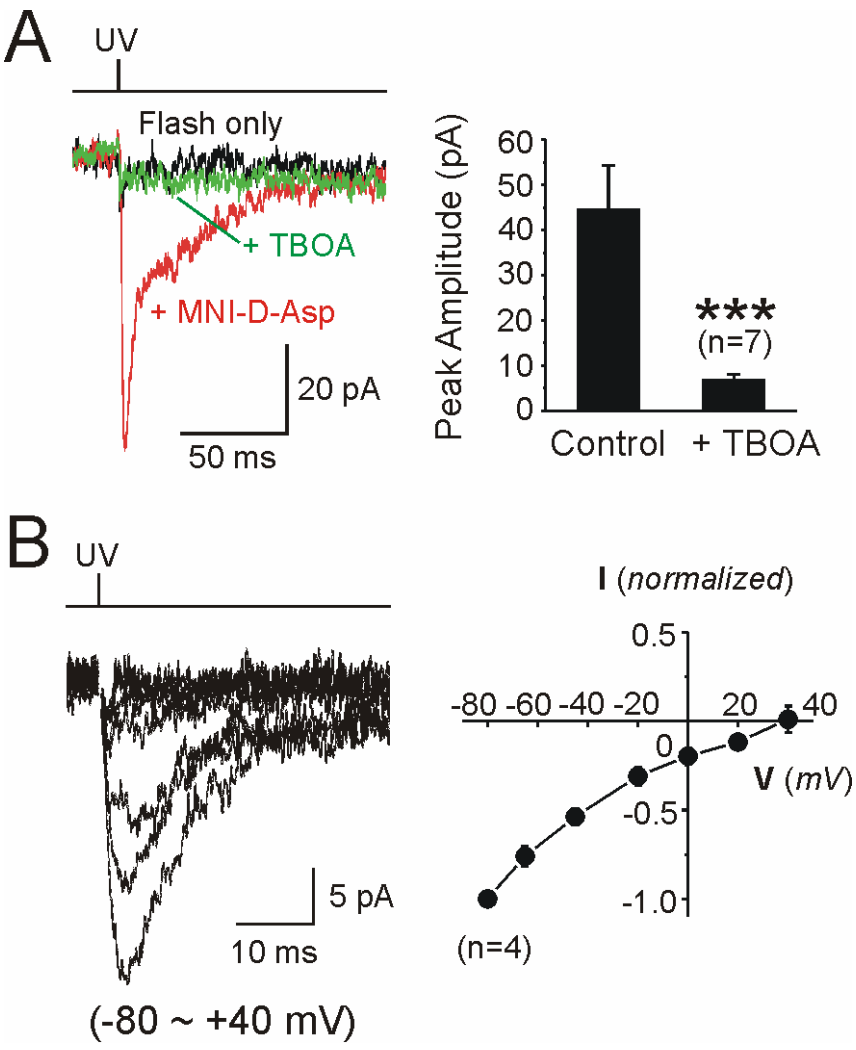
A
UV
Flash only
+ TBOA
+ MNI-D-Asp
20 pA
50 ms
Peak Amplitude (pA)
60
50
40
30
20
10
0
***
(n=7)
Control
+ TBOA
B
UV
5 pA
10 ms
(-80 ~ +40 mV)
I (normalized)
0.5
-80 -60 -40 -20
20
40
0
V (mV)
-0.5
-1.0
(n=4)

Figure V-3. The photolysis-evoked transporter current is absent in CA1 pyramidal neurons. *A*, Response of a CA1 pyramidal neuron in an adult rat hippocampus to the same stimulus as previously. The trace above shows the duration of UV exposure. The photolysis-evoked response was slightly larger than the UV-flash artifact, and was not inhibited by TBOA (200 μM). *B*, Same recordings performed in CA1 pyramidal neurons of an *EAAC1*$^{-/-}$ mouse (*bottom*) and a wild-type littermate (*top*). The photolysis-evoked current in *EAAC1*$^{+/+}$ was not significantly larger than that in *EAAC1*$^{-/-}$, suggesting that the residual currents are not mediated by the neuronal transporter EAAC1. All neurons were held at −65 mV using KSCN-based internal solution. All responses were recorded in the presence of AMPA, NMDA and $GABA_A$ receptor antagonists as well as TTX (see **Methods**).

Figure V- 3

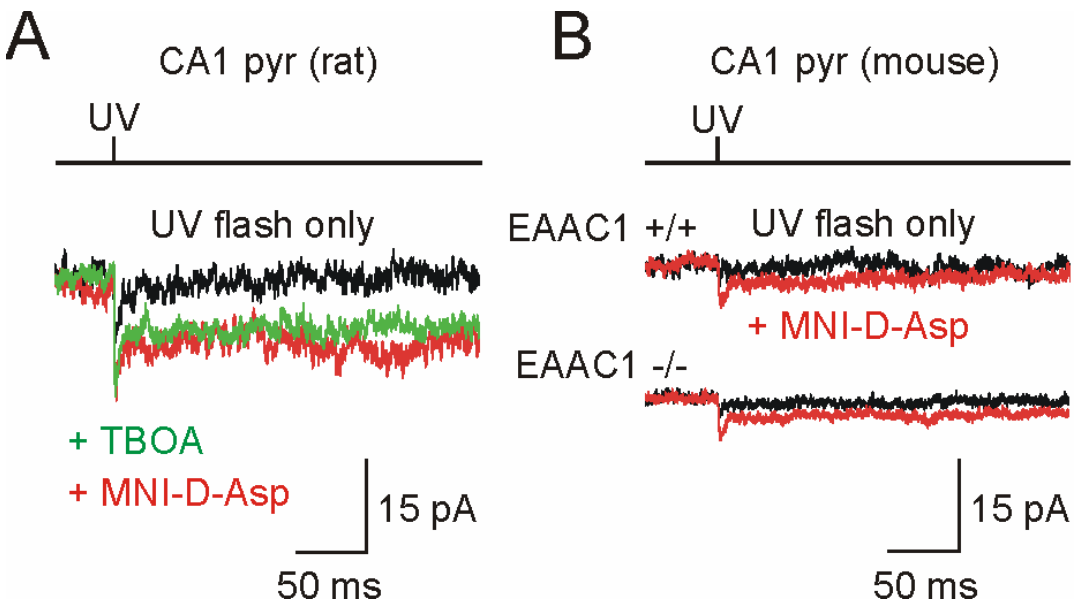
A
CA1 pyr (rat)
UV
UV flash only
+ TBOA
+ MNI-D-Asp
15 pA
50 ms
B
CA1 pyr (mouse)
UV
EAAC1 +/+
UV flash only
+ MNI-D-Asp
EAAC1 -/-
15 pA
50 ms

Figure V-4. GLT-1 mediates the photolysis-evoked transporter currents in CA3 pyramidal neurons. *A*, Photolysis-evoked responses recorded from CA3 pyramidal neurons in a *GLT-1*$^{-/-}$ mouse (*right*) and a wild-type littermate (*left*). Traces on the top show the duration of UV exposure. *B*, Summary of the peak amplitude of photolysis-evoked transporter currents in CA3 pyramidal neurons recorded from mice of different genotypes. The evoked transporter currents were absent in *GLT-1*$^{-/-}$ mice selectively (*** = $p < 0.001$; NS = not significant). Numbers in parentheses indicate the numbers of recordings. All neurons were held at −65 mV using KSCN-based internal solution. All responses were recorded in the presence of AMPA, NMDA and $GABA_A$ receptor antagonists as well as TTX (see **Methods**).

Figure V- 4

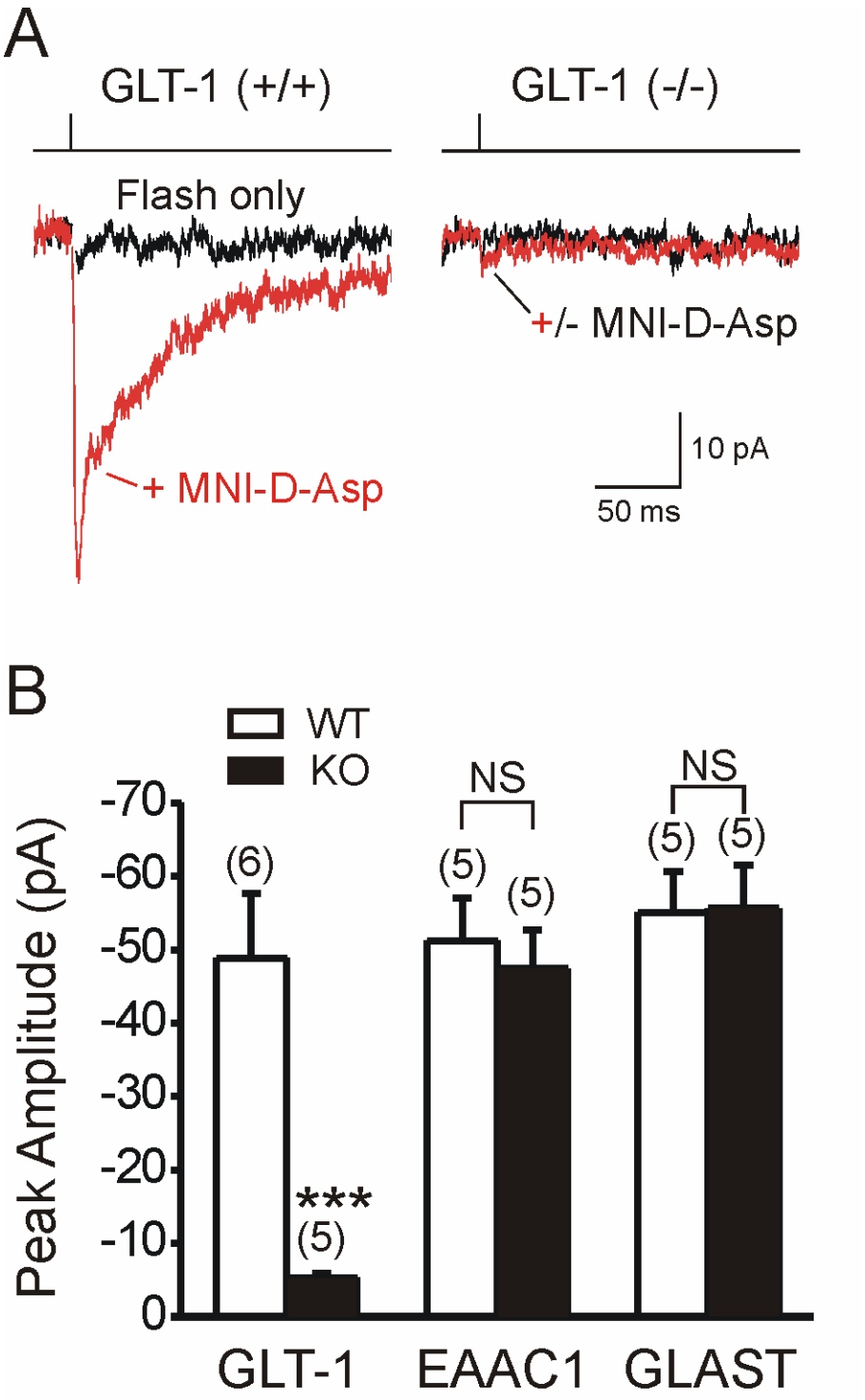
A
GLT-1 (+/+)
GLT-1 (-/-)
Flash only
+/- MNI-D-Asp
+ MNI-D-Asp
10 pA
50 ms
B
WT
KO
Peak Amplitude (pA)
-70
-60
-50
-40
-30
-20
-10
0
(6)
***
(5)
NS
(5)
(5)
NS
(5)
(5)
GLT-1
EAAC1
GLAST

Figure V-5. GLT-1 transporters are distributed on the soma and proximal dendrites of CA3 pyramidal neurons. *A*, A CA3 pyramidal neuron filled with Alexa dye 647 was illuminated. The CMNB-caged fluorescein was photolyzed by the laser UV light and emitted green fluorescent light upon excitation by 488 nm light. The spots of green fluorescent light therefore indicate the location and area that photolysis of MNI-D-aspartate occurred to activate transporters. *B*, Whole-cell recordings made from the cell body of the CA3 pyramidal neuron (as in *A*), showing the averaged responses upon photolysis at the four corresponding locations. The trace on the top shows the duration of UV exposure (5 ms).

Figure V- 5

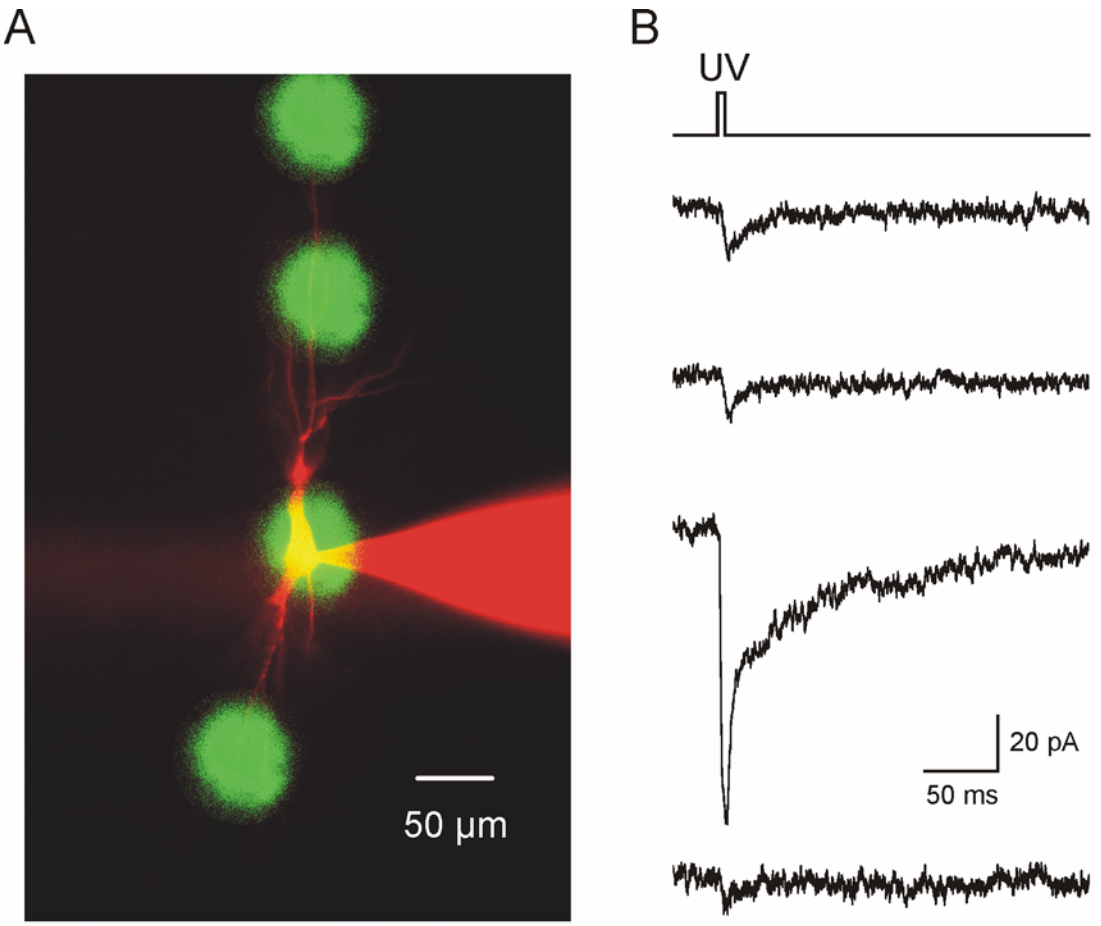

Concluding Remarks

The primary goal of this thesis was to understand the relative contributions of neuronal and glial transporters to the clearance of glutamate released at excitatory synapses, and to examine their differential impact on transmission. Using whole-cell patch-clamp methods, we combined pharmacological tools with genetically altered mice to examine transmission at two representative excitatory synapses in the adult rodent brain. We found that the neuronal transporter EAAT4 contributes to the uptake of ~10% of total released glutamate at the cerebellar climbing fiber-Purkinje cell synapse, and that EAAC1 does not contribute to the electrogenic transport of glutamate at this synapse. At hippocampal CA1-interneuron synapses, astroglial transporters GLAST and GLT-1, but not neuronal transporter EAAC1, contribute to the clearance of glutamate at extrasynaptic regions and regulate the activation of mGluRs at this synapse. Together, these results suggest that astroglial transporters, although positioned outside the synaptic cleft, contribute substantially more than neuronal transporters to the uptake of synaptically released glutamate.

The extreme diversity in synaptic morphology indicates that caution should be exercised when generalizing results from a few model synapses. Although less numerous, neuronal transporters also have been shown to influence clearance and receptor occupancy during transmission, presumably by being localized near receptors. At synapses devoid of astroglial processes, and at complex synapses that consist of multiple active zones with no intervening astroglia, neuronal glutamate transporters

may be of particular importance in terminating glutamate transients and regulating receptor occupancy. In addition to EAAC1 and EAAT4 as neuronal transporters, we observed in this study that the predominant glial transporter GLT-1 also mediates electrogenic glutamate uptake in hippocampal CA3 pyramidal neurons in the adult rodent brain. Mossy fiber-CA3 synapses are a typical large, complex synapses that have multiple release sites but very little intervening astroglial processes; it is therefore a prominent candidate location to study GLT-1 function in neurons during transmission. Finally, it is not clear why neurons express different sets of glutamate transporters (EAAC1, EAAT4 and GLT-1), which differ in their molecular composition as well as affinity for glutamate, conductance for anions, transport efficiency and turnover time. Future studies will test the hypothesis that different glutamate transporters expressed by neurons are subject to differential regulation; and that the difference in their biophysical properties determines their differential impact on synaptic transmission.

It is likely that synaptic structure and glial ensheathment are not static, even in the adult mammalian brain. Astrocyte processes can extend and retract from synapses under physiological or pathological conditions and therefore reposition glutamate transporters in relation to synapses. Previous studies have shown in the hypothalamus during lactation (Oliet et al., 2001) as well as in the cerebellum following selective expression of GluR2 in Bergmann glia (Iino et al., 2001), that astroglial cells retract their processes from excitatory synapses, which leads to impairment of glutamate clearance and alters transmission significantly. These studies suggest that plastic

changes in synaptic structure and ensheathment, as well as dynamic regulation of glutamate transporter activity in subcellular domains, could represent a widespread mechanism for influencing synaptic signaling over a period of seconds, hours, or days.

Although information about the individual roles of different glutamate transporters is emerging, the complex and dynamic regulation of synaptic structures as well as glutamate transporters themselves suggests that much work still needs to be done in order to create a complete picture of glutamate transporter involvement in excitatory transmission.

References

Aitken, P. G., and Somjen, G. G. (1986). The sources of extracellular potassium accumulation in the CA1 region of hippocampal slices. Brain Res *369*, 163-167.

Amaral, D. G., and Dent, J. A. (1981). Development of the mossy fibers of the dentate gyrus: I. A light and electron microscopic study of the mossy fibers and their expansions. J Comp Neurol *195*, 51-86.

Amit, B., Ben-Efraim, D. A., and Patchornik, A. (1976). LIght-sensitive amides. The photosolvolysis of substituted 1-acyl-7-nitroindolines. J Am Chem Soc *98*, 843-844.

Arnth-Jensen, N., Jabaudon, D., and Scanziani, M. (2002). Cooperation between independent hippocampal synapses is controlled by glutamate uptake. Nat Neurosci *5*, 325-331.

Arriza, J. L., Eliasof, S., Kavanaugh, M. P., and Amara, S. G. (1997). Excitatory amino acid transporter 5, a retinal glutamate transporter coupled to a chloride conductance. Proc Natl Acad Sci U S A *94*, 4155-4160.

Arriza, J. L., Fairman, W. A., Wadiche, J. I., Murdoch, G. H., Kavanaugh, M. P., and Amara, S. G. (1994). Functional comparisons of three glutamate transporter subtypes cloned from human motor cortex. J Neurosci *14*, 5559-5569.

Asztely, F., Erdemli, G., and Kullmann, D. M. (1997). Extrasynaptic glutamate spillover in the hippocampus: dependence on temperature and the role of active glutamate uptake. Neuron *18*, 281-293.

Attwell, D., and Gibb, A. (2005). Neuroenergetics and the kinetic design of excitatory

synapses. Nat Rev Neurosci *6*, 841-849.

Auger, C., and Attwell, D. (2000). Fast removal of synaptic glutamate by postsynaptic transporters. Neuron *28*, 547-558.

Balcar, V. J., and Johnston, G. A. (1972). The structural specificity of the high affinity uptake of L-glutamate and L-aspartate by rat brain slices. J Neurochem *19*, 2657-2666.

Barbour, B., Brew, H., and Attwell, D. (1991). Electrogenic uptake of glutamate and aspartate into glial cells isolated from the salamander (Ambystoma) retina. J Physiol (Lond) *436*, 169-193.

Barbour, B., Keller, B. U., Llano, I., and Marty, A. (1994). Prolonged presence of glutamate during excitatory synaptic transmission to cerebellar Purkinje cells. Neuron *12*, 1331-1343.

Batchelor, A. M., and Garthwaite, J. (1997). Frequency detection and temporally dispersed synaptic signal association through a metabotropic glutamate receptor pathway. Nature *385*, 74-77.

Batchelor, A. M., Madge, D. J., and Garthwaite, J. (1994). Synaptic activation of metabotropic glutamate receptors in the parallel fibre-Purkinje cell pathway in rat cerebellar slices. Neuroscience *63*, 911-915.

Baude, A., Nusser, Z., Roberts, J. D., Mulvihill, E., McIlhinney, R. A., and Somogyi, P. (1993). The metabotropic glutamate receptor (mGluR1 alpha) is concentrated at perisynaptic membrane of neuronal subpopulations as detected by immunogold reaction. Neuron *11*, 771-787.

Berger, U. V., and Hediger, M. A. (1998). Comparative analysis of glutamate transporter expression in rat brain using differential double in situ hybridization. Anat Embryol (Berl) *198*, 13-30.

Bergles, D. E., Dzubay, J. A., and Jahr, C. E. (1997). Glutamate transporter currents in bergmann glial cells follow the time course of extrasynaptic glutamate. Proc Natl Acad Sci U S A *94*, 14821-14825.

Bergles, D. E., and Jahr, C. E. (1997). Synaptic activation of glutamate transporters in hippocampal astrocytes. Neuron *19*, 1297-1308.

Bergles, D. E., and Jahr, C. E. (1998). Glial contribution to glutamate uptake at Schaffer collateral- commissural synapses in the hippocampus. J Neurosci *18*, 7709-7716.

Bergles, D. E., Tzingounis, A. V., and Jahr, C. E. (2002). Comparison of coupled and uncoupled currents during glutamate uptake by GLT-1 transporters. J Neurosci *22*, 10153-10162.

Bortolotto, Z. A., Clarke, V. R., Delany, C. M., Parry, M. C., Smolders, I., Vignes, M., Ho, K. H., Miu, P., Brinton, B. T., Fantaske, R.*, et al.* (1999). Kainate receptors are involved in synaptic plasticity. Nature *402*, 297-301.

Brasnjo, G., and Otis, T. S. (2001). Neuronal glutamate transporters control activation of postsynaptic metabotropic glutamate receptors and influence cerebellar long-term depression. Neuron *31*, 607-616.

Brasnjo, G., and Otis, T. S. (2004). Isolation of glutamate transport-coupled charge flux and estimation of glutamate uptake at the climbing fiber-Purkinje cell

synapse. Proc Natl Acad Sci U S A *101*, 6273-6278.

Brickley, S., Swanson, G., Contractor, A., Farrant, M., Sailer, A., Cull-Candy, S., and Heinemann, S. (1999). Functional GluR5-containing kainate receptors are restricted to extrasynaptic sties in Purkinje cells of the mouse cerebellum. J Physiol *521 P*, 90P.

Bureau, I., Dieudonne, S., Coussen, F., and Mulle, C. (2000). Kainate receptor-mediated synaptic currents in cerebellar Golgi cells are not shaped by diffusion of glutamate. Proc Natl Acad Sci U S A *97*, 6838-6843.

Canepari, M., Nelson, L., Papageorgiou, G., Corrie, J. E., and Ogden, D. (2001). Photochemical and pharmacological evaluation of 7-nitroindolinyl-and 4-methoxy-7-nitroindolinyl-amino acids as novel, fast caged neurotransmitters. J Neurosci Methods *112*, 29-42.

Canepari, M., Papageorgiou, G., Corrie, J. E., Watkins, C., and Ogden, D. (2001). The conductance underlying the parallel fibre slow EPSP in rat cerebellar Purkinje neurones studied with photolytic release of L-glutamate. J Physiol *533*, 765-772.

Chaudhry, F. A., Lehre, K. P., M., v. L. C., Ottersen, O. P., Danbolt, N. C., and J., S.-M. (1995). Glutamate Transporters In Glial Plasma Membranes: Highly Differentiated Localizations Revealed by Quantitative Ultrastructural Immunocytochemistry. Neuron *15*, 720.

Chen, W., Aoki, C., Mahadomrongkul, V., Gruber, C. E., Wang, G. J., Blitzblau, R., Irwin, N., and Rosenberg, P. A. (2002). Expression of a variant form of the glutamate transporter GLT1 in neuronal cultures and in neurons and astrocytes in

the rat brain. J Neurosci *22*, 2142-2152.

Chen, W., Mahadomrongkul, V., Berger, U. V., Bassan, M., DeSilva, T., Tanaka, K., Irwin, N., Aoki, C., and Rosenberg, P. A. (2004). The glutamate transporter GLT1α is expressed in excitatory axon terminals of mature hippocampal neurons. J Neurosci *24*, 1136-1148.

Chicurel, M. E., and Harris, K. M. (1992). Three-dimensional analysis of the structure and composition of CA3 branched dendritic spines and their synaptic relationships with mossy fiber boutons in the rat hippocampus. J Comp Neurol *325*, 169-182.

Clark, B. A., and Barbour, B. (1997). Currents evoked in Bergmann glial cells by parallel fibre stimulation in rat cerebellar slices. J Physiol (Lond) *502*, 335-350.

Clark, B. A., and Cull-Candy, S. G. (2002). Activity-dependent recruitment of extrasynaptic NMDA receptor activation at an AMPA receptor-only synapse. J Neurosci *22*, 4428-4436.

Cleveland, D. W., and Rothstein, J. D. (2001). From Charcot to Lou Gehrig: deciphering selective motor neuron death in ALS. Nat Rev Neurosci *2*, 806-819.

Commons, K. G., and Milner, T. A. (1995). Ultrastructural heterogeneity of enkephalin-containing terminals in the rat hippocampal formation. J Comp Neurol *358*, 324-342.

Conn, P. J., and Pin, J. P. (1997). Pharmacology and functions of metabotropic glutamate receptors. Annu Rev Pharmacol Toxicol *37*, 205-237.

Contractor, A., Swanson, G. T., Sailer, A., O'Gorman, S., and Heinemann, S. F. (2000). Identification of the kainate receptor subunits underlying modulation of excitatory

synaptic transmission in the CA3 region of the hippocampus. J Neurosci *20*, 8269-8278.

Cossart, R., Epsztein, J., Tyzio, R., Becq, H., Hirsch, J., Ben-Ari, Y., and Crepel, V. (2002). Quantal release of glutamate generates pure kainate and mixed AMPA/kainate EPSCs in hippocampal neurons. Neuron *35*, 147-159.

Danbolt, N. C. (2001). Glutamate uptake. Prog Neurobiol *65*, 1-105.

Dehnes, Y., Chaudhry, F. A., Ullensvang, K., Lehre, K. P., Storm-Mathisen, J., and Danbolt, N. C. (1998). The glutamate transporter EAAT4 in rat cerebellar Purkinje cells: a glutamate-gated chloride channel concentrated near the synapse in parts of the dendritic membrane facing astroglia. J Neurosci *18*, 3606-3619.

Diamond, J. S. (2001). Neuronal glutamate transporters limit activation of NMDA receptors by neurotransmitter spillover on CA1 pyramidal cells. J Neurosci *21*, 8328-8338.

Diamond, J. S., and Jahr, C. E. (1997). Transporters buffer synaptically released glutamate on a submillisecond time scale. J Neurosci *17*, 4672-4687.

Diamond, J. S., and Jahr, C. E. (2000). Synaptically released glutamate does not overwhelm transporters on hippocampal astrocytes during high-frequency stimulation. J Neurophysiol *83*, 2835-2843.

Dowd, L. A., Coyle, A. J., Rothstein, J. D., Pritchett, D. B., and Robinson, M. B. (1996). Comparison of Na+-dependent glutamate transport activity in synaptosomes, C6 glioma, and Xenopus oocytes expressing excitatory amino acid carrier 1 (EAAC1). Mol Pharmacol *49*, 465-473.

Dowd, L. A., and Robinson, M. B. (1996). Rapid stimulation of EAAC1-mediated Na+-dependent L-glutamate transport activity in C6 glioma cells by phorbol ester. J Neurochem *67*, 508-516.

Dunlop, J. (2001). Substrate exchange properties of the high-affinity glutamate transporter EAAT2. J Neurosci Res *66*, 482-486.

Dunlop, J., Eliasof, S., Stack, G., McIlvain, H. B., Greenfield, A., Kowal, D., Petroski, R., and Carrick, T. (2003). WAY-855 (3-amino-tricyclo[2.2.1.02.6]heptane-1,3-dicarboxylic acid): a novel, EAAT2-preferring, nonsubstrate inhibitor of high-affinity glutamate uptake. Br J Pharmacol *140*, 839-846.

Dzubay, J. A., and Jahr, C. E. (1999). The concentration of synaptically released glutamate outside of the climbing fiber-Purkinje cell synaptic cleft. J Neurosci *19*, 5265-5274.

Ellis-Davies, G. C., and Kaplan, J. H. (1994). Nitrophenyl-EGTA, a photolabile chelator that selectively binds Ca2+ with high affinity and releases it rapidly upon photolysis. Proc Natl Acad Sci U S A *91*, 187-191.

Euler, T., and Wassle, H. (1995). Immunocytochemical identification of cone bipolar cells in the rat retina. J Comp Neurol *361*, 461-478.

Fairman, W. A., Vandenberg, R. J., Arriza, J. L., Kavanaugh, M. P., and Amara, S. G. (1995). An excitatory amino-acid transporter with properties of a ligand-gated chloride channel. Nature *375*, 599-603.

Frerking, M., and Ohliger-Frerking, P. (2002). AMPA receptors and kainate receptors

encode different features of afferent activity. J Neurosci *22*, 7434-7443.

Freund, T. F., and Buzsáki, G. (1996). Interneurons of the hippocampus. Hippocampus *6*, 347-470.

Furuta, A., Rothstein, J. D., and Martin, L. J. (1997). Glutamate transporter protein subtypes are expressed differentially during rat CNS development. J Neurosci *17*, 8363-8375.

Gee, C. E., Woodhall, G., and Lacaille, J. C. (2001). Synaptically activated calcium responses in dendrites of hippocampal oriens-alveus interneurons. J Neurophysiol *85*, 1603-1613.

Gee, K. R., Niu, L., Schaper, K., Jayaraman, V., and Hess, G. P. (1999). Synthesis and photochemistry of a photolabile precursor of N-methyl-D-aspartate (NMDA) that is photolyzed in the microsecond time region and is suitable for chemical kinetic investigations of the NMDA receptor. Biochemistry *38*, 3140-3147.

Gegelashvili, G., Danbolt, N. C., and Schousboe, A. (1997). Neuronal soluble factors differentially regulate the expression of the GLT1 and GLAST glutamate transporters in cultured astroglia. J Neurochem *69*, 2612-2615.

Gonzalez, M. I., and Robinson, M. B. (2004). Neurotransmitter transporters: why dance with so many partners? Curr Opin Pharmacol *4*, 30-35.

Grewer, C., Madani Mobarekeh, S. A., Watzke, N., Rauen, T., and Schaper, K. (2001). Substrate translocation kinetics of excitatory amino acid carrier 1 probed with laser-pulse photolysis of a new photolabile precursor of D-aspartic acid. Biochemistry *40*, 232-240.

Grewer, C., and Rauen, T. (2005). Electrogenic glutamate transporters in the CNS: molecular mechanism, pre-steady-state kinetics, and their impact on synaptic signaling. J Membr Biol *203*, 1-20.

Grewer, C., Watzke, N., Wiessner, M., and Rauen, T. (2000). Glutamate translocation of the neuronal glutamate transporter EAAC1 occurs within milliseconds. Proc Natl Acad Sci U S A *97*, 9706-9711.

Hakuba, N., Koga, K., Gyo, K., Usami, S.-i., and Tanaka, K. (2000). Exacerbation of Noise-Induced Hearing Loss in Mice Lacking the Glutamate Transporter GLAST. J Neurosci *20*, 8750-8753.

Harrison, J., and Jahr, C. E. (2003). Receptor occupancy limits synaptic depression at climbing fiber synapses. J Neurosci *23*, 377-383.

Hausser, M., and Roth, A. (1997). Dendritic and somatic glutamate receptor channels in rat cerebellar Purkinje cells. J Physiol *501 (Pt 1)*, 77-95.

He, Y., Janssen, W. G., Rothstein, J. D., and Morrison, J. H. (2000). Differential synaptic localization of the glutamate transporter EAAC1 and glutamate receptor subunit GluR2 in the rat hippocampus. J Comp Neurol *418*, 255-269.

Hirasawa, M., Cho, A., Sreenath, T., Sauer, B., Julien, J. P., and Kulkarni, A. B. (2001). Neuron-specific expression of Cre recombinase during the late phase of brain development. Neurosci Res *40*, 125-132.

Huang, Y. H., and Bergles, D. E. (2004). Glutamate transporters bring competition to the synapse. Curr Opin Neurobiol *14*, 346-352.

Huang, Y. H., Dykes-Hoberg, M., Tanaka, K., Rothstein, J. D., and Bergles, D. E.

(2004). Climbing fiber activation of EAAT4 transporters and kainate receptors in cerebellar Purkinje cells. J Neurosci *24*, 103-111.

Huang, Y. H., Sinha, S. R., Fedoryak, O. D., Ellis-Davies, G. C., and Bergles, D. E. (2005). Synthesis and characterization of 4-methoxy-7-nitroindolinyl-D-aspartate, a caged compound for selective activation of glutamate transporters and N-methyl-D-aspartate receptors in brain tissue. Biochemistry *44*, 3316-3326.

Huang, Y. H., Sinha, S. R., Tanaka, K., Rothstein, J. D., and Bergles, D. E. (2004). Astrocyte glutamate transporters regulate metabotropic glutamate receptor-mediated excitation of hippocampal interneurons. J Neurosci *24*, 4551-4559.

Iino, M., Goto, K., Kakegawa, W., Okado, H., Sudo, M., Ishiuchi, S., Miwa, A., Takayasu, Y., Saito, I., Tsuzuki, K., and Ozawa, S. (2001). Glia-synapse interaction through Ca2+-permeable AMPA receptors in Bergmann glia. Science *292*, 926-929.

Isaacson, J. S., and Nicoll, R. A. (1993). The uptake inhibitor L-trans-PDC enhances responses to glutamate but fails to alter the kinetics of excitatory synaptic currents in the hippocampus. J Neurophysiol *70*, 2187-2191.

Jabaudon, D., Shimamoto, K., Yasuda-Kamatani, Y., Scanziani, M., Gahwiler, B. H., and Gerber, U. (1999). Inhibition of uptake unmasks rapid extracellular turnover of glutamate of nonvesicular origin. Proc Natl Acad Sci U S A *96*, 8733-8738.

Johnston, G. A. R., ed. (1981). Glutamate uptake and its possible role in neurotransmitter inactivation (Chichester, UK: Wiley).

Jonas, P., and Sakmann, B. (1992). Glutamate receptor channels in isolated patches from CA1 and CA3 pyramidal cells of rat hippocampal slices. J Physiol (Lond) *455*, 143-171.

Kang, J., Jiang, L., Goldman, S. A., and Nedergaard, M. (1998). Astrocyte-mediated potentiation of inhibitory synaptic transmission. Nat Neurosci *1*, 683-692.

Kanner, B. I., and Bendahan, A. (1982). Binding order of substrates to the sodium and potassium ion coupled L-glutamic acid transporter from rat brain. Biochemistry *21*, 6327-6330.

Katagiri, H., Tanaka, K., and Manabe, T. (2001). Requirement of appropriate glutamate concentrations in the synaptic cleft for hippocampal LTP induction. Eur J Neurosci *14*, 547-553.

Kidd, F. L., and Isaac, J. T. (2001). Kinetics and activation of postsynaptic kainate receptors at thalamocortical synapses: role of glutamate clearance. J Neurophysiol *86*, 1139-1148.

Kim, S. J., Kim, Y. S., Yuan, J. P., Petralia, R. S., Worley, P. F., and Linden, D. J. (2003). Activation of the TRPC1 cation channel by metabotropic glutamate receptor mGluR1. Nature *426*, 285-291.

Kinney, G. A., Overstreet, L. S., and Slater, N. T. (1997). Prolonged physiological entrapment of glutamate in the synaptic cleft of cerebellar unipolar brush cells. J Neurophysiol *78*, 1320-1333.

Lehre, K. P., and Danbolt, N. C. (1998). The number of glutamate transporter subtype molecules at glutamatergic synapses: chemical and stereological quantification in

young adult rat brain. J Neurosci *18*, 8751-8757.

Lehre, K. P., Levy, L. M., Ottersen, O. P., Storm-Mathisen, J., and Danbolt, N. C. (1995). Differential expression of two glial glutamate transporters in the rat brain: quantitative and immunocytochemical observations. J Neurosci *15*, 1835-1853.

Lehre, K. P., and Rusakov, D. A. (2002). Asymmetry of glia near central synapses favors presynaptically directed glutamate escape. Biophys J *83*, 125-134.

Lerma, J. (2003). Roles and rules of kainate receptors in synaptic transmission. Nat Rev Neurosci *4*, 481-495.

Lerma, J., Paternain, A. V., Rodriguez-Moreno, A., and Lopez-Garcia, J. C. (2001). Molecular physiology of kainate receptors. Physiol Rev *81*, 971-998.

Levy, L. M., Lehre, K. P., Walaas, S. I., Storm-Mathisen, J., and Danbolt, N. C. (1995). Down-regulation of glial glutamate transporters after glutamatergic denervation in the rat brain. Eur J Neurosci *7*, 2036-2041.

Levy, L. M., Warr, O., and Attwell, D. (1998). Stoichiometry of the glial glutamate transporter GLT-1 expressed inducibly in a Chinese hamster ovary cell line selected for low endogenous Na+-dependent glutamate uptake. J Neurosci *18*, 9620-9628.

Li, X., Atkinson, R., and King, S. (2001). Preparation and evaluation of new -canavanine derivatives as nitric oxide synthase inhibitors. Tetrahedron *57*, 6557-6565.

Logan, W. J., and Snyder, S. H. (1972). High affinity uptake systems for glycine, glutamic and aspaspartic acids in synaptosomes of rat central nervous tissues.

Brain Res *42*, 413-431.

Lujan, R., Nusser, Z., Roberts, J. D., Shigemoto, R., and Somogyi, P. (1996). Perisynaptic location of metabotropic glutamate receptors mGluR1 and mGluR5 on dendrites and dendritic spines in the rat hippocampus. Eur J Neurosci *8*, 1488-1500.

Maccaferri, G., and Dingledine, R. (2002). Control of feedforward dendritic inhibition by NMDA receptor-dependent spike timing in hippocampal interneurons. J Neurosci *22*, 5462-5472.

Maccaferri, G., Roberts, J. D., Szucs, P., Cottingham, C. A., and Somogyi, P. (2000). Cell surface domain specific postsynaptic currents evoked by identified GABAergic neurones in rat hippocampus in vitro. J Physiol *524 Pt 1*, 91-116.

Manzoni, O. J., Castillo, P. E., and Nicoll, R. A. (1995). Pharmacology of metabotropic glutamate receptors at the mossy fiber synapses of the guinea pig hippocampus. Neuropharmacology *34*, 965-971.

Martin, L. J., Brambrink, A. M., Lehmann, C., Portera-Cailliau, C., Koehler, R., Rothstein, J., and Traystman, R. J. (1997). Hypoxia-ischemia causes abnormalities in glutamate transporters and death of astroglia and neurons in newborn striatum. *42*, 335-348.

Mathews, G. C., and Diamond, J. S. (2003). Neuronal glutamate uptake Contributes to GABA synthesis and inhibitory synaptic strength. *23*, 2040-2048.

Matsuzaki, M., Ellis-Davies, G. C., Nemoto, T., Miyashita, Y., Iino, M., and Kasai, H. (2001). Dendritic spine geometry is critical for AMPA receptor expression in

hippocampal CA1 pyramidal neurons. Nat Neurosci *4*, 1086-1092.

McBain, C. J., DiChiara, T. J., and Kauer, J. A. (1994). Activation of metabotropic glutamate receptors differentially affects two classes of hippocampal interneurons and potentiates excitatory synaptic transmission. J Neurosci *14*, 4433-4445.

Miles, R., and Poncer, J. C. (1993). Metabotropic glutamate receptors mediate a post-tetanic excitation of guinea-pig hippocampal inhibitory neurones. J Physiol *463*, 461-473.

Min, M. Y., Rusakov, D. A., and Kullmann, D. M. (1998). Activation of AMPA, kainate, and metabotropic receptors at hippocampal mossy fiber synapses: role of glutamate diffusion. Neuron *21*, 561-570.

Mori, M., and Gerber, U. (2002). Slow feedback inhibition in the CA3 area of the rat hippocampus by synergistic synaptic activation of mGluR1 and mGluR5. J Physiol *544*, 793-799.

Norman, R. O., and Radda, G. K. (1961). J Chem Soc, 3030-3036.

Northington, F. J., Traystman, R. J., Koehler, R. C., Rothstein, J. D., and Martin, L. J. (1998). Regional and cellular expression of glial (GLT1) and neuronal (EAAC1) glutamate transporter proteins in ovine fetal brain. Neuroscience *85*, 1183-1194.

Oliet, S. H., Piet, R., and Poulain, D. A. (2001). Control of glutamate clearance and synaptic efficacy by glial coverage of neurons. Science *292*, 923-926.

Olverman, H. J., Jones, A. W., Mewett, K. N., and Watkins, J. C. (1988). Structure/activity relations of N-methyl-D-aspartate receptor ligands as studied by their inhibition of [3H]D-2-amino-5-phosphonopentanoic acid binding in rat brain

membranes. Neuroscience *26*, 17-31.

Otis, T. S., and Jahr, C. E. (1998). Anion currents and predicted glutamate flux through a neuronal glutamate transporter. J Neurosci *18*, 7099-7110.

Otis, T. S., and Kavanaugh, M. P. (2000). Isolation of current components and partial reaction cycles in the glial glutamate transporter EAAT2. J Neurosci *20*, 2749-2757.

Otis, T. S., Kavanaugh, M. P., and Jahr, C. E. (1997). Postsynaptic glutamate transport at the climbing fiber-Purkinje cell synapse. Science *277*, 1515-1518.

Otis, T. S., Wu, Y. C., and Trussell, L. O. (1996). Delayed clearance of transmitter and the role of glutamate transporters at synapses with multiple release sites. J Neurosci *16*, 1634-1644.

Ottersen, O. P., Laake, J. H., Reichelt, W., Haug, F. M., and Torp, R. (1996). Ischemic disruption of glutamate homeostasis in brain: quantitative immunocytochemical analyses. J Chem Neuroanat *12*, 1-14.

Palay, S. L., and Chan-Palay, V. (1974). In Cerebellar Cortex - Cytology and Organization (Berlin: Springer).

Paternain, A. V., Morales, M., and Lerma, J. (1995). Selective antagonism of AMPA receptors unmasks kainate receptor-mediated responses in hippocampal neurons. Neuron *14*, 185-189.

Patneau, D. K., and Mayer, M. L. (1990). Structure-activity relationships for amino acid transmitter candidates acting at N-methyl-D-aspartate and quisqualate receptors. J Neurosci *10*, 2385-2399.

Peghini, P., Janzen, J., and Stoffel, W. (1997). Glutamate transporter EAAC-1-deficient mice develop dicarboxylic aminoaciduria and behavioral abnormalities but no neurodegeneration. Embo J *16*, 3822-3832.

Perkel, D. J., Hestrin, S., Sah, P., and Nicoll, R. A. (1990). Excitatory synaptic currents in Purkinje cells. Proc R Soc Lond B Biol Sci *241*, 116-121.

Pettit, D. L., Wang, S. S., Gee, K. R., and Augustine, G. J. (1997). Chemical two-photon uncaging: a novel approach to mapping glutamate receptors. Neuron *19*, 465-471.

Pin, J. P., and Duvoisin, R. (1995). The metabotropic glutamate receptors: structure and functions. Neuropharmacology *34*, 1-26.

Rammes, G., Swandulla, D., Spielmanns, P., and Parsons, C. G. (1998). Interactions of GYKI 52466 and NBQX with cyclothiazide at AMPA receptors: experiments with outside-out patches and EPSCs in hippocampal neurones. Neuropharmacology *37*, 1299-1320.

Rao, V. L., Baskaya, M. K., Dogan, A., Rothstein, J. D., and Dempsey, R. J. (1998). Traumatic brain injury down-regulates glial glutamate transporter (GLT-1 and GLAST) proteins in rat brain. J Neurochem *70*, 2020-2027.

Rauen, T., and Kanner, B. I. (1994). Localization of the glutamate transporter GLT-1 in rat and macaque monkey retinae. Neurosci Lett *169*, 137-140.

Rauen, T., Rothstein, J. D., and Wassle, H. (1996). Differential expression of three glutamate transporter subtypes in the rat retina. Cell Tissue Res *286*, 325-336.

Reichelt, W., and Knopfel, T. (2002). Glutamate uptake controls expression of a slow

postsynaptic current mediated by mGluRs in cerebellar Purkinje cells. J Neurophysiol *87*, 1974-1980.

Renden, R., Taschenberger, H., Puente, N., Rusakov, D. A., Duvoisin, R., Wang, L. Y., Lehre, K. P., and von Gersdorff, H. (2005). Glutamate transporter studies reveal the pruning of metabotropic glutamate receptors and absence of AMPA receptor desensitization at mature calyx of held synapses. J Neurosci *25*, 8482-8497.

Rossi, D. J., Oshima, T., and Attwell, D. (2000). Glutamate release in severe brain ischaemia is mainly by reversed uptake. Nature *403*, 316-321.

Rothstein, J. D., Dykes-Hoberg, M., Pardo, C. A., Bristol, L. A., Jin, L., Kuncl, R. W., Kanai, Y., Hediger, M. A., Wang, Y., Schielke, J. P., and Welty, D. F. (1996). Knockout of glutamate transporters reveals a major role for astroglial transport in excitotoxicity and clearance of glutamate. Neuron *16*, 675-686.

Rothstein, J. D., Martin, L., Levey, A. I., Dykes-Hoberg, M., Jin, L., Wu, D., Nash, N., and Kuncl, R. W. (1994). Localization of neuronal and glial glutamate transporters. Neuron *13*, 713-725.

Rozas, J. L., Paternain, A. V., and Lerma, J. (2003). Noncanonical signaling by ionotropic kainate receptors. Neuron *39*, 543-553.

Saier, M. H., Jr. (1999). Eukaryotic transmembrane solute transport systems. Int Rev Cytol *190*, 61-136.

Scanziani, M., Gahwiler, B. H., and Charpak, S. (1998). Target cell-specific modulation of transmitter release at terminals from a single axon. Proc Natl Acad Sci U S A *95*, 12004-12009.

Schmitt, A., Asan, E., Puschel, B., Jons, T., and Kugler, P. (1996). Expression of the glutamate transporter GLT1 in neural cells of the rat central nervous system: non-radioactive in situ hybridization and comparative immunocytochemistry. Neuroscience *71*, 989-1004.

Sepkuty, J. P., Cohen, A. S., Eccles, C., Rafiq, A., Behar, K., Ganel, R., Coulter, D. A., and Rothstein, J. D. (2002). A neuronal glutamate transporter contributes to neurotransmitter GABA synthesis and epilepsy. *22*, 6372-6379.

Shepherd, G. M. (2004). The synaptic organization of the brain, 5th edn (New York: Oxford University Press).

Shigemoto, R., Kinoshita, A., Wada, E., Nomura, S., Ohishi, H., Takada, M., Flor, P. J., Neki, A., Abe, T., Nakanishi, S., and Mizuno, N. (1997). Differential presynaptic localization of metabotropic glutamate receptor subtypes in the rat hippocampus. J Neurosci *17*, 7503-7522.

Shigeri, Y., Shimamoto, K., Yasuda-Kamatani, Y., Seal, R. P., Yumoto, N., Nakajima, T., and Amara, S. G. (2001). Effects of threo-beta-hydroxyaspartate derivatives on excitatory amino acid transporters (EAAT4 and EAAT5). J Neurochem *79*, 297-302.

Shimamoto, K., Lebrun, B., Yasuda-Kamatani, Y., Sakaitani, M., Shigeri, Y., Yumoto, N., and Nakajima, T. (1998). DL-threo-beta-benzyloxyaspartate, a potent blocker of excitatory amino acid transporters. Mol Pharmacol *53*, 195-201.

Shimamoto, K., Shigeri, Y., Yasuda-Kamatani, Y., Lebrun, B., Yumoto, N., and Nakajima, T. (2000). Syntheses of optically pure beta-hydroxyaspartate

derivatives as glutamate transporter blockers. Bioorg Med Chem Lett *10*, 2407-2410.

Silver, R. A., Momiyama, A., and Cull-Candy, S. G. (1998). Locus of frequency-dependent depression identified with multiple-probability fluctuation analysis at rat climbing fibre-Purkinje cell synapses. J Physiol *510 (Pt 3)*, 881-902.

Slotboom, D. J., Konings, W. N., and Lolkema, J. S. (1999). Structural features of the glutamate transporter family. Microbiol Mol Biol Rev *63*, 293-307.

Spacek, J. (1980). Non-synaptic membrane specializations on the necks of Purkinje cell dentritic spines. J Anat *131*, 723-729.

Spacek, J. (1985). Three-dimensional analysis of dendritic spines. III. Glial sheath. Anat Embryol (Berl) *171*, 245-252.

Swanson, G. T., and Heinemann, S. F. (1998). Heterogeneity of homomeric GluR5 kainate receptor desensitization expressed in HEK293 cells. J Physiol *513 (Pt 3)*, 639-646.

Takahashi, M., Kovalchuk, Y., and Attwell, D. (1995). Pre- and postsynaptic determinants of EPSC waveform at cerebellar climbing fiber and parallel fiber to Purkinje cell synapses. J Neurosci *15*, 5693-5702.

Takahashi, M., Sarantis, M., and Attwell, D. (1996). Postsynaptic glutamate uptake in rat cerebellar Purkinje cells. J Physiol (Lond) *497*, 523-530.

Tamaru, Y., Nomura, S., Mizuno, N., and Shigemoto, R. (2001). Distribution of metabotropic glutamate receptor mGluR3 in the mouse CNS: differential location

relative to pre- and postsynaptic sites. Neuroscience *106*, 481-503.

Tanaka, J., Ichikawa, R., Watanabe, M., Tanaka, K., and Inoue, Y. (1997). Extra-junctional localization of glutamate transporter EAAT4 at excitatory Purkinje cell synapses. Neuroreport *8*, 2461-2464.

Tanaka, K., Watase, K., Manabe, T., Yamada, K., Watanabe, M., Takahashi, K., Iwama, H., Nishikawa, T., Ichihara, N., Kikuchi, T.*, et al.* (1997). Epilepsy and exacerbation of brain injury in mice lacking the glutamate transporter GLT-1. Science *276*, 1699-1702.

Tempia, F., Miniaci, M. C., Anchisi, D., and Strata, P. (1998). Postsynaptic current mediated by metabotropic glutamate receptors in cerebellar Purkinje cells. J Neurophysiol *80*, 520-528.

Theodosis, D. T., and Poulain, D. A. (1993). Activity-dependent neuronal-glial and synaptic plasticity in the adult mammalian hypothalamus. Neuroscience *57*, 501-535.

Thomson, A. M. (2000). Facilitation, augmentation and potentiation at central synapses. Trends Neurosci *23*, 305-312.

Tong, G., and Jahr, C. E. (1994). Block of glutamate transporters potentiates postsynaptic excitation. Neuron *13*, 1195-1203.

Torp, R., Danbolt, N. C., Babaie, E., Bjoras, M., Seeberg, E., Storm-Mathisen, J., and Ottersen, O. P. (1994). Differential expression of two glial glutamate transporters in the rat brain: an in situ hybridization study. Eur J Neurosci *6*, 936-942.

Torp, R., Hoover, F., Danbolt, N. C., Storm-Mathisen, J., and Ottersen, O. P. (1997).

Differential distribution of the glutamate transporters GLT1 and rEAAC1 in rat cerebral cortex and thalamus: an in situ hybridization analysis. Anat Embryol (Berl) *195*, 317-326.

Trotti, D., Peng, J. B., Dunlop, J., and Hediger, M. A. (2001). Inhibition of the glutamate transporter EAAC1 expressed in Xenopus oocytes by phorbol esters. Brain Res *914*, 196-203.

Tsvetkov, E., Shin, R. M., and Bolshakov, V. Y. (2004). Glutamate uptake determines pathway specificity of long-term potentiation in the neural circuitry of fear conditioning. Neuron *41*, 139-151.

Utsunomiya-Tate, N., Endou, H., and Kanai, Y. (1997). Tissue specific variants of glutamate transporter GLT-1. FEBS Lett *416*, 312-316.

Ventura, R., and Harris, K. M. (1999). Three-dimensional relationships between hippocampal synapses and astrocytes. J Neurosci *19*, 6897-6906.

von Kitzing, E., Jonas, P., and Sakmann, B. (1994). Quantal analysis of excitatory postsynaptic currents at the hippocampal mossy fiber-CA3 pyramidal cell synapse. Adv Second Messenger Phosphoprotein Res *29*, 235-260.

Voutsinos-Porche, B., Bonvento, G., Tanaka, K., Steiner, P., Welker, E., Chatton, J. Y., Magistretti, P. J., and Pellerin, L. (2003). Glial glutamate transporters mediate a functional metabolic crosstalk between neurons and astrocytes in the mouse developing cortex. Neuron *37*, 275-286.

Wadiche, J. I., Amara, S. G., and Kavanaugh, M. P. (1995). Ion fluxes associated with excitatory amino acid transport. Neuron *15*, 721-728.

Wadiche, J. I., Arriza, J. L., Amara, S. G., and Kavanaugh, M. P. (1995). Kinetics of a human glutamate transporter. Neuron *14*, 1019-1027.

Wadiche, J. I., and Jahr, C. E. (2001). Multivesicular release at climbing fiber-Purkinje cell synapses. Neuron *32*, 301-313.

Wadiche, J. I., and Jahr, C. E. (2005). Patterned expression of Purkinje cell glutamate transporters controls synaptic plasticity. Nat Neurosci *8*, 1329-1334.

Wadiche, J. I., and Kavanaugh, M. P. (1998). Macroscopic and microscopic properties of a cloned glutamate transporter/chloride channel. J Neurosci *18*, 7650-7661.

Watase, K., Hashimoto, K., Kano, M., Yamada, K., Watanabe, M., Inoue, Y., Okuyama, S., Sakagawa, T., Ogawa, S., Kawashima, N.*, et al.* (1998). Motor discoordination and increased susceptibility to cerebellar injury in GLAST mutant mice. Eur J Neurosci *10*, 976-988.

Wisden, W., and Seeburg, P. H. (1993). A complex mosaic of high-affinity kainate receptors in rat brain. J Neurosci *13*, 3582-3598.

Wong, M., Ess, K. C., Uhlmann, E. J., Jansen, L. A., Li, W., Crino, P. B., Mennerick, S., Yamada, K. A., and Gutmann, D. H. (2003). Impaired glial glutamate transport in a mouse tuberous sclerosis epilepsy model. Ann Neurol *54*, 251-256.

Xu-Friedman, M. A., Harris, K. M., and Regehr, W. G. (2001). Three-dimensional comparison of ultrastructural characteristics at depressing and facilitating synapses onto cerebellar Purkinje cells. J Neurosci *21*, 6666-6672.

Yuzaki, M., Forrest, D., Curran, T., and Connor, J. A. (1996). Selective activation of calcium permeability by aspartate in Purkinje cells. Science *273*, 1112-1114.

Zerangue, N., and Kavanaugh, M. P. (1996). Flux coupling in a neuronal glutamate transporter. Nature *383*, 634-637.

Zhang, L., and McBain, C. J. (1995). Potassium conductances underlying repolarization and after-hyperpolarization in rat CA1 hippocampal interneurones. J Physiol *488 (Pt 3)*, 661-672.

Curriculum Vitae

Name: Yanhua Huang

Date of Birth: April 10, 1978

Mailing Address: 725 N. Wolfe St., WBSB 914

Baltimore, MD 21205

Phone (work): (410) 955-6949

E-mail: yhuang@jhmi.edu

yhhuang@gmail.com

Education:

Aug. 2000 – Present: Johns Hopkins Medical Institutions, Baltimore, MD, USA

Expecting Ph.D. in Neuroscience by Jan. 2006.

Sept. 1996 – June 2000: Beijing University, Beijing, P. R. China

B.S. in Physiology and Biophysics

Research Experience:

May 2001 – Present: "Glutamate transporter function at excitatory synapses" in the laboratory of Dr. Dwight E. Bergles, Johns Hopkins University.

Aug. 2000 – May 2001: Doing rotations in the laboratories of Drs. Richard L. Huganir and David D. Ginty, Johns Hopkins University.

Sept. 1999 – June 2000: "Involvement of endogenous opioid systems in the modulation of nociception" in the laboratory of Dr. Long-Chuan Yu, Beijing University.

Publications:

Peer-Reviewed Journal Articles

Huang YH, Muralidharan S, Sinha SR, Kao JP, Bergles DE (2005) Ncm-D-aspartate: a novel caged D-aspartate suitable for activation of glutamate transporters and *N*-methyl-D-aspartate (NMDA) receptors in brain tissue. Neuropharmacology 49:831-842.

Rothstein JD, Patel S, Regan MR, Haenggeli C, Huang YH, Bergles DE, Jin L, Dykes Hoberg M, Vidensky S, Chung DS, Toan SV, Bruijn LI, Su ZZ, Gupta P, Fisher PB (2005) Beta-lactam antibiotics offer neuroprotection by increasing glutamate transporter expression. Nature 433:73-77.

Huang YH, Sinha SR, Fedoryak OD, Ellis-Davies GC, Bergles DE (2005) Synthesis and characterization of 4-methoxy-7-nitroindolinyl-D-aspartate, a caged compound for selective activation of glutamate transporters and *N*-Methyl-D-aspartate (NMDA) receptors in brain tissue. Biochemistry 44:3316-3326.

Huang YH, Sinha SR, Tanaka K, Rothstein JD, Bergles DE (2004) Astrocyte glutamate transporters regulate metabotropic glutamate receptor-mediated excitation of hippocampal interneurons. J Neurosci 24:4551-4559.

Huang YH, Dykes-Hoberg M, Tanaka K, Rothstein JD, Bergles DE (2004) Climbing fiber activation of EAAT4 transporters and kainate receptors in cerebellar Purkinje cells. J Neurosci 24:103-111.

Chung HJ, Huang YH, Lau L-F, Huganir RL (2004) Regulation of the NMDA receptor complex and trafficking by activity-dependent phosphorylation of the NR2B subunit PDZ ligand. J Neurosci 24: 10248-10259

Lu JT, Huang YH, Palmer PP, Xie GX, Gabriel A, Grond S, Yu LC (2001) Blockade

effects of (Nphe1) Nociceptin(1-13)-NH(2) on anti-nociception induced by intrathecal administration of nociceptin in rats. Regul Pept 101:81-85.

Huang Y, Brodda-Jansen G, Lundeberg T, Yu LC (2000) Anti-nociceptive effects of calcitonin gene-related peptide in nucleus raphe magnus of rats: an effect attenuated by naloxone. Brain Res 873:54-59.

Review paper

Huang YH, Bergles DE (2004) Glutamate transporters bring competition to the synapse. Curr Opin Neurobiol 14:346-352.

Honors and Awards:

1996 – 1997	Outstanding Student Award, Beijing University.
1997 – 1998	Guang Hua Scholarship, Beijing University.
1998 – 1999	Guang Cai Scholarship, Beijing University.
1999 – 2000	Centennial Elite Scholarship, Beijing University.
April, 2005	Paul Ehrlich Award (Young Investigator Award) Johns Hopkins University School of Medicine.

Membership: Member of Society for Neuroscience (USA)